

# Origin of felsic achondrites Graves Nunataks 06128 and 06129, and ultramafic brachinites and brachinite-like achondrites by partial melting of volatile-rich primitive parent bodies

James M.D. Day<sup>a,b,\*</sup>, Richard J. Walker<sup>b</sup>, Richard D. Ash<sup>b</sup>, Yang Liu<sup>c</sup>, Douglas Rumble III<sup>d</sup>, Anthony J. Irving<sup>e</sup>, Cyrena A. Goodrich<sup>f</sup>, Kimberly Tait<sup>g</sup>, William F. McDonough<sup>b</sup>, Lawrence A. Taylor<sup>c</sup>

<sup>a</sup> *Geosciences Research Division, Scripps Institution of Oceanography, La Jolla, CA 92093-0244, USA*

<sup>b</sup> *Department of Geology, University of Maryland, College Park, MD 20742, USA*

<sup>c</sup> *Planetary Geosciences Institute, Department of Earth and Planetary Sciences, University of Tennessee, Knoxville, TN 37996, USA*

<sup>d</sup> *Geophysical Laboratory, Carnegie Institution of Washington, Washington, DC 20015-1305, USA*

<sup>e</sup> *Department of Earth and Space Sciences, University of Washington, Seattle, WA 98195, USA*

<sup>f</sup> *Planetary Science Institute, Tucson, AZ 85719, USA*

<sup>g</sup> *Royal Ontario Museum, Department of Natural History, Toronto, ON M5S 2C6, Canada*

Received 31 May 2011; accepted in revised form 13 December 2011; available online 20 December 2011

## Abstract

New major- and trace-element abundances, highly siderophile element (HSE: Os, Ir, Ru, Pt, Pd, Re) abundances, and oxygen and rhenium–osmium isotope data are reported for oligoclase-rich meteorites Graves Nunataks 06128 and 06129 (GRA 06128/9), six brachinites (Brachina; Elephant Moraine 99402/7; Northwest Africa (NWA) 1500; NWA 3151; NWA 4872; NWA 4882) and three olivine-rich achondrites, which are referred to here as brachinite-like achondrites (NWA 5400; NWA 6077; Zag (b)). GRA 06128/9 represent examples of felsic and highly-sodic melt products from an asteroid that may provide a differentiation complement to brachinites and/or brachinite-like achondrites. The new data, together with our petrological observations, are consistent with derivation of GRA 06128/9, brachinites and the three brachinite-like achondrites from nominally volatile-rich and oxidised ‘chondritic’ precursor sources within their respective parent bodies. Furthermore, the range of  $\Delta^{17}\text{O}$  values ( $\sim 0\text{‰}$  to  $-0.3\text{‰}$ ) among the meteorites indicates generation from isotopically heterogeneous sources that never completely melted, or isotopically homogenised.

It is possible to generate major- and trace-element compositions similar to brachinites and the three studied brachinite-like achondrites as residues of moderate degrees (13–30%) of partial melting of primitive chondritic sources. This process was coupled with inefficient removal of silica-saturated, high Fe/Mg felsic melts with compositions similar to GRA 06128/9. Melting of the parent bodies of GRA 06128/9, brachinites and brachinite-like achondrites halted well before extensive differentiation, possibly due to the exhaustion of the short-lived radionuclide  $^{26}\text{Al}$  by felsic melt segregation. This mechanism provides a potential explanation for the cessation of run-away melting in asteroids to preserve achondrites such as GRA 06128/9, brachinites, brachinite-like achondrites, acapulcoite-lodranites, ureilites and aubrites.

Moderate degrees of partial melting of chondritic material and generation of Fe–Ni–S-bearing melts are generally consistent with HSE abundances that are within factors of  $\sim 2\text{--}10 \times$  CI-chondrite abundances for GRA 06128/9, brachinites and the three brachinite-like achondrites. However, in detail, brachinite-like achondrites NWA 5400, NWA 6077 and Zag (b) are interpreted to have witnessed single-stage S-rich metal segregation, whereas HSE in GRA 06128/9 and brachinites have more

\* Corresponding author at: Scripps Institution of Oceanography, Geosciences Research Division, La Jolla, CA 92093-0244, USA. Tel.: +1 858 534 5431.

E-mail address: [jmdday@ucsd.edu](mailto:jmdday@ucsd.edu) (J.M.D. Day).

complex heritages. The HSE compositions of GRA 06128/9 and brachinites require either: (1) multiple phases in the residue (e.g., metal and sulphide); (2) fractionation after generation of an initial melt, again involving multiple phases; (3) fractional fusion, or; (4) a parent body with non-chondritic relative HSE abundances. Petrological and geochemical observations permit genetic links (i.e., same parent body) between GRA 06128/9 and brachinites and similar formation mechanisms for brachinites and brachinite-like achondrites.

© 2011 Elsevier Ltd. All rights reserved.

## 1. INTRODUCTION

The transformation of aggregates of nebular material into fully-fledged planets consisting of metallic Fe–Ni cores and silicate mantles and crusts represents a fundamental process. Refined understanding of the nature of this process will lead to improved models for metal–silicate equilibration, the evolution of silicate–magma oceans, hydrospheres and atmospheres, planetary habitability, and ultimately, form a template for understanding the genesis of extra-solar worlds. Planetary differentiation processes recorded in asteroidal meteorites offer complementary information to studies of igneous rocks from larger planetary bodies. Some asteroidal achondrites are believed to be derived from partially melted bodies. They offer valuable insights to the earliest stages of planetary differentiation, as they provide snap-shots of limited melting and melt segregation in asteroids. Such meteorites, commonly referred to as ‘primitive’ achondrites (c.f., Prinz et al., 1980, 1983), are typically characterised by near-chondritic bulk compositions and mineral assemblages. Texturally, these rocks range from metamorphosed- and anatectic-chondritic materials, such as winonaites (Benedix et al., 1998) and acapulcoites (e.g., Mittlefehldt et al., 1996), to lithologies that have witnessed variable degrees of partial melting, melt extraction, or are themselves partial melt products, such as lodranites (e.g., Mittlefehldt et al., 1996; McCoy et al., 1997), ureilites (e.g., Warren et al., 2006; Goodrich et al., 2007), brachinites (e.g., Mittlefehldt et al., 2003), and silicate inclusions within IAB and IIICD iron meteorites (e.g., McCoy et al., 1993; Choi et al., 1995).

A new class of partially melted achondrite was recently recognised; the paired, oligoclase-rich achondrite meteorites Graves Nunataks 06128 and 06129 (GRA 06128/9). These distinctly ‘non-primitive’ achondrites are probably related to partially melted (‘primitive’) achondrites, and provide new insights into partial melting processes within volatile-rich, and relatively oxidised asteroid parent bodies in the early Solar System (Day et al., 2009a,b; Shearer et al., 2010). It has been suggested that GRA 06128/9 may be related to brachinites (Zeigler et al., 2008), and this link has been explored through petrological and geochemical observations (Day et al., 2009a,b). It has also been argued that melting processes responsible for the GRA 06128/9 meteorites may be similar to those that produced minor Na-plagioclase-rich components preserved in some chondrites, ureilites, winonaites and silicate inclusions in IAB iron meteorites (Arai et al., 2008; Shearer et al., 2010).

Here we consider the origins of GRA 06128/9, brachinites, and brachinite-like achondrites, collectively, and whether they can be associated through genetic- (i.e., same

parent body) or process-related links (i.e., different parent bodies, but similar formation and differentiation processes). We define brachinite-like ultramafic achondrite meteorites as being like brachinites with respect to having compositions dominated by olivine with subsidiary augite, and having  $\Delta^{17}\text{O}$  values that are similar to brachinites and between  $\sim 0\text{‰}$  and  $-0.3\text{‰}$  (relative to the terrestrial fraction line of  $\lambda = 0.526$ ; Rumble et al., 2007). In contrast to brachinites, however, brachinite-like achondrites have more magnesian compositions for their silicates (i.e., olivine), and can contain orthopyroxene. We provide updated petrology, as well as new mineral and whole-rock trace-element abundances, including highly siderophile element (HSE: Os, Ir, Ru, Pt, Pd, Re) abundances, as well as Os and O isotope data for GRA 06128/9, six brachinites (Brachina; Elephant Moraine [EET] 99402/7; Northwest Africa [NWA] 1500; NWA 3151; NWA 4872; NWA 4882), and three brachinite-like achondrites (NWA 5400; NWA 6077; Zag (b)). The Re–Os isotopic data and HSE abundances were especially targeted in order to gain a better understanding of the silicate–sulphide–metal segregation processes that acted on partially-melted asteroidal bodies (e.g., Rankenburg et al., 2008; Walker et al., 2008; Day et al., 2009a).

## 2. SAMPLES AND ANALYTICAL METHODS

### 2.1. Samples

Macroscopic observations and general details of GRA 06128, GRA 06129, brachinites Brachina, EETA 99402, EETA 99407, NWA 1500, NWA 3151, NWA 4872, NWA 4882, and brachinite-like achondrites NWA 5400, NWA 6077 and Zag (b) are provided in the [Online annex](#) accompanying this article.

### 2.2. Petrography and electron microprobe analysis

Mineral modes in three polished sections (GRA 06128, 42; GRA 06128, 51; and GRA 06129, 22) were determined using the Feature-Scan Phase Distribution software package of an Oxford instrument energy dispersive spectrometer interfaced to a *Cameca SX 50* electron microprobe (EMP) at the University of Tennessee (Taylor et al., 1996). All other polished section modes were measured using thresholds for individual minerals, calculated according to analysed mineral compositions and then quantitatively analysed using *Image J* image analysis software with uncertainties of better than  $\pm 5\%$  (Day et al., 2006a). Major- and minor-element analyses were performed on four sections of the GRA 06128/9 meteorites using the *Cameca SX 50* EMP at the University of Tennessee. Mineral compositions were

determined in wave-length dispersive spectral mode using an accelerating potential of 15 keV, a 20 nA beam current, with beam focus of 1  $\mu\text{m}$ . Peak and background counting times of 20–30 s and standard PAP correction procedures were used. Glass and plagioclase compositions were determined using a 10 nA beam current, a 5–10  $\mu\text{m}$  beam size, and longer counting times to avoid mobilisation of Na, K, or Cl. Natural and synthetic standards were used for calibration and measured periodically within analytical sessions to ensure optimum data quality. Detection limits ( $3\sigma$  above background) were  $<0.03$  wt.% for  $\text{SiO}_2$ ,  $\text{TiO}_2$ ,  $\text{Al}_2\text{O}_3$ ,  $\text{MgO}$ ,  $\text{CaO}$ ,  $\text{Na}_2\text{O}$  and  $\text{K}_2\text{O}$ ,  $<0.05$  wt.% for  $\text{Cr}_2\text{O}_3$ ,  $\text{MnO}$ ,  $\text{FeO}$ ,  $\text{P}_2\text{O}_5$ , and  $<0.05$ – $0.1$  wt.% for all other elements listed (e.g., Day et al., 2006b).

For NWA 5400 and EET 99402, petrography and mineralogy were performed at the University of Maryland. Major- and minor-element analyses of sulphides and metals were performed using a *JEOL JXA-8900* EMP. Mineral compositions were determined in wave-length dispersive spectral mode using an accelerating potential of 15 keV, a 20 nA beam current, with a 1  $\mu\text{m}$  beam focus. Peak and background counting times of 20–30 s and standard ZAF (PAP) correction procedures were used. Natural and synthetic standards were used for calibration, and were measured periodically within analytical sessions. Detection limits ( $3\sigma$  above background) were  $<0.03$  wt.%.

### 2.3. Laser ablation ICP-MS analysis

Concentrations of minor- and trace-elements in minerals from NWA 5400, EET 99402, 47, GRA 06128, 51 and GRA 06129, 25 polished sections were determined using a *New Wave Research UP213* (213 nm) laser-ablation system coupled to a *Thermo-Finnigan Element 2* inductively coupled plasma-mass spectrometer (ICP-MS) at the University of Maryland. Olivine, pyroxene, plagioclase, phosphate, chromite, ilmenite, metal and sulphide were analysed using individual spots with a 15–80  $\mu\text{m}$ -diameter, a laser repetition rate of 7 Hz and a photon fluence of 2–2.5  $\text{J}/\text{cm}^2$ . Th/ThO production was between 0.06% and 0.07% for analytical sessions. Ablation analysis took place in a 3  $\text{cm}^3$  ablation cell. The cell was flushed with a He gas flow of 1 L/min to enhance production and transport of fine aerosols, and was mixed with an Ar carrier gas flow of 0.4 L/min before reaching the torch. Each analysis consisted of  $\sim 60$  s data collection. Backgrounds on the sample gas were collected for  $\sim 20$  s followed by  $\sim 40$  s of laser ablation. Washout time between spots was  $>120$  s. Data were collected in time-resolved mode so effects of inclusions, mineral zoning, and possible penetration of the laser beam to underlying phases could be evaluated. Plots of counts per second versus time were examined for each analysis, and integration intervals for the gas background and the sample analysis were selected using LAM-TRACE software. Each LA-ICP-MS analysis was normalised to values of CaO (silicates and phosphates), FeO (oxides), and Fe (metals and sulphides) measured by EMP. LA-ICP-MS time-resolved patterns showed that the ablated volumes were generally homogeneous. Replicate LA-ICP-MS analyses of the BIR-2 g glass standard, run twice at the beginning and

end of analytical sessions for 8–12 unknowns, yielded an external precision of better than  $\pm 5\%$  ( $2\sigma$  relative standard deviation) for all measured trace- and major-element compositions in silicates and phosphates. Replicate LA-ICP-MS analyses of the JBS sulphide standard, run twice at the beginning and end of analysis of 4–12 unknowns of metals, oxides and sulphides, yielded external precision of better than  $\pm 4\%$  ( $2\sigma$  relative standard deviation) for the HSE, Mo and W.

### 2.4. Whole-rock major- and trace-element abundance analysis

Major-element analyses of GRA 06128/9 are reported in Day et al. (2009a). Trace-element analyses of whole-rock powders were performed by solution ICP-MS techniques at the University of Maryland. Prior to disaggregation, exterior surfaces exposed to sawing or splitting implements were thoroughly buffed with carborundum, and samples were then washed with high purity water. Sample powders were prepared in a dust-free environment using an agate mortar and pestle dedicated to processing brachinite-like samples. The mortar and pestle were leached for  $>48$  h using  $\sim 0.5$  M HCl, abraded with pure-silica powder and washed with ultra-pure water and dried between uses. Qualitative analysis (count rates versus pure 0.8 M  $\text{HNO}_3$  diluent and a 1 ppb multi-element standard) of leachate from the mortar and pestle shows negligible minor or trace-element concentrations, implying no cross-contamination to samples during disaggregation. Sample aliquants were ground to fine powders, with some samples requiring greater crushing force than others.

For trace-element analysis, 30–50 mg aliquots of well-homogenised powder were digested in a 4:1 mixture of concentrated Teflon-distilled (TD) HF and  $\text{HNO}_3$  inside Teflon Parr bombs at  $>180$   $^\circ\text{C}$  for  $>72$  h in an oven. Digestion vessels were then allowed to cool, were uncapped, and solutions were taken to incipient dryness. Residues were repeatedly taken into solution with concentrated TD  $\text{HNO}_3$  and dried down to remove any residual fluorides. Samples were doped with indium for internal normalisation and drift correction, and diluted by a factor of 2500 in 3% TD  $\text{HNO}_3$ . International standards BCR-1, BIR-1, BHVO-2 and PCC-1 were prepared using the same procedure as samples and include basaltic and dunitic standards for matrix matching. Solutions were measured using the *Element 2* ICP-MS. Samples were introduced using a cyclonic spray chamber with oxide production  $\sim 3\%$ . Raw data were corrected offline for blank contributions (low [ $<0.1\%$  of measured concentration] and consistent), drift (negligible during analysis), and were calibrated and monitored relative to accepted values of international standards BHVO-2, BIR-2 and BCR-1 for accuracy. Reproducibility (as  $1\sigma$  relative standard deviation) was  $<4\%$  for most elements with the exception of Ti (4.7%), Mo (8.6%), Zn (20.4%) and Se (30.4%) for ‘unknown’ runs of USGS basalt standard BHVO-2, and  $<6\%$  for ‘unknown’ runs of USGS peridotite standard PCC-1.

Table 1

Modal mineralogy (% area) and summary of major-element mineral chemistry for GRA 06128/9 and some brachinites and brachinite-like achondrites.

Sample ID	GRA 06128, 42 <sup>a</sup>	GRA 06128, 51 <sup>a</sup>	GRA 06128 <sup>b</sup> , PC	GRA 06129, 22 <sup>a</sup> , EMM	GRA 06129, 23 <sup>c</sup> , DMM	GRA 06129, 24 <sup>d</sup> , PC	GRA 06128/9, Average <sup>2</sup>	Av. mineral chemistry <sup>3</sup>	NWA 5400 <sup>a</sup> , DMM	NWA 5400 <sup>c</sup> , PC	Av. mineral chemistry <sup>3</sup>	NWA 6077 <sup>e</sup>	Divnoe <sup>f</sup> , Zag (b) <sup>g</sup>	NWA 595 <sup>h</sup>	NWA 1500 <sup>i</sup>	Av. mineral chemistry <sup>3</sup>			
Plagioclase	78.5	71.1	90	74.1	81	82	79.5 ± 6.6	An <sub>14.6±0.4</sub>	Tr.	–	–	None-Present	1.5	–	–	1.0 ± 0.6	An <sub>27-38</sub>		
Olivine	8.4	14.2	4	9.0	8	9	8.8 ± 3.3	Fe <sub>39.9±0.4</sub>	80.6	79	Fe <sub>69.6-69.9</sub>	Fe <sub>69.3-69.8</sub>	74.6	68	82.5 ± 11	95.7 ± 0.6	Fe <sub>65-80</sub>		
Pyroxene	8.8	10.9	1	10.1	9	7	7.8 ± 3.6	–	16.4	19.4	–	–	14.3	18	17.5 ± 11	2.4 ± 0.6	–		
Orthopyroxene	4.0	4.0	–	5.0	–	1	3.5 ± 1.7	En <sub>52.9±0.3</sub> Wo <sub>2.3±0.1</sub>	Present	10.5	En <sub>73.5</sub> Wo <sub>2.1</sub>	En <sub>75.7</sub> Wo <sub>2.0</sub>	Present	8	6.5 ± 5.0	–	En <sub>70-81</sub> Wo <sub>0.5-3</sub>		
Clinopyroxene	4.8	7.0	–	5.1	–	6	5.7 ± 1.0	En <sub>37.7±0.4</sub> Wo <sub>42.4±0.8</sub>	Present	8.9	En <sub>45.5</sub> Wo <sub>45.1</sub>	En <sub>46.6</sub> Wo <sub>43.8</sub>	Present	10	11 ± 6	2.4 ± 0.6	En <sub>42-46</sub> Wo <sub>42-45</sub>		
Chromite	0.02	0.07	Tr.	0.10	Tr.	Tr.	0.06 ± 0.04	Cr# = 0.86	2.0	1.4	Cr# = 0.82	Present	Present	<1	Tr.	0.9 ± 0.5	Cr# = 0.75		
Sulphide/metal	0.24	0.25	Tr.	2.50	Tr.	Tr.	1 ± 1.3	–	1.0	–	–	Present	9.5	13.5	Tr.	Present	–		
Fe-sulphide	0.19	0.20	Tr.	2.30	Tr.	Tr.	0.9 ± 1.2	–	–	Tr.	–	Present	Present	12	Tr.	Present	–		
Pentlandite	0.05	0.05	Tr.	0.20	Tr.	Tr.	0.10 ± 0.09	<26 wt.% Ni	–	–	–	–	–	–	–	–	–		
Fe-Ni metal	Tr.	Tr.	Tr.	Tr.	Tr.	Tr.	Tr.	–	–	Tr.	Taenite	Present	Present	1.5	Tr.	Present	–		
Ilmenite	0.05	0.08	Tr.	0.10	Tr.	Tr.	0.08 ± 0.03	–	–	–	–	–	–	–	–	–	–		
Phosphates	3.64	2.87	5	2.50	0.5	1	2.6 ± 1.7	–	<0.1	Tr.	–	Present	Present	<1	–	Present	–		
Cl-rich apatite	1.63	1.54	–	1.80	–	–	1.7 ± 0.1	3.3–5.5 wt.% Cl	<0.1	Tr.	–	Present	–	–	–	Present	3.6–5.2wt.% Cl		
Na-merrillite	2.01	1.33	–	0.70	–	–	1.3 ± 0.7	2.2–2.5 wt.% Na <sub>2</sub> O	–	–	–	–	–	–	–	–	–		
Alteration	0.40	0.45	Present	1.60	Present	Present	0.8 ± 0.7	–	Present	Present	–	Present	–	Present	–	–	–		
Total	100	100	100	100	99	99	–	–	100	100	–	–	98	100	100	100	–		
Sample ID	Brachina <sup>j</sup> , ALH 84025 <sup>k</sup> , PC	ALH 84025 <sup>k</sup> , PC	ALH 84025, 6 <sup>l</sup> , EMM	ALH 84025, 26 <sup>l</sup> , EMM	Eagles Nest <sup>m</sup> , PC	EET 99402, EET 99402/7 <sup>l</sup> , EMM	EET 99402/7 <sup>l</sup> , Calculated PC	Hughes 026 <sup>k</sup> , PC	NWA 3151 <sup>n,h</sup> , PC	NWA 4872 <sup>n</sup> , PC	NWA 4882 <sup>n</sup> , PC	NWA 4969 <sup>n,h</sup> , PC	NWA 4874 <sup>h</sup> , PC	NWA 4876 <sup>h</sup> , PC	NWA 5191 <sup>h</sup> , PC	Brachinites	Av. mineral chemistry <sup>3</sup>		
Method <sup>1</sup>	PC	PC	PC	EMM	EMM	PC	EMM	Calculated PC	PC	PC	PC	PC	PC	PC	PC	Average <sup>2</sup>	Range	EMP	
Plagioclase	9.9	–	–	–	–	–	8.1	7.7	<0.1	Present	–	Present	2.5	2	2	–	8.6 ± 9	None-9.9	An <sub>14-40</sub>
Olivine	80.4	79	90.2	83.3	86.9	81	86	86.2	92.7	90	85	85 to 90	89	90	90	90	86 ± 10	79 to 95	Fe <sub>64-70</sub>
Pyroxene	5.5	15	4.2	9.4	6.4	6	5	4.4	5.2	Minor	3	Present	6	4	5	7	6.4 ± 3.4	4 to 20	–
Orthopyroxene	Tr.	–	–	–	–	–	–	–	1.6	Minor	–	–	None-Present	–	–	Minor	<1.6	0 to 15	Wo <sub>2-4</sub> En <sub>68-70</sub>
Clinopyroxene	5.5	15	4.2	9.4	6.4	6	5	4.4	3.6	Minor	3	Present	6	4	5	7	6.2 ± 3.6	3.6 to 15	Wo <sub>38-47</sub> En <sub>43-49</sub>
Chromite	0.5	2	0.8	0.84	0.57	<2	0.79	0.75	0.8	Present	5	Present	1.5	3	Present	1 to 2	1.3 ± 1.4	0.5 to 5	Cr# = 0.71–0.82
Sulphide/metal	3.2	3	4.6	6.36	6.06	7	0.11	1	<1.3	Present	4	Present	<1	1	<3	Minor	3.9 ± 2.3	0.1 to 6.4	–
Fe-sulphide	2.9	3	4	5.4	5.4	–	0.11	1	1.2	Present	2	Present	Present	–	Present	Minor	2.8 ± 1.9	0.1 to 5.4	–
Pentlandite	0.3	–	–	–	–	–	–	–	–	–	–	–	–	–	–	–	–	–	–
Fe-Ni metal	Tr.	<1	0.6	0.96	0.66	–	–	–	<0.1	Present	2	Present	Present	1	Present	Minor	<2	0 to 1	Taenite
Ilmenite	–	–	–	–	–	–	–	–	–	–	–	–	–	–	–	–	–	–	–
Phosphates	0.5	–	Tr.	0.16	Tr.	Tr.	Tr.	Tr.	0.1	–	3	–	–	1	–	–	<3	0 to 0.5	–
Cl-rich apatite	0.5	Tr.	Tr.	–	–	–	–	–	–	–	3	–	–	1	–	–	<3	–	–
Na-merrillite	–	–	–	–	–	–	–	–	–	–	–	–	–	–	–	–	–	–	–
Alteration	Present	–	–	–	–	5	–	–	Present	Present	Present	Present	Present	–	–	–	Absent-present	Absent-present	–
Total	100	100	100	100	100	99	100	100	100	90	100	100	100	100	100	100	–	–	–

References – <sup>a</sup>Data from this study or reported previously in Day et al. (2009a); <sup>b</sup>Zeigler et al. (2008); <sup>c</sup>Shearer et al. (2010); <sup>d</sup>Mikouchi and Miyamoto (2008); <sup>e</sup>Irving et al. (2009); <sup>f</sup>Petaev et al. (1994); <sup>g</sup>Delaney et al. (2000); <sup>h</sup>Goodrich et al. (2011); <sup>i</sup>Goodrich et al. (2006); <sup>j</sup>Nehru et al. (1983, 1996); <sup>k</sup>Warren and Kallemeyn, 1989 (ALH 84025, 7&12); ALH 84025, 1&5, reported in Warren and Kallemeyn, 1989; <sup>l</sup>Mittlefehldt et al. (2003); <sup>m</sup>Swindle et al. (1998); <sup>n</sup>Rumble et al. (2008); <sup>o</sup><http://www.lpi.usra.edu/meteor/>.

<sup>1</sup> EMM = Elemental mapping methods; PC = point counting; DMM = Digitised mapping methods; EMP = Electron microprobe analysis (WDS).

<sup>2</sup> All reported errors in the table are 1σ St.Dev.

<sup>3</sup> See text for details.

## 2.5. Rhenium–Os isotope and HSE abundance analysis

Osmium isotope and HSE abundance analyses were performed at the University of Maryland as described in Day et al. (2009a, 2010). Homogenised powder aliquots were digested in sealed borosilicate Carius tubes, with isotopically enriched multi-element spikes ( $^{99}\text{Ru}$ ,  $^{106}\text{Pd}$ ,  $^{185}\text{Re}$ ,  $^{190}\text{Os}$ ,  $^{191}\text{Ir}$ ,  $^{194}\text{Pt}$ ), and 6–9 mL of a 1:2 mixture of TD HCl and purged TD  $\text{HNO}_3$ . Samples were digested to a maximum temperature of 270 °C in an oven for 36–96 h. Osmium was triply extracted from the acid using  $\text{CCl}_4$  and then back-extracted into HBr, prior to purification by micro-distillation (Birck et al., 1997). Rhenium and the other HSE were recovered and purified from the residual solutions using standard anion exchange separation techniques. Isotopic compositions of Os were measured in negative-ion mode on a *ThermoFisher Triton* thermal ionisation mass spectrometer (N-TIMS) instrument for most samples, with the exception of Brachina, which was measured using an NBS-type N-TIMS. Rhenium, Pd, Pt, Ru and Ir were measured using an *Aridus* desolvating nebuliser coupled to an *Element 2* ICP-MS. Offline corrections for Os involved an oxide correction, an iterative fractionation correction using  $^{192}\text{Os}/^{188}\text{Os} = 3.08271$ , a  $^{190}\text{Os}$  spike subtraction, and finally, an Os blank subtraction. External precision for  $^{187}\text{Os}/^{188}\text{Os}$ , determined by repeated measurement of the UMCP *Johnson-Matthey* standard was better than  $\pm 2.1\%$  ( $2\sigma$ ;  $0.11372 \pm 23$ ;  $n = 25$ ). Duplicate measurements of unknowns were also in this range. Measured Re, Ir, Pt, Pd and Ru isotopic ratios for sample solutions were corrected for mass fractionation using the deviation of the standard average run on the day over the natural ratio for the element. External reproducibility on HSE analyses using the *Element 2* was better than 0.5% for 0.1 ppb solutions and 0.3% for 1 ppb solutions, and all reported values are blank corrected. Total procedural blanks ( $n = 7$ ) run with the samples had  $^{187}\text{Os}/^{188}\text{Os} = 0.156 \pm 0.053$ , with quantities (in picograms) of  $2.3 \pm 0.4$  [Re],  $9.9 \pm 12.2$  [Pd],  $5.8 \pm 6.6$  [Pt],  $6.1 \pm 1.9$  [Ru],  $1.7 \pm 0.9$  [Ir] and  $0.9 \pm 0.6$  [Os]. These blanks resulted in negligible corrections to samples.

## 2.6. Oxygen isotope analysis

Oxygen isotope analyses of EET 99402 were performed at the Geophysical Laboratory, Carnegie Institution of Washington as outlined in Day et al. (2009a). The rigorous cleaning procedure employed prior to fluorination removes terrestrial alteration, leaving fresh mineral grains. Data are reported as  $\delta^{18}\text{O}$  and  $\delta^{17}\text{O}$  notation ( $\delta^{\text{X}}\text{O}$  is the per mil [‰] deviation of  $^{\text{X}}\text{O}/^{16}\text{O}$  in  $n$  from the international standard [std] V-SMOW given by the relationship:  $\delta^{\text{X}}\text{O} = 1000 \times ((^{\text{X}}\text{O}/^{16}\text{O})_n / (^{\text{X}}\text{O}/^{16}\text{O})_{\text{std}} - 1)$ , where X is  $^{17}\text{O}$  or  $^{18}\text{O}$  and  $n$  denotes the unknown), and as  $\Delta^{17}\text{O}$  notation, which represents deviations from the terrestrial fractionation line ( $\lambda = 0.526$  (Rumble et al., 2007);  $\Delta^{17}\text{O} = 1000 \ln ((\delta^{17}\text{O}/1000) + 1) - 0.526 \times 1000 \ln ((\delta^{18}\text{O}/1000) + 1)$ ) (Miller, 2002). The value of 0.526 was obtained by linear regression of values for  $\delta^{17}\text{O}$  and  $\delta^{18}\text{O}$  of terrestrial silicate minerals (Rumble et al., 2007). As a monitor of external precision, analysis of aliquots of Gore Mountain garnet

(USNM 107144) were repeated every day during the course of the study. A value of 6.0‰ was measured in respect to UWG-2 (Valley et al. 1995; Rumble et al., 1997). The two sigma standard deviations of the Gore Mountain garnet analyses were  $\delta^{18}\text{O} = \pm 0.17$ ;  $\delta^{17}\text{O} = \pm 0.09$ ; and  $\Delta^{17}\text{O} = \pm 0.03$ .

## 3. RESULTS

Modal abundances and average mineral compositional data for GRA 06128/9, brachinites, and brachinite-like achondrites are presented in Table 1. Representative major-element data for minerals, either measured in this study, or compiled from literature sources are presented in Tables 2 and 3. Mineral trace-element data for GRA 06128/9, NWA 5400 and EET 99402/7 are presented in Table 4. Trace-element and HSE abundance data and Os and O isotope compositions are presented in Tables 5–7. Whole-rock major-element data are presented in the Online annex.

### 3.1. Petrography and major-element mineral chemistry

#### 3.1.1. GRA 06128 and GRA 06129

The GRA 06128/9 achondrites have a blocky or slab-like appearance, and a stratified fabric that has been partly attributed to intense parallel fracturing (Satterwhite and McBride, 2007; Treiman et al., 2008). This fabric is also related to mineral segregations, including mafic (olivine and pyroxene) bands, stringers and pods (Figs. 1 and 2a and b) set within a matrix of generally coarser-grained oligoclase grains. GRA 06128/9 are partially brecciated but represent a single lithology, with GRA 06129 appearing more intensely fractured than GRA 06128 (Fig. 2a and b). In unbrecciated regions, GRA 06128/9 have a granoblastic texture, and exhibit ranges in grain-size for the major silicate phases (<0.1 to >0.5 mm, diameter), and are partially to totally re-equilibrated, with no evidence for zoning.

GRA 06128/9 dominantly consist of oligoclase (area modal abundance = 71–90%; Table 1) with lesser orthopyroxene and clinopyroxene (<1–11%), olivine (4–14.2%), Chlorapatite and merrillite (0.5–5%), troilite and pentlandite (0.2–2.5%), and spinel and ilmenite (<0.2%); FeNi metal is a minor phase. In detail, GRA 06128, 42 and 51 contain more merrillite and less sulphide than GRA 06129, 22, consistent with mineralogical heterogeneity at cm-scales (e.g., Fig. 2). Alteration is pervasive and occurs as rusty regions on grain boundaries; gypsum as well as Fe-sulphates and Fe-oxides have been recognised in GRA 06128/9 (Arai et al., 2008; Liu et al., 2008; Treiman et al., 2008; Zeigler et al., 2008; Day et al., 2009a; Shearer et al., 2010). Shearer et al. (2010) identified three types of alteration and noted Fe-S-rich veins cross-cutting fusion crust in GRA 06128, demonstrating terrestrial alteration, as confirmed by terrestrial  $\Delta^{17}\text{O}$  values measured for unleached fragments of GRA 06128/9 (Satterwhite and McBride, 2007).

Major mineral phases display ranges in grain size. Large (up to 2 mm) subhedral plagioclase grains possess granoblastic textures with polysynthetic twinning. Transformation twinning (c.f., microcline) is observed in some plagioclase grains. Anhedral olivine grains (>1 mm long) have rims of

Table 2

Representative major element compositions (wt.%  $\pm 1\sigma$  standard deviation) of constituent minerals in GRA 06128/9.

Section	Plagioclase (79.5 $\pm$ 6.6 modal %)								Olivine (8.8 $\pm$ 3.3 modal %)								
	GRA 06128, 42		GRA 06128, 51		GRA 06129, 22		GRA 06129, 25		GRA 06128, 42		GRA 06128, 51		GRA 06129, 22		GRA 06129, 25		
n=	65		66		29		48		35		32		36		50		
SiO <sub>2</sub>	63.8	0.7	64.7	0.4	65.0	0.6	65.1	0.6	SiO <sub>2</sub>	32.8	0.3	33.0	0.2	33.6	0.3	33.9	0.4
Al <sub>2</sub> O <sub>3</sub>	20.8	0.3	21.3	0.2	21.6	0.2	21.5	0.3	TiO <sub>2</sub>	<0.03		<0.03		<0.03		<0.03	
MgO	<0.03		<0.03		<0.03		<0.03		Cr <sub>2</sub> O <sub>3</sub>	<0.03		<0.03		<0.03		<0.03	
CaO	2.84	0.21	2.66	0.11	3.09	0.09	3.07	0.10	MgO	17.3	0.2	17.7	0.2	18.1	0.2	18.0	0.3
FeO	0.20	0.34	0.10	0.14	0.10	0.11	0.11	0.12	CaO	0.10	0.04	0.10	0.02	0.11	0.02	0.09	0.02
Na <sub>2</sub> O	9.77	0.14	9.77	0.12	9.77	0.13	9.80	0.16	MnO	0.69	0.05	0.70	0.04	0.70	0.04	0.75	0.05
K <sub>2</sub> O	0.33	0.04	0.35	0.02	0.32	0.02	0.32	0.02	FeO	48.8	0.4	48.1	0.4	47.9	0.5	48.8	0.7
Total	97.8		98.8		99.9		99.9		NiO	–		–		–		0.06	0.03
An	13.6	1.0	12.8	0.5	14.6	0.4	14.5	0.4	Total	99.7		99.6		100.4		101.5	
Ab	84.5	0.9	85.2	0.5	83.6	0.4	83.7	0.4	Fo	38.8	0.3	39.6	0.4	40.2	0.3	39.6	0.3
Or	1.9	0.2	2.0	0.1	1.8	0.1	1.8	0.1									
Section	Clinopyroxene (5.7 $\pm$ 1.0 modal %)								Orthopyroxene (3.5 $\pm$ 1.7 modal %)								
	GRA 06128, 42		GRA 06128, 51		GRA 06129, 22		GRA 06129, 25		GRA 06128, 42		GRA 06128, 51		GRA 06129, 22		GRA 06129, 25		
n=	44		39		36		49		29		15		15		15		
SiO <sub>2</sub>	51.6	0.5	51.7	0.2	52.3	0.4	52.3	0.5	SiO <sub>2</sub>	51.0	0.5	51.0	0.2	52.1	0.3	52.0	0.4
TiO <sub>2</sub>	0.38	0.05	0.38	0.05	0.42	0.06	0.47	0.08	TiO <sub>2</sub>	0.17	0.03	0.17	0.02	0.16	0.01	0.18	0.06
Al <sub>2</sub> O <sub>3</sub>	0.42	0.03	0.43	0.03	0.45	0.05	0.49	0.07	Al <sub>2</sub> O <sub>3</sub>	0.17	0.02	0.19	0.05	0.19	0.04	0.18	0.02
Cr <sub>2</sub> O <sub>3</sub>	0.41	0.05	0.42	0.04	0.44	0.05	0.46	0.06	Cr <sub>2</sub> O <sub>3</sub>	0.08	0.03	0.09	0.03	0.10	0.02	0.10	0.04
MgO	12.9	0.1	13.1	0.2	13.1	0.2	12.8	0.2	MgO	17.9	0.1	18.2	0.2	18.4	0.1	18.1	0.3
CaO	20.3	0.6	20.4	0.5	20.1	0.6	20.2	0.9	CaO	1.08	0.05	1.12	0.06	1.11	0.03	1.32	0.72
MnO	0.31	0.04	0.31	0.04	0.32	0.04	0.34	0.04	MnO	0.60	0.05	0.60	0.03	0.59	0.03	0.63	0.04
FeO	12.5	0.7	12.1	0.4	12.2	0.6	12.6	0.8	FeO	28.4	0.4	27.9	0.3	27.7	0.3	27.8	0.8
Na <sub>2</sub> O	0.33	0.02	0.33	0.02	0.34	0.03	0.37	0.04	Na <sub>2</sub> O	0.02	0.01	0.01	0.01	0.01	0.01	0.01	0.01
Total	99.1		99.2		99.7		100.1		Total	99.4		99.2		100.3		100.3	
En	37.3	0.4	38.0	0.3	38.0	0.4	37.3	0.6	En	51.7	0.4	52.5	0.4	52.9	0.2	52.2	0.5
Fs	20.4	1.1	19.6	0.7	19.9	1.0	20.6	1.4	Fs	46.1	0.4	45.1	0.4	44.8	0.3	45.1	1.1
Wo	42.3	1.2	42.4	0.9	42.1	1.2	42.1	1.8	Wo	2.2	0.1	2.3	0.1	2.3	0.1	2.7	1.5
Section	Apatite (1.7 $\pm$ 0.1 modal %)						Merrillite (1.3 $\pm$ 0.7 modal %)										
	GRA 06128, 42		GRA 06128, 51		GRA 06129, 22		GRA 06128, 42		GRA 06128, 51		GRA 06129, 22						
n=	41		27		34		50		28		21						
P <sub>2</sub> O <sub>5</sub>	41.0	0.4	40.7	0.3	41.5	0.6	P <sub>2</sub> O <sub>5</sub>	45.6	0.3	45.2	0.4	45.9	0.5				
MgO	0.04	0.09	0.03	0.04	0.03	0.01	MgO	2.91	0.11	2.69	0.17	2.82	0.10				
CaO	53.5	0.3	53.5	0.2	54.2	0.5	CaO	46.7	0.4	46.8	0.2	47.2	0.6				
FeO	0.19	0.08	0.26	0.17	0.22	0.09	FeO	1.51	0.35	1.61	0.15	1.58	0.17				
Na <sub>2</sub> O	0.01	0.07	0.40	0.05	0.41	0.04	Na <sub>2</sub> O	2.00	0.08	2.38	0.08	2.38	0.06				
H <sub>2</sub> O	0.04	0.08	0.06	0.09	0.17	0.16	Total	98.7		98.7		99.9					
F	1.23	0.28	0.98	0.22	0.85	0.17											
Cl	4.69	0.43	4.88	0.32	4.67	0.60											
O = F	–0.52	0.12	–0.41	0.09	–0.36	0.07											
O = Cl	–1.06	0.10	–1.10	0.07	–1.05	0.13											
Total	99.1		99.2		100.6												
Section	Troilite (0.9 $\pm$ 1.2 modal %)						Pentlandite (0.10 $\pm$ 0.09 modal %)						Metal (trace %)				
	GRA 06128, 42		GRA 06128, 51		GRA 06129, 25		GRA 06128, 42		GRA 06128, 51		GRA 06129, 25		GRA 06128, 42				
n=	32		15		18		25		10		7		6				
Fe	61.7	0.6	61.9	0.7	63.3	1.4	Fe	38.5	2.3	38.0	0.9	41.2	3.3	Fe	26.3	1.4	
Ni	0.05	0.06	0.03	0.02	0.13	0.27	Ni	25.6	3.7	25.5	1.2	23.7	2.5	Ni	69.4	1.0	
Co	0.01	0.01	0.01	0.01	0.03	0.04	Co	1.10	0.90	2.51	0.29	1.69	0.96	Co	0.90	0.06	
S	36.6	0.5	36.1	0.5	36.4	0.8	S	32.7	1.9	32.7	0.4	32.9	0.7	S	1.98	2.46	
P	<0.03		<0.001	0.001			P	<0.03		<0.03				P	<0.03		
Si	0.04	0.04	0.01	0.01	0.06	0.05	Si	0.17	0.26	<0.03		0.06	0.06	Si	0.44	0.52	
Total	98.4		98.0		99.9		Total	98.1		98.8		99.6		Total	99.0		

(continued on next page)

Table 2 (continued)

Section	Ti-chromite (0.06 ± 0.04 modal %)								Ilmenite (0.08 ± 0.03 modal %)								
	GRA 06128, 42 n=	GRA 06128, 51 18	GRA 06129, 22 17	GRA 06129, 25 5	GRA 06128, 42 12	GRA 06128, 51 24	GRA 06129, 22 6	GRA 06129, 25 10	GRA 06128, 42 12	GRA 06128, 51 24	GRA 06129, 22 6	GRA 06129, 25 10	GRA 06129, 22 6	GRA 06129, 25 10			
SiO <sub>2</sub>	0.04	0.01	0.03	0.02	0.02	0.01	0.12	0.11	SiO <sub>2</sub>	0.03	0.02	0.06	0.13	0.03	0.01	0.19	0.14
TiO <sub>2</sub>	13.2	1.6	11.7	1.0	12.6	1.7	12.8	2.7	TiO <sub>2</sub>	49.3	7.8	51.5	1.5	52.8	0.6	53.9	0.7
Al <sub>2</sub> O <sub>3</sub>	2.98	0.28	4.09	0.48	4.04	0.46	3.86	0.90	Al <sub>2</sub> O <sub>3</sub>	0.26	0.57	0.15	0.33	0.29	0.05	0.09	0.06
V <sub>2</sub> O <sub>3</sub>	2.32	0.28	2.40	0.13	2.52	0.29			Cr <sub>2</sub> O <sub>3</sub>	3.29	7.63	0.48	1.09	0.02	0.01	0.24	0.05
Cr <sub>2</sub> O <sub>3</sub>	35.4	3.2	36.2	1.8	36.2	2.5	36.4	4.5	MgO	1.66	0.23	1.23	0.17	1.93	0.25	1.61	0.19
MgO	1.46	0.10	1.16	0.12	1.45	0.18	1.34	0.17	CaO	0.04	0.03	0.04	0.04	0.02	0.02	0.03	0.04
CaO	0.03	0.02	0.02	0.01	0.01	0.01	0.03	0.02	MnO	0.60	0.05	0.62	0.04	0.66	0.07	0.62	0.05
MnO	0.31	0.04	0.29	0.05	0.34	0.05	0.28	0.03	FeO	43.4	1.0	44.2	0.7	43.9	0.7	44.4	0.8
FeO	41.4	1.5	40.6	0.9	41.5	1.8	41.4	2.5	Fe <sub>2</sub> O <sub>3</sub>	0		0					
Fe <sub>2</sub> O <sub>3</sub>	1.31	0.05	1.45	0.03	1.30	0.06	1.74	0.11	Na <sub>2</sub> O							0.04	0.04
Total	98.4		97.9		99.9		98.1		Total	98.6		98.2		99.7		101.1	

clinopyroxene, orthopyroxene, and phosphates. Compositions of silicate minerals are extremely uniform (Fig. 3; Table 2); these grains display inter- and intra-grain homogeneity at all scales and in all sections studied. Plagioclase has the composition of oligoclase ( $\text{An}_{14.6 \pm 0.4} \text{Ab}_{83.6 \pm 0.4} \text{Or}_{1.8 \pm 0.1}$ ). Olivines have near-constant forsterite content ( $\text{Fo}_{39.9 \pm 0.4}$ ), relatively constant CaO ( $0.10 \pm 0.03\%$ ), Cr<sub>2</sub>O<sub>3</sub> ( $0.01 \pm 0.01\%$ ), and high MnO ( $0.71 \pm 0.05\%$ ) for all morphologies and sizes of grains measured. Orthopyroxenes are  $\text{En}_{52.9 \pm 0.3} \text{Wo}_{2.3 \pm 0.1}$  with Mg# of  $54.1 \pm 0.4$ ; and augites are  $\text{En}_{37.7 \pm 0.4} \text{Wo}_{42.4 \pm 0.8}$  with Mg# of  $65.5 \pm 1.1$ . Co-existing orthopyroxene and augite yield temperatures of between 670 °C (Shearer et al., 2010) and 810 °C (Liu et al., 2008; Day et al., 2009a). It is notable that the olivine in GRA 06128/9 is in chemical disequilibrium with both pyroxenes (Fig. 3), being more Fe-rich (predicted equilibrium composition =  $\text{Fo}_{50 \pm 5}$ ) than expected from the Mg–Fe exchange between these phases (von Seckendorf and O'Neill, 1993), possibly reflecting slow cooling, as inferred from thin (5 µm) exsolution lamellae observed in augite grains.

Large phosphate grains typically show intergrowths of chlorapatite and merrillite. These intergrowths have been interpreted to occur through merrillite replacement by chlorapatite (Treiman et al., 2008), as well as protection of merrillite from this process at grain boundaries (Shearer et al., 2010). A typical merrillite–apatite intergrowth assemblage is shown in Fig. 4. There is no obvious indication of protection or replacement, and the chlorapatite and merrillite appear to be inter-grown. Grains of chlorapatite can be quite large, with two subhedral grains in GRA 06128, 42 and 51 being up to 2 mm across (Fig. 2a), and are as large as 5 mm across in some sections (Zeigler et al., 2008). Apatite contains variable Cl ( $4.7 \pm 0.5 \text{ wt.}\%$ ) and the F concentrations vary from 0.5–1.9 wt.% (Av. =  $1.0 \pm 0.3\%$ ). Inter-grown merrillite contains 2.2–2.5 wt.% Na<sub>2</sub>O, which is higher than the Na contents present in lunar rocks and most martian meteorites, but similar to the composition of merrillite present in martian meteorite ALH 84001 and in some pallasites (Jolliff et al., 2006). The Mg# of merrillite varies from 68 to 82 – higher than for the Mg# of coexisting silicates.

Almost all large sulphide grains (10–60 µm) are intergrowths of pentlandite and troilite. Smaller pentlandite

and FeS droplets (~5 µm) are ubiquitously enclosed in silicate phases. Small FeNi metal grains (1–3 µm) are found associated with pentlandite as inclusions in silicate minerals. The composition of large sulphide grains is essentially FeS (troilite). Pentlandite lamellae ( $[\text{FeNi}]_9\text{S}_8$ ) in the large sulphide grains contain up to 26 wt.% Ni and 2.3–3.3 wt.% Co. Coexisting pentlandite and troilite reflect exsolution of pentlandite from a monosulphide solid solution at a temperature of ~865 °C, under a slow-cooling condition at a relatively high S fugacity (Taylor and Liu, 2009), indicative of a possible immiscible sulphide melt during crystallisation. The small pentlandite inclusions in silicate minerals contain low Co (0.5–0.6 wt.%), but otherwise are similar to pentlandite lamellae. FeNi metals associated with these pentlandite inclusions are of a composition near awaruite ( $\text{Ni}_3\text{Fe}$ ), with about 0.9 wt.% Co (Table 2). The association of pentlandite and FeNi metal suggests a melt with low S content (Craig and Kullerud, 1968) and implies inconsistency between the two sulphide (± metal) associations. Anhedral ilmenite and titaniferous chromite grains occur as individual grains or as intergrowths. Ilmenite contains 1–1.9 wt.% MgO. Titaniferous chromite contains up to 39.8 wt.% Cr<sub>2</sub>O<sub>3</sub> with 1.8–2.7 wt.% V<sub>2</sub>O<sub>3</sub> and Mg# of 4.5–6.7 and is compositionally homogeneous (Online annex). Chromite in the GRA 06128/9 samples contains between 0.5% and 2.7 wt.% Fe<sub>2</sub>O<sub>3</sub>.

### 3.1.2. Brachinites and brachinite-like achondrites

Since the identification of Brachina as an asteroidal achondrite (Nehru et al., 1983), the brachinite group has grown to become a small, but significant clan of achondrite meteorites. At the time of writing (2011), achondrites with brachinite affinities (i.e., rocks composed predominantly – 80% or greater – of modal olivine with  $\sim \text{Fo}_{64-71}$ , containing Ca-rich pyroxene, having limited ranges in mineral compositions, and having  $\Delta^{17}\text{O}$  ranging from 0‰ to  $-0.3\%$ ) include: Brachina (80% olivine,  $\text{Fo}_{70}$ ; Nehru et al., 1983); ALH 84025 (79–90% olivine,  $\text{Fo}_{67.7}$ ; Warren and Kallemeyn, 1989); Eagles Nest (81% olivine,  $\text{Fo}_{68}$ ; Swindle et al., 1998); Reid 013 (90–95% olivine,  $\text{Fo}_{66.8}$ ; also known as Nova 003, informally called Window Butte; Nehru et al., 1992, 1996; Goodrich et al., 2011); Hughes 026 (93%

Table 3

Representative major element compositions (wt.%  $\pm 1\sigma$  standard deviation) of constituent minerals in brachinites and brachinite-like achondrites.

		Olivine																
Section	Brachina	ALH 84025			EET 99402		EET 99407		NWA 595	Zag (b)	Divnoe	Divnoe	Divnoe	NWA 1500	NWA 5191			
n=	(N 83)	(WK 89)	5 (M 03)		6 (M 03)		5 (M 03)		22 (G 11)	(D 00)	(D 00)	81 (P 94)	37 (P 94)	3 (G 06)	22 (G 11)			
SiO <sub>2</sub>	37.2	36.9	37.1	0.1	36.8	0.2	36.6	0.1	37.4	0.1	38.3	36.9	37.4	38.0	36.8	0.1	36.8	0.1
Cr <sub>2</sub> O <sub>3</sub>			0.046	0.004	0.028	0.005	0.015	0.005	0.028	0.008	0.03	0.02	0.06	0.02	0.04	0.01	0.035	0.015
MgO	34.9	33.8	32.9	0.1	31.1	0.3	31.2	0.1	36.5	0.4	42.3	38.4	38.7	39.9	32.8	0.1	33.3	0.3
CaO	0.27	0.1	0.098	0.005	0.26	0.02	0.1	0.003	0.082	0.012	0.07	0.04	0.02	0.03	0.09	0.01	0.131	0.022
MnO	0.42	0.42	0.423	0.004	0.401	0.006	0.404	0.004	0.462	0.012	0.54	0.46	0.45	0.42	0.43	0.01	0.434	0.009
FeO	26.8	28.8	29.5	0.1	30.7	0.1	31.0	0.1	25.7	0.4	18.9	24.2	23.6	21.7	31.2	0.1	30.0	0.3
NiO	0.08		0.02	0.006			0.017	0.007										
Total	99.7	100.0	100.0		99.3		99.3		100.2		100.1	99.9	100.2	100.0	101.4		100.7	
Fo	69.8	67.7	66.5		64.4		64.2		71.7		80	73.9	74.5	76.67	65.2		66.4	
		Clinopyroxene																
Section	Brachina	ALH 84025			EET 99402		EET 99407		Zag (b)	Divnoe	Divnoe	NWA 1500	NWA 595	NWA 5191	Reid 013	Hughes 026		
n=	(N 83)	(WK 89)	5 (M 03)		5 (M 03)		5 (M 03)		(D 00)	(D 00)	(P 94)	(G 06)	14 (G 11)	84 (G 11)	6 (G 11)	8 (G 11)		
SiO <sub>2</sub>	53.3	53.4	53.2	0.1	52.9	0.2	53.1	0.2	53.7	52.4	52.9	53.5	53.1	53.4	53.8	53.5	53.6	
TiO <sub>2</sub>	0.32	0.17	0.16	0.01	0.13	0.01	0.14	0.01	0.28	0.09	0.18	0.15	0.12	0.14	0.09	0.12	0.14	
Al <sub>2</sub> O <sub>3</sub>	0.75	0.67	0.72	0.01	1.03	0.02	1.07	0.01	0.15	0.76	1.05	0.97	0.73	0.78	0.99	0.74	1.01	
Cr <sub>2</sub> O <sub>3</sub>	0.98	0.84	0.96	0.02	0.77	0.01	0.81	0.02	0.71	0.56	0.86	0.70	0.50	0.62	0.75	0.61	0.76	
MgO	16.5	16.0	15.9	0.1	15.2	0.1	15.4	0.1	15.7	16.2	17.2	15.6	15.8	16.1	15.3	15.7	15.2	
CaO	18.4	20.9	21.0	0.2	22.9	0.1	22.4	0.1	21.1	21.9	19.1	22.0	22.0	21.6	22.7	22.0	22.6	
MnO	0.30	0.23	0.22	0.01	0.15	0.01	0.16	0.01	0.26	0.25	0.24	0.18	0.16	0.20	0.15	0.18	0.16	
FeO	7.90	6.80	7.00	0.06	6.00	0.10	6.60	0.10	6.73	6.67	6.98	6.70	6.90	6.10	6.10	7.09	6.19	
Na <sub>2</sub> O	0.61	0.49	0.48	0.01	0.37	0.01	0.38	0.01		0.39	0.35	0.30	0.36		0.47	0.37	0.42	
Total	99.1	99.5	99.6		99.4		100.1		98.7	98.8	98.8	100.2	99.6	99.3	100.4	100.3	100.1	
En	48.3	45.9	45.5	25.3	43.4	26.0	43.8	19.0	45.4	45.3	49.3	44.3	44.5	45.9	43.7	44.1	43.5	
Fs	13.0	11.0	11.3	14.2	9.6	36.5	10.5	35.5	10.9	10.5	11.3	10.7	10.9	9.8	9.7	11.2	9.9	
Wo	38.7	43.1	43.2	60.6	47.0	37.4	45.7	45.5	43.7	44.2	39.4	45.0	44.6	44.4	46.7	44.6	46.5	
		Plagioclase						Orthopyroxene										
Section	Brachina	Brachina	EET 99402		Divnoe	NWA 1500		Brachina	Divnoe	Zag (b)	Zag (b)	NWA 595	NWA 595	NWA 1500	NWA 5191			
n=	(N 83)	(N 83)	5 (M 03)		47 (P 94)	(G 06)		(N 83)	(D 00)	(D 00)	(D 00)	12 (G 11)	5 (G 11)	80 (G 06)	17 (G 11)			
SiO <sub>2</sub>	62.5	68.7	57.2	0.2	59.8	58.3	61.6	SiO <sub>2</sub>	54.9	54.0	53.7	55.7	54.4	54.0	53.9	54.3	54.2	
Al <sub>2</sub> O <sub>3</sub>	23.2	22.9	27.2	0.1	26.3	26.4	24.3	TiO <sub>2</sub>	0.12	0.11	0.28	0.12	0.07	0.02	0.05	0.02	0.02	
MgO			0.03	0.01	0.01			Al <sub>2</sub> O <sub>3</sub>	0.40	0.45	0.11	0.04	0.40	0.04	0.33	0.04	0.11	
CaO	4.60	1.60	8.30	0.10	7.50	7.90	5.56	Cr <sub>2</sub> O <sub>3</sub>	0.38	0.17	0.18	0.35	0.22	0.07	0.16	0.08	0.13	
FeO			0.10	0.03	0.02	0.11	0.26	MgO	25.1	27.1	25.6	30.1	26.7	27.3	25.7	28.4	26.1	
Na <sub>2</sub> O	9.00	6.00	6.88	0.04	6.99	7.20	8.30	CaO	2.00	1.56	1.15	0.52	1.10	0.75	1.09	0.49	1.40	
K <sub>2</sub> O	0.26	1.37	0.04	0.01	0.09	0.03	0.11	MnO	0.42	0.45	0.42	0.49	0.40	0.44	0.39	0.47	0.40	
Total	99.6	100.6	99.8		100.7	99.9	100.1	FeO	16.3	14.7	16.3	11.9	16.2	17.1	18.3	16.2	17.9	
								Na <sub>2</sub> O	0.08				0.03	0.01	0.02	0.01	0.02	

(continued on next page)

Table 3 (continued)

Section <i>n</i> =	Plagioclase						Total	Orthopyroxene								
	Brachina (N 83)	Brachina (N 83)	EET 99402 5 (M 03)	Divnoe 47 (P 94)	NWA 1500 (G 06)			Brachina (N 83)	Divnoe (D 00)	Zag (b) (D 00)	Zag (b) (D 00)	NWA 595 12 (G 11)	NWA 595 5 (G 11)	NWA 1500 80 (G 06)	NWA 5191 17 (G 11)	
An	21.6	8.6	39.9	37.0	37.8	26.8	99.7	98.5	97.7	99.3	99.5	99.7	99.9	100.0	100.3	
Ab	76.9	80.2	59.9	62.4	62.1	73.7										
Or	1.5	11.2	0.2	0.5	0.1	0.5	En	70.3	74.3	71.9	81.0	73.0	72.9	69.9	75.0	70.3
							Fs	25.6	22.6	25.8	18.0	24.9	25.6	27.9	24.0	27.0
							Wo	4.0	3.1	2.3	1.0	2.2	1.4	2.1	0.9	2.7
Section <i>n</i> =	Sulphide						Total	Metal								
	NWA 5400 30		EET 99402, 47 14		NWA 1500 (G 06)			ALH 84025 5 (M 03)		NWA 5400 12		NWA 1500 17 (G 06)		ALH 84025 5 (M 03)		
Ni	0.59	0.88	0.12	0.19			0.39	0.04	Ni	18.9	0.6	1.3	0.2	29.7	0.1	
S	37.6	0.9	37.4	0.5	36.9		36.4	0.1	S	0.03	0.02	<0.03				
Fe	62.1	2.4	63.1	0.9	62.7		62.7	0.1	Fe	77.0	2.9	98.0	0.6	69.0	0.1	
Co	0.15	0.05	0.13	0.07			0.06	0.02	Co	1.45	0.04			1.58	0.01	
Cu	0.03	0.02	0.01	0.02					Cu	0.04	0.02					
Total	100.4		100.7		100.1		100.1			97.4		99.5		99.5		
Section <i>n</i> =	Chromite							Total	Phosphate							
	Brachina (N 83)	ALH 84025 8 (WK 89)	ALH 84025 9 (M 03)	EET 99402 6 (M 03)	EET 99407 7 (M 03)	Divnoe 64 (P 94)	NWA 1500 108 (G 06)		Brachina (N 83)	NWA 1500 (S 98)	Eagles Nest (G 06)	Divnoe 3 (P 94)				
SiO <sub>2</sub>	0.03	0.01	<0.01	<0.01	<0.01	0.04	0.03	P <sub>2</sub> O <sub>5</sub>	40.6	29.4	40.6	0.2	45.7			
TiO <sub>2</sub>	2.48	1.40	1.27	0.01	0.97	0.01	0.96	0.01	MgO	0.47	0.11	–	3.43			
Al <sub>2</sub> O <sub>3</sub>	7.30	7.60	7.52	0.07	13.69	0.06	13.40	0.10	CaO	52.3	0.4	54.2	0.1	46.7		
V <sub>2</sub> O <sub>3</sub>	0.54	<0.01	0.40	0.01	0.37	0.01	0.37	0.01	FeO	0.74	50.07	0.89	0.37	1.12		
Cr <sub>2</sub> O <sub>3</sub>	53.2	57.0	59.7	0.2	52.6	0.1	53.1	0.1	Na <sub>2</sub> O	0.74	1.56	0.27	0.06	2.53		
MgO	6.80	4.00	3.50	0.10	4.29	0.03	4.37	0.03	F	–	–	1.04	0.52	–		
CaO	–	<0.01	<0.01	<0.01	<0.01	<0.01	<0.01	0.01	Cl	5.50	–	4.40	1.13	–		
MnO	0.32	0.18	0.10	0.01	0.08	0.01	0.08	0.01	Total	100.4	81.6	101.3		99.5		
FeO	24.8	27.9	29.1	0.2	28.5	0.1	28.4	0.1								
Fe <sub>2</sub> O <sub>3</sub>	4.57	0.72	0	0	0	0	0	0								
Total	100.0	98.8	100.4		100.1		100.3									

Abbreviations = N 83; Nehru et al. (1983); WK 89; Warren and Kallemeyn, 1989; P 94; Petaev et al. (1994); S 98; Swindle et al. (1998); D 00; Delaney et al. (2000); M 03; Mittlefehldt et al. (2003); G 06; Goodrich et al. (2006); G 11; Goodrich et al. (2011).

Table 4

Representative mineral trace element data (in ppm) for Graves Nunataks 06128/9, NWA 5400 and EET 99402.

	Olivine				High-Ca pyroxene				Plagioclase			Cl-apatite			Merrillite		
	GRA 06128	GRA 06129	EET 99402	NWA 5400	GRA 06128	GRA 06129	EET 99402	NWA 5400	GRA 06129	EET 99402	NWA 5400	GRA 06128	GRA 06129	NWA 5400	GRA 06128	GRA 06129	NWA 5400
P	–	348	–	–	–	–	–	–	–	–	–	–	–	–	–	–	–
Sc	7.1	8.2	10.1	4.46	144	205	94	86	0.7	1.6	1.5	4.4	1.4	49.0	10.0	14.5	17.4
Ti	–	50.9	87.4	131.8	–	3137	1249	1897	470	114	–	–	–	–	–	–	–
V	26	13	23	22.3	847	798	375	398	0.6	5.3	–	–	–	–	–	–	–
Cr	121	30.8	320	499	3321	3372	4415	5859	<3.51	385	–	–	–	–	–	–	–
Mn	276	–	–	–	1352	2541	–	–	6.3	2.9	–	–	–	–	–	–	–
Co	–	238	–	–	–	–	–	–	–	–	–	–	–	–	–	–	–
Ni	–	542	–	–	–	–	–	–	–	–	–	–	–	–	–	–	–
Cu	–	3.0	–	–	–	–	–	–	–	–	–	–	–	–	–	–	–
Zn	–	57.1	–	–	–	–	–	–	–	–	–	–	–	–	–	–	–
Ga	0.48	0.58	0.9	<3.01	8.4	8.8	5.9	4.9	93.4	31.4	–	–	–	–	–	–	–
Ge	6.6	9.3	16.71	2	28.2	31.8	54.4	9.7	5.6	62.6	–	–	–	–	–	–	–
Rb	<0.9	–	<1.39	<0.53	<0.65	<0.44	<0.65	<0.39	3.6	<1.16	–	–	–	–	–	–	–
Sr	0.167	–	<84.63	<32.51	2.79	2.93	<30	<25	69.0	178	228	114	124	294	50	42	279
Y	0.116	–	<0.19	0.07	2.61	5.72	2.48	5.80	<0.1	0.126	0.970	9.8	5.7	16.5	218.8	338.6	83.5
Zr	3.393	–	<0.67	0.30	128.5	114.4	<0.26	2.087	0.100	<0.37	0.388	24.0	16.1	0.8	2.2	0.5	0.9
Nb	0.002	–	<0.20	0.003	0.048	<0.07	0.020	0.020	0.040	0.047	0.030	0.16	0.05	0.08	0.10	0.09	<0.1
Ba	<0.2	–	<2.65	0.84	<0.14	<0.32	<1.26	2.06	36.86	1.95	–	–	–	–	–	–	–
La	0.004	–	<0.13	<0.04	0.068	0.102	0.012	0.060	0.036	<0.15	0.594	5.26	4.47	3.83	39.85	60.41	26.60
Ce	0.013	–	0.005	0.011	0.254	0.468	0.074	0.319	0.071	0.030	1.833	10.26	9.35	12.59	95.64	150.80	66.30
Pr	0.002	–	<0.03	0.002	0.049	0.102	0.025	0.075	0.018	0.004	0.137	1.24	1.11	1.50	13.55	22.07	10.67
Nd	0.015	–	<0.30	0.009	0.327	0.702	0.203	0.595	0.117	0.027	0.794	5.30	4.84	8.57	66.94	116.70	54.36
Sm	0.009	–	<0.14	0.006	0.127	0.388	0.152	0.365	0.047	0.014	0.140	1.31	1.24	2.52	21.25	35.34	14.54
Eu	0.002	–	<0.25	<0.06	0.049	0.056	0.062	0.066	0.026	0.678	0.915	1.44	0.90	1.44	4.09	3.93	4.15
Gd	0.011	–	<0.31	<0.20	0.273	0.640	0.256	0.634	0.142	<0.46	<2.54	1.41	1.54	3.98	25.68	49.39	20.98
Tb	0.002	–	<0.09	0.001	0.069	0.140	0.064	0.122	0.024	0.017	0.019	0.29	0.22	0.59	5.31	8.84	2.99
Dy	0.024	–	0.008	0.007	0.528	1.046	0.418	0.943	0.142	0.012	0.465	1.74	1.28	3.98	36.16	59.45	17.90
Ho	0.006	–	0.001	0.003	0.120	0.252	0.101	0.226	0.032	0.003	0.038	0.35	0.25	0.76	7.79	12.62	3.68
Er	0.035	–	0.021	0.003	0.384	0.670	0.323	0.642	0.111	0.016	0.118	0.94	0.72	1.47	20.97	32.16	9.03
Tm	0.003	–	0.012	<0.02	0.059	0.108	0.053	0.096	0.025	0.003	0.038	0.14	0.07	0.19	2.81	3.93	1.38
Yb	0.035	–	0.062	0.032	0.491	0.752	0.421	0.696	0.155	0.005	0.090	0.99	0.45	1.06	18.92	23.75	8.54
Lu	0.004	–	<0.04	0.010	0.083	0.144	0.075	0.099	0.0001	0.004	0.019	0.14	0.06	0.13	2.58	3.16	1.05
Hf	0.249	–	0.013	0.014	5.42	4.04	0.004	0.079	0.010	0.023	<0.01	0.44	0.29	0.02	0.28	0.27	0.02
Ta	0.0002	–	<0.09	0.003	0.005	<0.04	<0.06	0.010	<0.04	<0.01	0.002	0.05	0.03	0.002	0.03	0.05	0.01
W	0.001	–	–	–	0.020	<2.55	–	–	0.005	–	–	–	–	–	–	–	–
Pb	0.010	–	<0.19	0.978	0.086	0.060	0.075	0.281	0.100	1.939	2.684	5.79	1.15	0.78	0.65	0.11	<0.47
Th	<0.01	–	<0.07	0.001	0.003	<0.03	0.001	0.004	<0.04	0.0005	0.050	4.19	1.24	0.23	3.08	0.93	0.29
U	0.0001	–	0.001	0.009	0.002	<0.03	0.0001	0.030	<0.01	0.083	0.172	2.61	0.51	0.17	0.28	0.04	0.49

Asteroid differentiation

Table 5

Whole-rock trace element data for GRA 06128/9, brachinites and brachinite-like achondrites.

ppm	GRA 06128, 22	GRA 06129, 9	EETA 99402, 44	Brachina 3151	NWA 4872	NWA 4882	NWA 1500	NWA 5400	NWA 6077	Zag (b)	BHVO-2 ( <i>n</i> = 5)		RSD %	BHVO- 2*	PCC1 ( <i>n</i> = 4)		RSD %	PCC1*	
Li	2.70	1.83	1.87	2.56	2.02	1.60	1.83	1.68	2.50	1.99	1.87	4.82	0.07	1.5	4.8	1.17	0.05	4.2	–
P <sub>2</sub> O <sub>5</sub>	2.560	3.074	0.097	0.301	0.097	0.065	0.096	0.078	0.179	0.067	0.274	0.004	1.6	0.27	0.046	0.001	2.4	–	
Sc	8.23	11.28	7.19	8.81	9.49	4.68	5.07	7.12	8.56	8.23	10.55	34.21	0.40	1.2	32	8.47	0.10	1.2	8.37
Ti	885.8	358.7	93.6	348.8	124.5	54.2	60.0	109.7	239.7	142.1	166.7	15472	727	4.7	16,00	23.0	1.1	4.9	–
V	91.7	47.7	67.7	79.6	118.1	55.2	77.1	78.0	109.7	72.7	100.1	325.9	8.8	2.7	317	35.4	0.9	2.5	25.7
Cr	978	265	3696	4040	7106	3293	4601	5071	6465	3432	5350	300	7	2.5	280	2750	59	2.1	–
MnO	0.179	0.108	0.327	0.327	0.417	0.392	0.354	0.385	0.370	0.359	0.380	0.164	0.006	3.5	0.17	0.108	0.006	5.4	–
FeO	17.5	11.9	26.8	25.7	37.6	33.0	30.3	30.8	25.2	26.9	26.9	11.2	0.4	3.3	11.4	7.1	0.3	4.6	–
Co	245	285	181	278	375	263	319	190	304	452	186	47.4	1.4	3.0	45	119	2	2.1	103
Ni	2105	3177	406	1758	1734	1312	1758	657	2848	4629	1519	127	2	1.6	119	2081	17	0.8	2171
Cu	38.9	30.7	4.0	31.2	34.1	11.9	18.3	4.4	17.8	31.1	19.1	141	4	2.5	127	7.7	0.2	2.7	6.7
Zn	22.0	17.4	11.5	182.0	204.6	33.7	41.2	209.9	62.4	30.8	16.7	115	24	20.4	103	29.6	1.8	6.0	–
Ga	40.0	46.4	3.81	7.85	3.49	1.82	2.13	2.72	2.56	1.22	2.12	22.1	0.3	1.6	22	0.68	0.02	3.1	–
Ge	3.86	3.38	6.85	10.80	12.09	6.90	6.79	1.89	11.82	10.39	17.88	1.61	0.02	1.3	1.6	1.04	0.05	4.4	–
Se	0.352	0.277	0.176	0.275	0.334	0.157	0.258	0.141	0.187	0.262	0.152	0.194	0.059	30.4	0.1	0.138	0.004	3.2	–
Rb	1.316	1.487	0.051	1.870	0.124	0.049	0.160	0.048	0.846	0.044	0.152	9.03	0.16	1.8	9.11	0.0731	0.0009	1.3	–
Sr	50.75	60.99	13.71	16.98	2.47	0.74	3.42	0.93	7.95	1.20	0.81	421.0	8.1	1.9	396	0.397	0.013	3.3	0.344
Y	6.405	9.572	0.152	1.817	0.156	0.052	0.097	0.175	0.584	0.472	0.472	30.1	0.6	2.0	26	0.088	0.003	2.9	0.082
Zr	5.692	7.276	0.557	6.450	0.245	0.132	0.274	0.171	0.946	2.949	0.846	188	4	2.3	172	0.308	0.016	5.3	0.14
Nb	0.423	0.154	0.012	0.170	0.022	0.012	0.019	0.011	0.116	0.019	0.049	19.6	0.7	3.7	18.1	0.0215	0.0012	5.6	0.02
Mo	2.176	1.627	0.559	1.011	1.219	0.512	1.025	0.185	1.204	1.109	0.691	3.996	0.344	8.6	4	0.421	0.015	3.5	–
Sn	0.459	0.319	0.333	1.396	1.045	1.817	0.758	0.155	2.918	0.385	0.399	1.719	0.046	2.7	1.7	1.206	0.059	4.9	–
Cs	0.021	0.033	0.003	0.134	0.005	0.002	0.008	0.003	0.133	0.004	0.013	0.1075	0.0035	3.3	0.1	0.0078	0.0002	2.4	–
Ba	22.5	24.1	0.36	86.6	1.29	0.68	36.6	2.7	37.2	0.11	0.27	129.9	3.0	2.3	131	0.8479	0.0083	1.0	0.79
La	1.379	1.704	0.0056	0.526	0.021	0.0046	0.0497	0.0084	0.202	0.028	0.009	16.5	0.4	2.4	15.2	0.0353	0.0018	5.0	0.0293
Ce	3.498	4.091	0.0153	1.240	0.047	0.0094	0.1022	0.0248	0.448	0.085	0.036	40.6	1.2	2.9	37.5	0.0669	0.0033	5.0	0.0547
Pr	0.511	0.631	0.0026	0.175	0.006	0.0012	0.0115	0.0044	0.056	0.015	0.008	5.59	0.16	2.9	5.35	0.0086	0.0003	3.3	0.00662
Nd	2.785	3.332	0.0200	0.891	0.032	0.0065	0.0611	0.0263	0.266	0.097	0.058	28.1	0.6	2.3	24.5	0.0358	0.0009	2.5	0.0255
Sm	0.799	0.954	0.0095	0.243	0.009	0.0020	0.0114	0.0105	0.071	0.038	0.027	6.62	0.11	1.7	6.07	0.0069	0.0002	2.5	0.00458
Eu	0.480	0.532	0.0579	0.103	0.004	0.0012	0.0075	0.0035	0.022	0.011	0.004	2.16	0.04	1.7	2.07	0.0013	0.0001	4.3	0.00079
Gd	1.042	1.242	0.0163	0.297	0.015	0.0024	0.0143	0.0185	0.090	0.056	0.046	6.79	0.17	2.5	6.24	0.0081	0.0002	2.0	0.00513
Tb	0.181	0.227	0.0033	0.050	0.003	0.0006	0.0020	0.0035	0.015	0.011	0.010	0.988	0.026	2.6	0.92	0.0014	0.0003	2.2	0.00101
Dy	1.220	1.603	0.0267	0.357	0.024	0.0059	0.0143	0.0274	0.108	0.081	0.079	5.756	0.098	1.7	5.31	0.0123	0.0004	3.1	0.00921
Ho	0.252	0.334	0.0069	0.077	0.006	0.0019	0.0036	0.0067	0.025	0.019	0.019	1.083	0.030	2.7	0.98	0.0036	0.00004	0.8	0.00256
Er	0.656	0.926	0.0242	0.226	0.024	0.0090	0.0146	0.0237	0.079	0.062	0.062	2.823	0.065	2.3	2.54	0.0151	0.0003	2.1	0.011
Tm	0.087	0.122	0.0048	0.035	0.005	0.0023	0.0030	0.0048	0.013	0.011	0.011	0.361	0.011	3.1	0.33	0.0032	0.00004	1.2	–
Yb	0.516	0.727	0.0444	0.237	0.046	0.0238	0.0295	0.0407	0.101	0.083	0.083	2.210	0.077	3.5	2	0.0296	0.0012	4.1	0.0214
Lu	0.071	0.100	0.0099	0.038	0.010	0.0057	0.0064	0.0082	0.018	0.015	0.015	0.306	0.007	2.2	0.274	0.0063	0.0003	4.9	0.00421
Hf	0.156	0.194	0.0161	0.193	0.007	0.0031	0.0078	0.0045	0.036	0.077	0.027	4.844	0.097	2.0	4.36	0.0104	0.0003	3.0	0.00379
Ta	0.034	0.015	0.0043	0.015	0.006	0.0031	0.0045	0.0022	0.015	0.005	0.006	1.201	0.028	2.3	1.14	0.0082	0.0001	0.8	–
W	0.329	0.255	0.0790	0.182	0.088	0.0373	0.0786	0.0713	1.467	0.512	0.165	0.273	0.008	3.1	0.21	0.0847	0.0035	4.1	–
Pb	0.196	0.192	0.0851	3.504	0.180	0.0853	0.3902	0.0281	3.041	0.075	0.130	1.846	0.045	2.4	1.6	12.18	0.18	1.4	–
Th	0.101	0.117	0.0013	0.128	0.005	0.0012	0.0059	0.0011	0.100	0.001	0.001	1.369	0.030	2.2	1.22	0.0150	0.0008	5.5	0.011
U	0.046	0.036	0.0021	0.036	0.009	0.0005	0.0182	0.0008	0.076	0.001	0.001	0.440	0.013	2.8	0.403	0.0060	0.0003	5.0	0.0042

Recommended values for reference materials USGS BHVO-2 (basalt, BHVO-2\*) and PCC1 (peridotite, PCC1\*) from Barrat et al. (2008) and references therein.

Table 6  
Highly siderophile element and osmium isotope data for GRA 06128/9, brachinites and brachinite-like achondrites.

Sample	Mass (g)	Os ng g <sup>-1</sup>	Ir ng g <sup>-1</sup>	Ru ng g <sup>-1</sup>	Pt ng g <sup>-1</sup>	Pd ng g <sup>-1</sup>	Re ng g <sup>-1</sup>	Re* ng g <sup>-1</sup>	Pd/Os	Pt/Os	<sup>187</sup> Os/ <sup>188</sup> Os ±2σ	<sup>187</sup> Re/ <sup>188</sup> Os ±2σ	<sup>187</sup> Re*/ <sup>188</sup> Os	<sup>187</sup> Os/ <sup>188</sup> Os <sub>i</sub>
<i>GRA 06128 and GRA 06129</i>														
GRA 06128, 22	0.208	175.1	78.58	301.4	125.9	53.55	16.06	16.01	0.31	0.72	0.13100	0.00009	0.442	0.0961
GRA 06128, 22	0.310	120.1	89.23	245.0	114.6	69.13	11.64	9.45	0.58	0.95	0.12614	0.00005	0.467	0.0893
GRA 06128, 22	0.491	148.2	90.88	326.9	112.3	46.05	12.23	12.23	0.31	0.76	0.12761	0.00007	0.398	0.0962
GRA 06129, 9	0.257	265.0	95.56	378.1	143.0	54.93	24.30	24.35	0.21	0.54	0.13117	0.00005	0.442	0.0963
GRA 06129, 9	0.087	197.7	103.4	388.6	131.5	56.64	19.67	17.07	0.29	0.67	0.12904	0.00008	0.479	0.0912
GRA 06129, 9	0.308	187.5	102.2	375.6	117.7	60.48	15.74	16.52	0.32	0.63	0.12973	0.00006	0.405	0.0978
GRA 06129, 9	0.548	155.8	101.5	337.7	123.9	54.60	13.37	13.17	0.35	0.80	0.12837	0.00005	0.414	0.0957
<i>Brachinites</i>														
Brachina	0.063	156.0	142.6	228.9	110.6	67.45	10.12	9.93	0.43	0.71	0.12041	0.00014	0.312	0.0958
EET 99402, 44	0.480	35.16	14.55	56.45	12.51	6.500	2.404	2.99	0.18	0.36	0.12851	0.00005	0.329	0.1025
NWA 1500	0.213	43.31	18.07	57.27	26.94	14.48	3.709	3.71	0.33	0.62	0.12877	0.00002	0.413	0.0962
NWA 4872	0.151	123.9	54.07	201.8	49.66	23.49	11.35	10.55	0.19	0.40	0.12861	0.00001	0.442	0.0938
NWA 4872	0.768	112.2	51.52	196.9	43.30	22.12	7.754	9.59	0.20	0.39	0.12874	0.00008	0.333	0.1024
NWA 4882	0.096	146.0	56.78	223.4	54.15	23.44	9.346	12.54	0.16	0.37	0.12887	0.00003	0.308	0.1045
NWA 4882	0.246	118.4	47.74	223.1	46.04	22.21	10.33	10.22	0.19	0.39	0.12905	0.00010	0.421	0.0958
NWA 3151	0.111	230.1	96.26	490.0	39.38	31.48	2.265	20.47	0.14	0.17	0.13005	0.00001	0.047	0.1263
NWA 3151	0.226	178.6	79.32	371.0	49.53	47.47	6.939	15.79	0.27	0.28	0.12985	0.00009	0.187	0.1151
<i>Brachinite-like achondrites</i>														
Zag (b)	0.129	98.27	88.83	173.9	245.7	89.49	9.175	7.57	0.91	2.50	0.12550	0.00002	0.450	0.0900
Zag (b)	0.123	285.1	315.8	573.6	730.5	135.5	27.07	23.86	0.48	2.56	0.12804	0.00008	0.458	0.0919
NWA 5400	0.073	2516	2093	2563	3069	159.8	59.91	201.1	0.06	1.22	0.12661	0.00005	0.115	0.1176
NWA 5400	0.053	2995	2568	2409	3467	175.7	71.52	238.6	0.06	1.16	0.12650	0.00005	0.115	0.1174
NWA 5400	0.065	2197	2299	2312	3093	173.9	60.17	177.2	0.08	1.41	0.12689	0.00006	0.132	0.1165
NWA 5400	0.064	2010	2057	2064	2886	139.5	57.63	163.7	0.07	1.44	0.12719	0.00006	0.138	0.1163
NWA 5400	0.068	2373	2333	2252	3273	159.8	61.61	188.6	0.07	1.38	0.12645	0.00006	0.125	0.1166
NWA 6077	0.176	289.3	252.5	486.2	547.4	227.4	29.91	24.31	0.79	1.89	0.12816	0.00001	0.498	0.0888
NWA 6077	0.173	528.6	469.3	859.1	1174	251.5	54.85	44.20	0.48	2.22	0.12801	0.00007	0.500	0.0885

Re\* is amount of rhenium calculated in the sample using the Os concentration and <sup>187</sup>Os/<sup>188</sup>Os value and assuming long-term chondritic Re/Os. <sup>187</sup>Os/<sup>188</sup>Os<sub>i</sub> calculated for 4.56 Ga.

Asteroid differentiation

Table 7  
Oxygen isotope data for GRA 06128/9, brachinites and brachinite-like achondrites.

Sample	$\delta^{17}\text{O}$	1 $\sigma$ stdev	$\delta^{18}\text{O}$	1 $\sigma$ stdev	$\Delta^{17}\text{O}^a$	1 $\sigma$ stdev	First reported <sup>b</sup>	Laboratory <sup>c</sup>
GRA 06128, 22	2.457		5.052		−0.201		Day et al. (2009a,b)	GL
GRA 06128, 22	2.330		4.822		−0.207		Day et al. (2009a,b)	GL
GRA 06128	2.447		5.047		−0.208		Zeigler et al. (2008)	GL
GRA 06128	2.179		4.552		−0.216		Zeigler et al. (2008)	GL
<i>Av. GRA 06128</i>	2.35	0.11	4.87	0.20	−0.208	0.005		
GRA 06129, 9	2.421		4.968		−0.193		Day et al., (2009a,b)	GL
GRA 06129, 9	2.334		4.777		−0.179		Day et al., (2009a,b)	GL
GRA 06129	2.820		5.740		−0.199		Shearer et al. (2010)	UNM
GRA 06129	2.880		5.920		−0.234		Shearer et al. (2010)	UNM
GRA 06129	2.850		5.830		−0.216		Shearer et al. (2010)	UNM
<i>Av. GRA 06129</i>	2.38	0.04	4.87	0.10	−0.186	0.007	( <i>Just GL</i> )	
NWA 5400	2.681		5.061		0.018		Shukolyukov et al. (2010)	GL
NWA 5400	2.741		5.223		−0.007		Shukolyukov et al. (2010)	GL
NWA 5400	2.446		4.683		−0.018		Shukolyukov et al. (2010)	GL
NWA 5400	2.632		4.953		0.026		Shukolyukov et al. (2010)	GL
<i>Av. NWA 5400</i>	2.63	0.11	4.98	0.20	0.005	0.018		
NWA 6077	2.667		5.180		−0.058		Rumble, unpublished	GL
NWA 6077	2.932		5.536		0.019		Rumble, unpublished	GL
<i>Av. NWA 6077</i>	2.80	0.13	5.36	0.18	−0.019	0.039		
EETA 99402	2.059		4.034		−0.064		This study	GL
	2.207		4.390		−0.103		This study	GL
	2.214		4.498		−0.153		This study	GL
	2.251		4.534		−0.135		This study	GL
<i>Av. EETA 99402</i>	2.18	0.07	4.36	0.20	−0.114	0.034		
Brachina	1.586		3.600		−0.308		Irving and Rumble, (2006)	GL
	1.380		3.210		−0.309		Irving and Rumble, (2006)	GL
<i>Av. Brachina</i>	1.48	0.10	3.41	0.20	−0.309	0.0005		
NWA 4872	2.061		4.354		−0.230		Rumble et al. (2008)	GL
	2.012		4.308		−0.255		Rumble et al. (2008)	GL
<i>Av. NWA 4872</i>	2.04	0.02	4.33	0.02	−0.242	0.012		
NWA 4882	2.064		4.368		−0.234		Rumble et al. (2008)	GL
	2.095		4.455		−0.249		Rumble et al. (2008)	GL
<i>Av. NWA 4882</i>	2.08	0.02	4.41	0.04	−0.242	0.007		
Divnoe	2.537		5.359		−0.282		Rumble et al. (2008)	GL
	2.523		5.369		−0.301		Rumble et al. (2008)	GL
	2.627		5.580		−0.308		Rumble et al. (2008)	GL
<i>Av. Divnoe</i>	2.56	0.05	5.44	0.10	−0.297	0.011		
Zag (b)	2.279		4.703		−0.195		Rumble et al. (2008)	GL
	2.135		4.410		−0.185		Rumble et al. (2008)	GL
<i>Av. Zag (b)</i>	2.21	0.07	4.56	0.15	−0.190	0.005		
NWA 595	2.604		5.187		−0.125		Rumble, unpublished	GL
	2.720		5.399		−0.120		Rumble, unpublished	GL
	2.356		4.769		−0.153		Rumble, unpublished	GL
	2.327		4.780		−0.188		Rumble, unpublished	GL
<i>Av. NWA 595</i>	2.50	0.17	5.03	0.27	−0.146	0.027		
NWA 3151	2.402		4.835		−0.142		Rumble, unpublished	GL
	2.416		4.924		−0.175		Rumble, unpublished	GL
	2.436		4.830		−0.105		Rumble, unpublished	GL
<i>Av. NWA 3151</i>	2.42	0.01	4.86	0.04	−0.141	0.028		

<sup>a</sup> Terrestrial fractionation line defined as  $\lambda = 0.526$ .

<sup>b</sup> Sources reported in the text.

<sup>c</sup> GL = Geophysical Laboratory, Carnegie Institution of Washington and using methods outlined here; UNM = University of New Mexico.

olivine, Fo<sub>66.2</sub>; informally called Australia 1; Nehru et al., 1996; Goodrich et al., 2011); Reid 027 (Grossman, 1998); EET 99402/7 (86% olivine, Fo<sub>66.4</sub>; Mittlefehldt et al., 2003); NWA 1500 (95–96% olivine, Fo<sub>65–73</sub>; Goodrich et al., 2011); NWA 3151 (Fo<sub>64.3</sub>; Irving et al., 2005); NWA 4042, NWA 4872, NWA 4874, NWA 4969, and

NWA 4882 (85–90% olivine, Fo<sub>64.9–65.9</sub>; Rumble et al., 2008); NWA 4876 (Connolly et al., 2008); NWA 5191 (90–95% olivine, Fo<sub>66.4</sub>; Goodrich et al., 2011).

Brachinite-like ultramafic achondrite meteorites are dominantly composed of olivine with subsidiary augite, and have  $\Delta^{17}\text{O}$  values between  $\sim 0\text{‰}$  and  $-0.3\text{‰}$ . However,

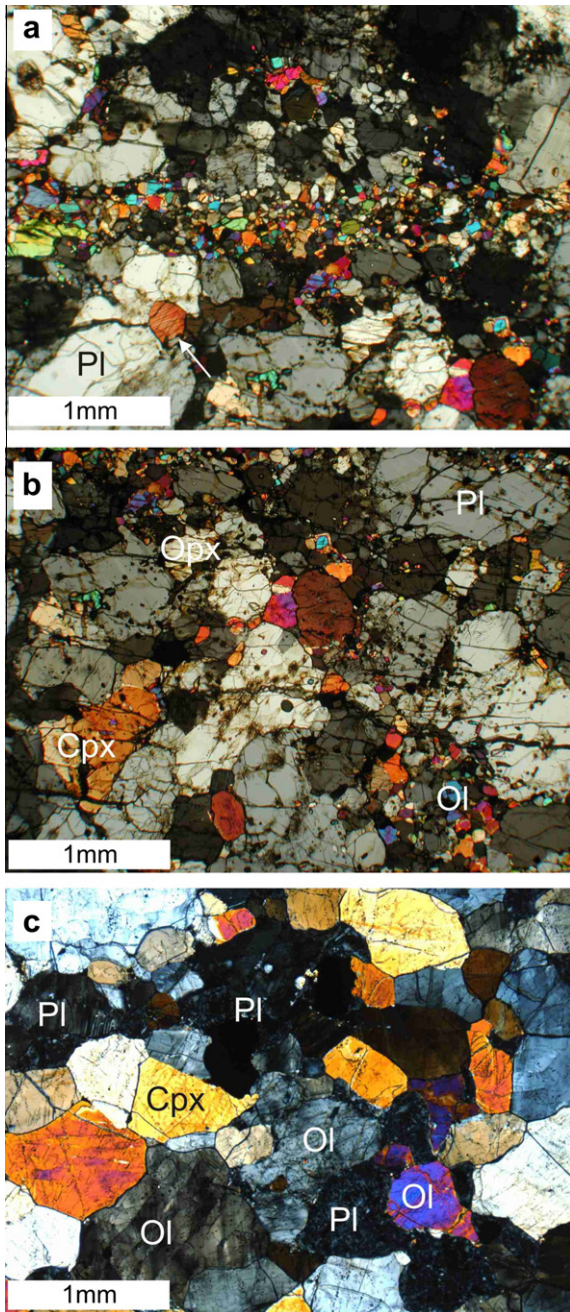


Fig. 1. Cross-polarised light photomicrographs of petrological features in the GRA 06128/9 and EET 99402/7 meteorites. Panel (a) illustrating a prominent  $\sim 0.5$  mm thick band composed predominantly of  $<0.1$  mm olivine and pyroxene crystals within coarser grained ( $0.5$ – $>1$  mm) oligoclase feldspar (Pl) in GRA 06128, 25. Note the presence of exsolution lamellae in some pyroxenes (arrow). (b) Prominent pods, typically of finer grained olivine (Ol) and pyroxene, occur within oligoclase feldspar in GRA 06128 and GRA 06129 (lower right hand corner of the image). Orthopyroxene (Opx) and clinopyroxene (Cpx) occur in approximately sub-equal proportions in GRA 06128/9. (c) EET 99402/7 is composed predominantly of fractured and unfractured (Ol) olivines with sub-ordinate clinopyroxene (Cpx). Plagioclase has been converted to a diaplectic glass (maskelynite).

these meteorites have more magnesian compositions for their silicates (i.e., olivine) than brachinites, and also contain orthopyroxene. Such meteorites include: NWA 595 (80% olivine,  $Fo_{71.7}$ ; Irving et al., 2005; Goodrich et al., 2011); Divnoe (75% olivine,  $Fo_{73.9}$ ; Petaev et al., 1994; Delaney et al., 2000); Zag (b) (68% olivine,  $Fo_{80}$ ; Delaney et al., 2000); NWA 5400 and NWA 6077 ( $Fo_{69.3-69.8}$ ; Table 1). Mineral grains in brachinites and brachinite-like achondrites are generally homogeneous (Table 3). Below we provide an updated petrology for brachinites and brachinite-like achondrites.

Brachinites and brachinite-like achondrites can broadly be defined as olivine-rich rocks (modal olivine – 68–95%; by terrestrial terminology, wehrlites and dunites; see Day et al., 2009c for discussion of terrestrial terminology for extra-terrestrial rocks), containing Ca-rich pyroxene (3.6–15%) and accessory phases of plagioclase, orthopyroxene, chromite, sulphide, metal and phosphates (Table 1). Some brachinite-like rocks, such as the poikilitic textured NWA 595, or Zag (b), can contain up to 15% orthopyroxene (e.g., harzburgite) (Delaney et al., 2000; Goodrich et al., 2011). The brachinites have been variously described as equigranular (Nehru et al., 1983, 1996; Warren and Kallemeyn, 1989), xenomorphic granular (Mittlefehldt et al., 2003), polygonal-granular (Irving et al., 2005), and proto-granular (e.g., NWA 5400; Irving et al., 2009). Olivine and clinopyroxene range considerably in grain size, from relatively fine-grained (0.1–0.3 mm, Brachina; Nehru et al., 1983), to medium-grained ( $\sim 0.7$  mm; Hughes 026, NWA 4874, NWA 4882; Nehru et al., 1996; Rumble et al., 2008), and to coarse-grained (up to 2.7 mm; ALH 84025; Warren and Kallemeyn, 1989), with some stones showing bimodal distribution of olivine (e.g., NWA 4872; 0.6 mm and 0.18 mm average grain sizes; Rumble et al., 2008; NWA 5400; 0.1–1.5 mm grain lengths; Irving et al., 2009; Weisberg et al., 2009; this study). Typically, samples with large olivine and Ca-rich pyroxene grains show bimodal grain size distributions (e.g., ALH 84025, average grain size 0.7 mm, grains up to 2.7 mm; EET 99402/7, 0.5–1.5 mm (Fig. 1c); NWA 4969 and NWA 4872; Warren and Kallemeyn, 1989; Mittlefehldt et al., 2003; Rumble et al., 2008). Grain sizes for accessory crystals (i.e., chromite, FeS, plagioclase) rarely exceed 0.7 mm (Warren and Kallemeyn, 1989; Swindle et al., 1998; Mittlefehldt et al., 2003), with the notable exception of troilite grains in ALH 84025 (up to 1.6 mm across; Warren and Kallemeyn, 1989) and plagioclase ‘clumps’ in EET 99402/7 (Fig. 2; up to 1.5 mm across).

Brachinites and brachinite-like achondrites often show variable distribution of rock-forming minerals, indicated by modal variations between sections (e.g., olivine and orthopyroxene in Zag (b); Delaney et al., 2000). In the case of the relatively coarse-grained sample NWA 5400, the rock is composed predominantly of olivine (79–80.5 vol.%) with subordinate pyroxene (16.4–19.4 vol.%; sub-equal proportions of orthopyroxene [50–54%] and clinopyroxene [46–50%]), chromite (1.4–2 vol.%), Cl-rich apatite, troilite ( $<0.3$  mm length), altered FeNi metal (as iron hydroxide), and fresh taenite ( $<0.2$  mm length) totalling no more than 1 vol.% of the sample (Table 1); the mineralogy of NWA 5400 is similar to that observed for NWA 6077, which also

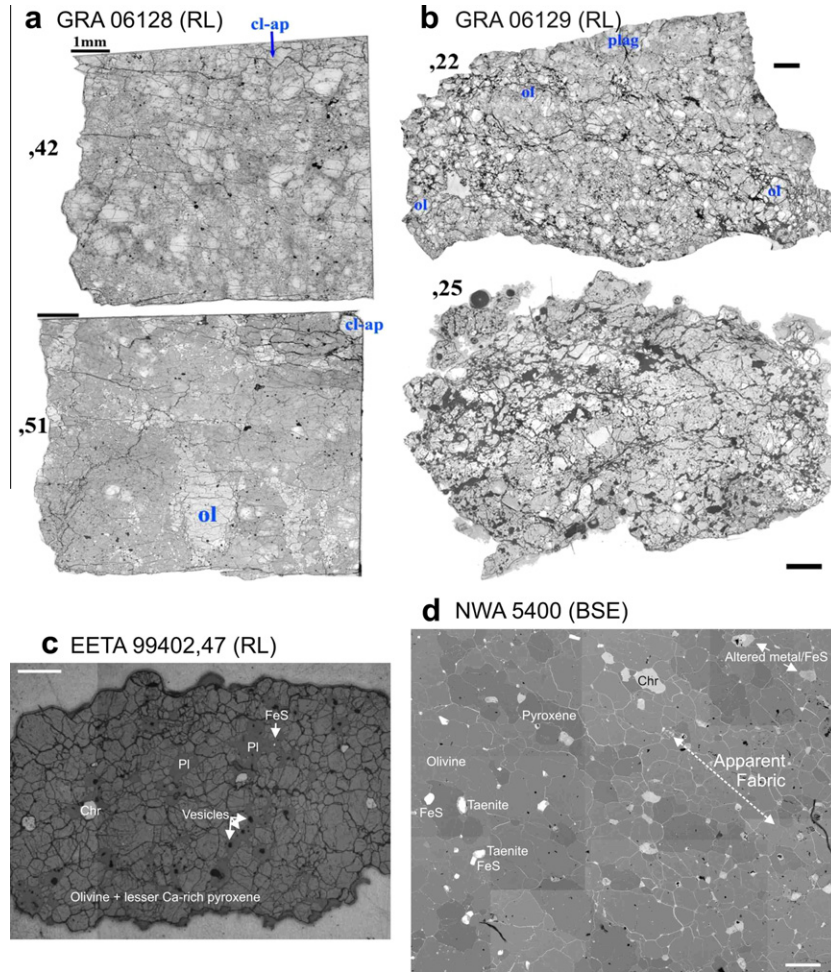


Fig. 2. Photo-mosaics of (a) GRA 06128 (.42 & .51) and (b) GRA 06129 (.22 & .25) polished sections described here, illustrating the distribution of minerals in the meteorites, and the differences in appearance of GRA 06128 and GRA 06129 polished sections. Also shown are (c) a composite reflected light (RL) image of the thick section of EET 99402, 47, and (d) composite back scattered electron (BSE) collage of NWA 5400. Note the apparent fabric preserved in NWA 5400 revealed by pyroxene, and the uneven preservation of taenite metals and FeS. Diaplectic plagioclase glass (PI) in EET 99402 contains vesicles associated with shock-melting of the plagioclase, and the meteorite appears to have been strongly deformed. Scale bars are 1 mm. Mineral abbreviations: cl-ap = Cl-rich apatite; ol = olivine; plag = plagioclase.

contains pyrrhotite (Table 1). There is a coarse fabric in NWA 5400, with partitioning of pyroxenes and the heterogeneous distribution of metal and sulphide grains (Fig. 2).

Olivine in brachinites show homogeneous compositions within each meteorite, with variations among meteorites spanning a range in Fe/Mg ( $Fe_{64-72}$ ; Tables 1 and 2). As noted above, some brachinite-like achondrite meteorites such as Zag (b), NWA 595 and Divnoe lie outside of this range at higher Mg/Fe for their olivine ( $Fe_{71-81}$ ; Delaney et al., 2000), possibly reflecting reduction of Fe-rich olivine in these stones. Preferred orientation of olivine grains has been observed for ALH 84025 (Warren and Kallemeyn, 1989) and EET 99402/7 (Mittlefehldt et al., 2003) suggesting that these rocks have witnessed only minor metamorphic equilibration. Petrofabric analysis of EET 99402/7 and ALH 84025 indicates lineations and probable foliations of olivine grains (Mittlefehldt et al., 2003). Other brachinites have equant olivine grains and  $120^\circ$  triple junctions between olivine grains, indicative of equilibration (Nehru

et al., 1983). Some olivines in brachinites contain small (10–25  $\mu\text{m}$ ), rounded, mono- to poly-mineralic inclusions of anorthoclase glass, phosphate, sulphide, chromite and FeNi-metal (e.g., Brachina and EET 99402/7; Nehru et al., 1983; Mittlefehldt et al., 2003); such inclusions in other brachinites are less abundant, or absent (e.g., ALH 84025; Warren and Kallemeyn, 1989). Olivine grains in NWA 5400 can contain small (typically <25  $\mu\text{m}$ ) inclusions of plagioclase, often associated with Cl-rich apatite. Olivine in NWA 5400 has an average composition of  $Fe_{69.8}$ , FeO/MnO up to 70.8, and has relatively high CaO contents (0.11 wt.%). Olivine in Zag (b) contains embedded micro-scale orthopyroxene ‘channels’, often containing Fe–Ni metal (Delaney et al., 2000).

Calcium-rich pyroxenes in brachinites show a restricted range in compositions, averaging to Mg-rich augite ( $Wo_{46.3}En_{43.4}Fs_{10.3}$ ). Ca-rich pyroxenes sometimes enclose small grains of olivine (Swindle et al., 1998) and can also include <15  $\mu\text{m}$  unidentified silicate, sulphide and opaque

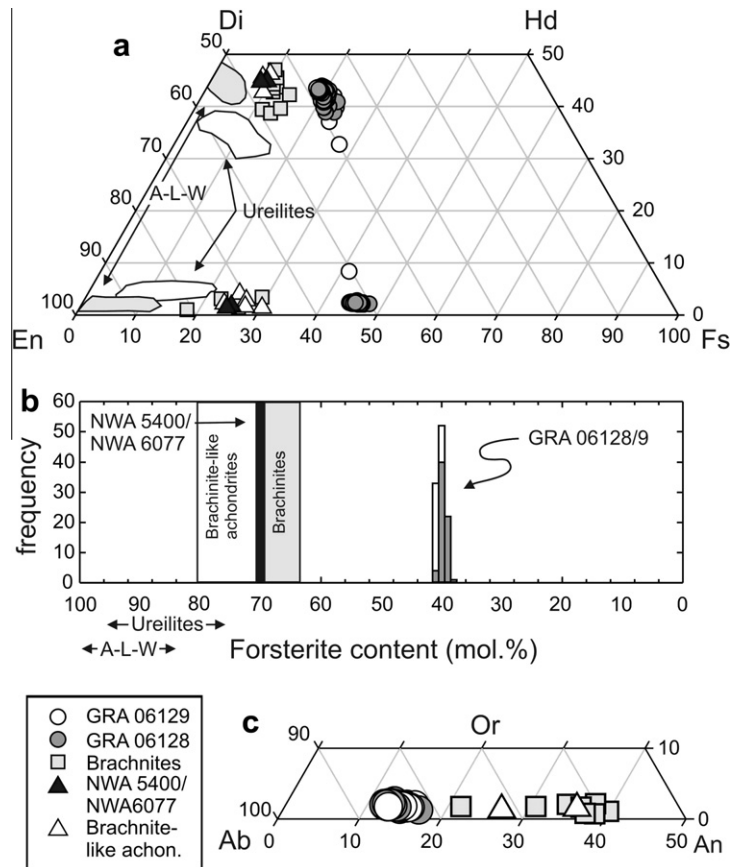


Fig. 3. Plots of compositional variations for major silicate mineral constituents in GRA 06128/9, brachinites and brachinite-like achondrites. (a) Quadrilateral plot for pyroxene compositions; (b) olivine forsterite content frequency plot for GRA 06128/9, and fields of data for brachinites, and brachinite-like achondrites; (c) ternary plot for plagioclase compositions. Fields for ureilites and acapulcoite–lodranite–winnonaites (A–L–W) from Goodrich et al. (2011).

inclusions (Mittlefehldt et al., 2003). Otherwise Ca-rich pyroxenes occur as interstitial grains between olivine in a number of brachinites (Tables 1 and 3). Low-Ca pyroxene also occurs as inclusions within Brachina (Nehru et al., 1983) and Hughes 026 (Nehru et al., 1996), or as fine-grained assemblages in brachinites (Goodrich et al., 2011). Brachinite-like achondrites, including NWA 595, Zag (b) and Divnoe all contain orthopyroxene grains, which, when coupled with more Mg-olivines, represent more reducing conditions for these meteorites compared with brachinites. The high-Ca pyroxene in NWA 5400 is diopside and the low-Ca pyroxene is Fe-rich enstatite (Table 1; Fig. 3). Two-pyroxene thermometry for brachinites indicates temperatures of 825–1070 °C, in close agreement with olivine-pyroxene (965–1246 °C) and olivine-chromite (800–1080 °C) thermometry (Nehru et al., 1996). Plagioclase is absent in the majority of brachinites and brachinite-like achondrites (Tables 1 and 3), but where it occurs it has a limited range in composition, being K-poor ( $Ab_{63.4}An_{36.3}Or_{0.3}$ ). Plagioclase grains in EET 99402/7 have been partially maskelynitised, devitrified and degassed (Mittlefehldt et al., 2003; this study, Fig. 2c), which probably explains observations that portions of these meteorites appear ‘melted together’ (McBride and McCoy, 2000; c.f., Fig. 2).

Chromite occurs interstitially and as inclusions in brachinites, and show two dominant chromite compositions, namely brachinites with low-Al chromites (Cr# = 82–84; Eagles Nest, ALH 84025) and those with higher Al compositions (Cr# = 71–74; EET 99402/7, Hughes 026, NWA brachinites). Chromite in NWA 5400 (Cr# = 82; ~1.4 wt.%  $TiO_2$ ; 0.3 wt.% ZnO) is similar in composition to that of low-Al chromites in brachinites (e.g., ALH 84025; Cr# = 84; ~1.3 wt.%  $TiO_2$ ; 0.4 wt.% ZnO). Chromites span a restricted range of compositions in Cr–2Ti–Al and Cr– $Fe^{2+}$ –Al space and typically have low  $Fe_2O_3$  (<0.7 wt.%, with the exception of Brachina ~4.5 wt.%), based on stoichiometry (Online annex).

Sulphide minerals occur dominantly as troilite, but minor pentlandite has been reported in some brachinites (e.g., Brachina; Nehru et al., 1983). Sulphides occur as (1) large (up to 1.6 mm across) grains in ALH 84025 (Warren and Kallemeyn, 1989), (2) interstitially and intergrown with minor pentlandite and Ni-rich metal in Brachina (Nehru et al., 1983), (3) inclusions within major silicate minerals in EET 99402/7 and ALH 84025 (Mittlefehldt et al., 2003), and (4) thin veins emanating from larger equant troilites (Warren and Kallemeyn, 1989). The major sulphide phase observed in NWA 5400 is troilite, but a Ni-rich

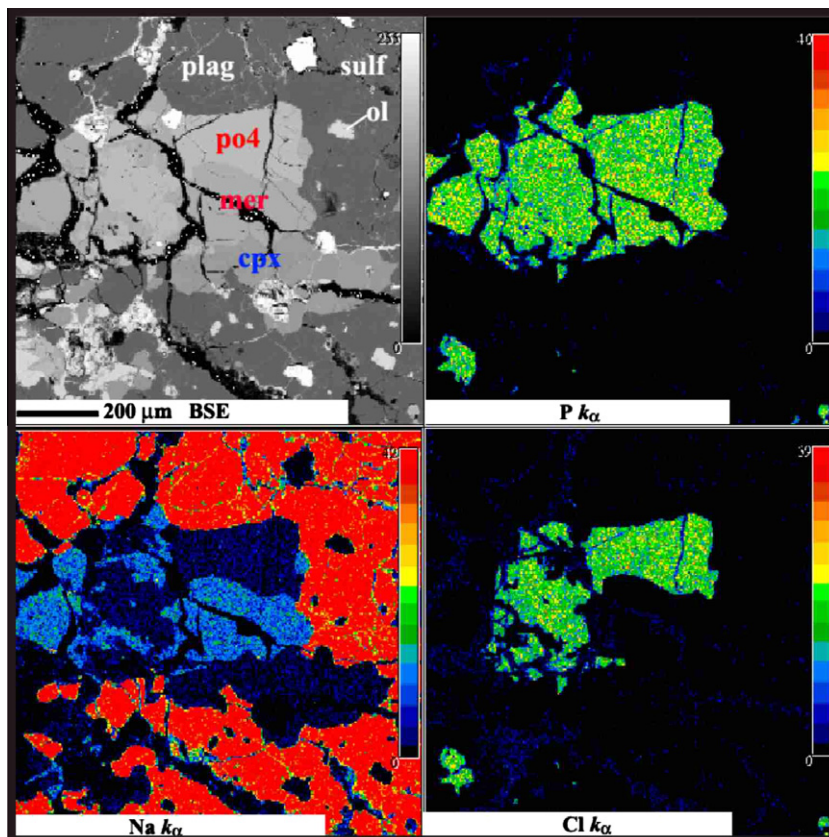


Fig. 4. Phosphate grain relations in GRA 06129. Back-scattered electron image (upper left panel), and phosphate (upper right panel), sodium (lower left panel) and chlorine (lower right panel) X-ray maps of merrillite and Cl-rich apatite grains enclosed within oligoclase and clinopyroxene.

(1.1–6.8 wt.%) ‘FeS’ phase, associated with altered metal grains, also occurs. Taenite, with a minor Co component ( $1.45 \pm 0.04$  wt.%), is the main metal phase in NWA 5400. Quantitative analyses of altered or semi-altered metal and sulphide grains gave low totals (<85%), so are not reported, but the metals are consistent with being either altered taenite or kamacite. No direct evidence for kamacite was observed, but Irving et al. (2009) reported altered metal was kamacite for the sample they studied; altered FeNi metal also occurs in NWA 6077 (Table 1).

Merrillite and Cl-rich apatite grains occur in both Hughes 026 (Nehru et al., 1996), and NWA 4872 (Rumble et al., 2008). Brachina contains Cl-rich apatite in inclusions within olivine (Nehru et al., 1983) and NWA 4874 also contains merrillite (Rumble et al., 2008). Chlorine-rich (up to 6 wt.%) apatite occurs as an accessory mineral between silicate grain boundaries, and within olivine in NWA 5400. As with GRA 06128/9, phosphates in brachinites and brachinite-like achondrites probably have a magmatic origin, but it is also likely they have been affected by sub-solidus processes (e.g., Day et al., 2009a).

Brachinites have been variably shocked. Nehru et al. (1983) reported no evidence of shock in Brachina, whereas EET 99402/7 contains both maskelynitised plagioclase and deformed olivine (Fig. 1c), suggesting a shock-stage of S3 (Mittlefehldt et al., 2003). Many brachinites have been

discovered in hot desert regions and show evidence of terrestrial weathering, including partial oxidation of metal, limonite on grain boundaries and Fe-enrichment in phosphates (e.g., Nehru et al., 1983; Swindle et al., 1998). Cold desert samples like EET 99402/7 and ALH 84025 are less altered (Mittlefehldt et al., 2003). Both NWA 5400 and NWA 6077 have experienced some minor terrestrial weathering, resulting in partial alteration of primary metals, as well as veining within fractures by calcite, clay minerals and iron hydroxides.

### 3.2. Mineral trace-element compositions

Representative trace element abundances of minerals measured by LA-ICP-MS for GRA 06128/9, EET 99402 and NWA 5400 are presented in Table 4, and represented diagrammatically in Fig. 5. Olivine and orthopyroxene in these meteorites have low rare earth element (REE) abundances ( $<1 \times$  CI-chondrite), with heavy REE (HREE)  $>$  light REE (LREE; La/Yb =  $<0.2$ ). Olivine from GRA 06129 measured by LA-ICP-MS yielded lower Ni (415–966 ppm) and Co (230–250 ppm) contents than those measured by ion microprobe (Ni = 1177–1584; Co = 500–592), but V (8–15 ppm) and Ti (44–65 ppm) contents are similar (V = 8–10 ppm; Ti = 75–95 ppm; Shearer et al., 2010), possibly indicating heterogeneous distribution of Ni and Co

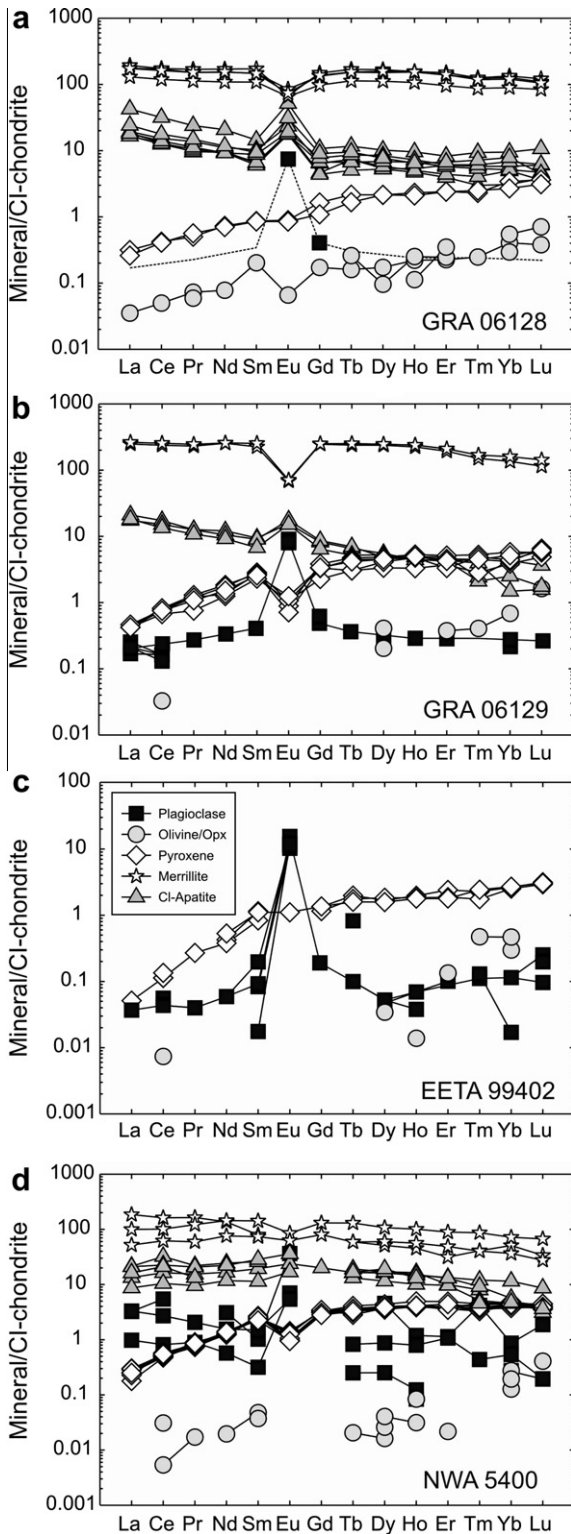


Fig. 5. CI-chondrite normalised rare earth element (+Lu) patterns for silicate and phosphate minerals in (a) GRA 06128, (b) GRA 06129, (c) EET 99402 and (d) NWA 5400 measured by laser ablation ICP-MS. Note differences in scale for figure panels. Total errors are equal to or smaller than symbols. CI-chondrite normalisation from McDonough and Sun (1995).

between samples. Plagioclase grains in GRA 06128/9, EET 99402 and NWA 5400 have similar REE abundances, with variable positive Eu anomalies ( $\text{Eu}/\text{Sm}_n = 22\text{--}250$ ; where  $n = \text{CI-chondrite normalised}$ ). We determined lower Ba (35–39 ppm) and Sr (68–73 ppm) concentrations in plagioclase from GRA 06129 relative to that measured by Shearer et al. (2010) (Ba = 77 ppm, Sr = 94.5 ppm). Strontium concentrations in plagioclases from EET 99402 (164–190 ppm) and NWA 5400 (87–312 ppm) are higher than for GRA 06128/9, and EET 99402 plagioclase have low Ba (<2 ppm).

High-Ca pyroxenes from GRA 06128/9, EET 99402 and NWA 5400 all exhibit convex-upward REE patterns, with increasing CI-chondrite normalised abundances from La to Sm (Fig. 5;  $\text{La}/\text{Sm}_n = 0.04\text{--}0.34$ ). High-Ca pyroxenes from GRA 06129 and NWA 5400 possess larger negative Eu anomalies ( $\text{Eu}^*$ ;  $\text{Eu}/((\text{Sm} \times \text{Gd})^{0.5})_n = 0.24\text{--}0.50$ ) than GRA 06128 ( $\text{Eu}^* = 0.8$ ) and EET 99402 ( $\text{Eu}^* = 0.9$ ). Indeed, GRA 06128 ( $\text{La}/\text{Yb}_n = 0.34$ ) shows subtle mineral major-element and trace-element composition, as well as petrological differences (Section 3.1.1), when compared with GRA 06129 ( $\text{La}/\text{Yb}_n = 0.17$ ). GRA 06128/9 high-Ca pyroxenes have higher Sc, Ti, V, Hf and lower Cr contents when compared with high-Ca pyroxenes from EET 99402 and NWA 5400 (Table 4). Phosphates occur in GRA 06128/9 and NWA 5400, but were not observed in the sections of EET 99402 that we studied. Merrillite grains in GRA 06128/9 and NWA 5400 have high concentrations of the REE ( $\sim 50\text{--}215 \times \text{CI-chondrite}$ ;  $\text{La}/\text{Yb}_n = 1.7 \pm 0.7$ ) and negative Eu anomalies ( $\text{Eu}^* = 0.3\text{--}0.8$ ; Fig. 5). Chlorine-rich apatite exhibits, on average, 11 times lower REE abundances ( $7\text{--}19 \times \text{CI-chondrite}$ ) than merrillite grains, with more pronounced LREE enrichment relative to HREE ( $\text{La}/\text{Yb}_n = 4.3 \pm 3.0$ ), and Eu anomalies that are slightly positive (NWA 5400 =  $\sim 1.2$ ) to strongly positive (GRA 06128 =  $3.2 \pm 0.6$ ; GRA 06129 =  $2.0 \pm 0.2$ ). A single chromite grain from GRA 06128 contains no detectable REE, and 1.2 ppm Hf and 42 ppm Zr. A single ilmenite grain from the same sample contains no detectable REE, and 40 ppm Hf, 610 ppm Nb, 3370 ppm Zr and 2430 ppm V.

Sulphides in GRA 06128/9 and EET 99402 and sulphides and metal in NWA 5400 are the primary hosts of the HSE and moderately siderophile elements (MSE: including Mo and W; Online annex). Abundances of the HSE and Mo are below detection limits for ilmenite and chromite grains in GRA 06128/9. Concentrations of Os, Ir, Ru and Mo in chromite grains from EET 99402 are highly variable, ranging from  $\sim 0.1$  to  $\sim 2 \times \text{CI-chondrite}$ . The remaining HSE (Rh, Pt, Pd, Re, Au) are below in-run limits of detection. The GRA 06128/9 sulphide population shows heterogeneous distribution of HSE within FeS and pentlandite, as well as between GRA 06128 and GRA 06129, with sulphides from the latter having generally higher HSE abundances. Sulphides in GRA 06128 have similar Ru concentrations to those measured in GRA 06129, but lower Re, Os and Ir abundances, indicating some degree of HSE fractionation within sulphides in the meteorites. The sulphides in GRA 06128/9 have elevated Ru/Os (CI-chondrite normalised  $\text{Ru}/\text{Os} = \sim 100$ ) and low Ir/Os (CI-chondrite normalised  $\text{Ir}/\text{Os} = \sim 0.8$ ) (Fig. 6). Fractionation of HSE in GRA 06128/9 sulphides is also expressed

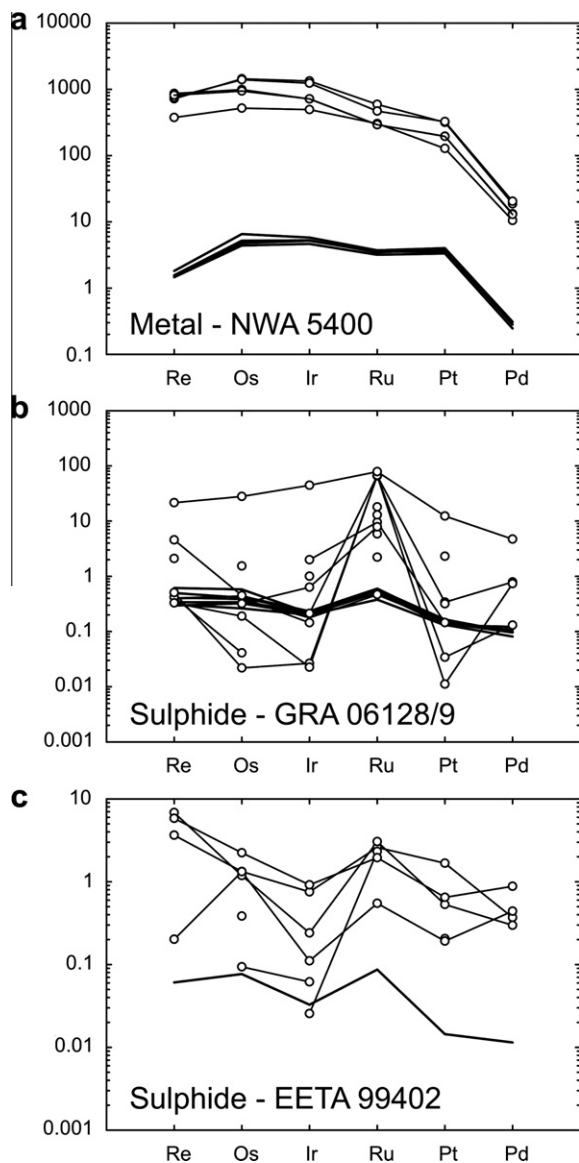


Fig. 6. CI-chondrite normalised HSE patterns for fresh (a) metal grains in NWA 5400; (b) pentlandite and troilite grains in GRA 06128/9, and (c) troilite grains in EET 99402/7, measured by LA-ICP-MS (open circles and lines), versus whole-rock HSE contents (bold lines; see Section 3.3.2). Total errors are equal to or smaller than symbols. Note differences in scale for figure panels. CI-chondrite normalisation from Horan et al. (2003).

by the elevated Au concentrations. HSE abundances within GRA 06128/9 sulphides range from 0.01 to nearly  $80 \times$  CI-chondrite, with Mo concentrations at  $\sim 1 \times$  CI-chondrite. The highest HSE concentrations may reflect metal-rich inclusions hosted within GRA 06128/9 sulphides. HSE abundances in sulphide grains from EET 99402 are in approximately chondritic relative abundances, with the exception of low CI-chondrite normalised Ir/Os ( $\sim 0.4$ ) (Fig. 6). Fresh metal grains in NWA 5400 have 6–88 times higher HSE, Mo and W abundances than associated sulphides, and both phases show pronounced depletions in Pd, Au, and to a lesser extent Mo ( $8\text{--}50 \times$  CI-chondrite),

relative to Re, Os, Ir, Ru, Rh, Pt and W ( $\sim 100\text{--}1000 \times$  CI-chondrite) (Fig. 6).

### 3.3. Whole-rock geochemistry

#### 3.3.1. Major- and trace-element compositions

The major-element composition of GRA 06128/9 is heterogeneous. This is not surprising, given the size of the sample aliquots analysed ( $<3$  g), and the mineralogical heterogeneity observed (e.g., Figs. 1 and 2). GRA 06128/9 splits have high  $\text{Al}_2\text{O}_3$  (16–18 wt.%), CaO (5.6–7.4 wt.%;  $\text{CaO}/\text{Al}_2\text{O}_3 = 0.5$ ) and  $\text{Na}_2\text{O}$  (5.4–5.6 wt.%), reflecting high oligoclase contents (Day et al., 2009a). The moderately volatile elements,  $\text{Na}_2\text{O}$  and  $\text{K}_2\text{O}$  are in near chondritic proportions with  $\text{K}_2\text{O}/\text{Na}_2\text{O} = 0.04$  (Day et al., 2009b; Shearer et al., 2010). The Mg-number of the whole-rock is 38–39, in agreement with the measured Mg-number of olivine and pyroxene in the samples. In detail, we find higher  $\text{P}_2\text{O}_5$  (1.8–3.2 wt.%),  $\text{TiO}_2$  (0.08–0.15 wt.%),  $\text{SiO}_2$  (54.6–57.6 wt.%) and lower  $\text{Na}_2\text{O}$  and S than the splits of GRA 06129 measured by Shearer et al. (2010), reflecting the control of modal mineralogy in the samples (phosphate on Ca and P, sulphide on S, oxides on Ti). NWA 5400 has relatively high MgO (29.6 wt.%) with an Mg-number = 61.5 (Irving et al., 2009). NWA 5400 also contains 0.18 wt.%  $\text{P}_2\text{O}_5$ , 0.95 wt.%  $\text{Cr}_2\text{O}_3$ , and 0.98 wt.%  $\text{Al}_2\text{O}_3$ . Measured concentrations by solution ICP-MS of  $\text{P}_2\text{O}_5$ , MnO and FeO (Table 5) are similar to fused bead measurements of GRA 06128/9 (Online annex). Brachinites and brachinite-like achondrites have low  $\text{P}_2\text{O}_5$  abundances (0.065–0.241 wt.%), high MnO (0.327–0.417 wt.%) and FeO between 25.7 and 37.6 wt.%.

Trace element abundances for GRA 06128/9, brachinites, and brachinite-like ultramafic achondrites are presented in Table 5 and Fig. 7. The new whole-rock REE data for GRA 06128, 22 and GRA 06129, 9 are similar to those measured for the same samples by LA-ICP-MS of fused beads (Day et al., 2009a) and by solution reported by Shearer et al. (2010), albeit the absolute concentrations of these elements, measured in this study, are higher. We note that there is a reasonably good correlation between  $\text{P}_2\text{O}_5$  and REE contents in samples of GRA 06128/9, consistent with REE contents being a function of phosphate content within analysed rock fragments. Higher concentrations of Cr and Zr, relative to measurements in Day et al. (2009a) and Shearer et al. (2010) probably reflect the greater efficiency of the higher-pressure/temperature dissolution technique used in this study. Measured Co (245–285 ppm), Ni (2105–3177 ppm), Sr (50.1–61.0 ppm) and Ba (22.5–24.1 ppm) are similar to those reported by Shearer et al. (2010); large variations in concentration probably reflect modal proportions of phases (e.g., Co and Ni in pentlandite). The low reported Ni, Co and Cu from LA-ICP-MS analysis probably reflect generation of sulphide-rich beads (nuggets) that formed in the fused beads analysed by Day et al. (2009a). The whole-rock REE pattern for GRA 06128/9 is relatively flat ( $\text{La}/\text{Yb}_n = 1.6\text{--}1.8$ ) with a positive Eu anomaly ( $\text{Eu}^* = 1.5\text{--}1.6$ ) (Fig. 7a). GRA 06128/9 possess pronounced Pb, Ti, Zr and Hf anomalies, as well as low Nb and Ta, similar to brachinites (Fig. 7b).

Brachinites (Brachina; EET 99402; NWA 1500; NWA 3151; NWA 4872; NWA 4882) exhibit a considerable range in REE abundances and CI-chondrite normalised REE patterns (Fig. 7a), from low REE abundances (NWA 4872), with a strongly positive Eu-anomaly for EET 99402 ( $Eu^* = 14.2$ ), to the highest REE abundances ( $\sim 1.7 \times$  CI-chondrite) for Brachina. The LREE/HREE ratio of brachinites varies from LREE-depleted (EET 99402, La/

$Yb_n = 0.1$ ) to relatively LREE-rich (Brachina, La/ $Yb_n = 1.5$ ). Brachinite-like achondrites NWA 5400 (La/ $Yb_n = 1.4$ ), NWA 6077 (La/ $Yb_n = 0.2$ ), and Zag (b) (La/ $Yb_n = 0.1$ ) lie within the range of brachinite REE compositions and together exhibit both modest positive and negative Eu anomalies ( $Eu^* = 0.3-14.2$ ). Brachinites have high Cr (3432–7106 ppm), Co (181–452 ppm) and Ni contents (406–4629 ppm), and low Sr (0.8–17 ppm). Brachina,

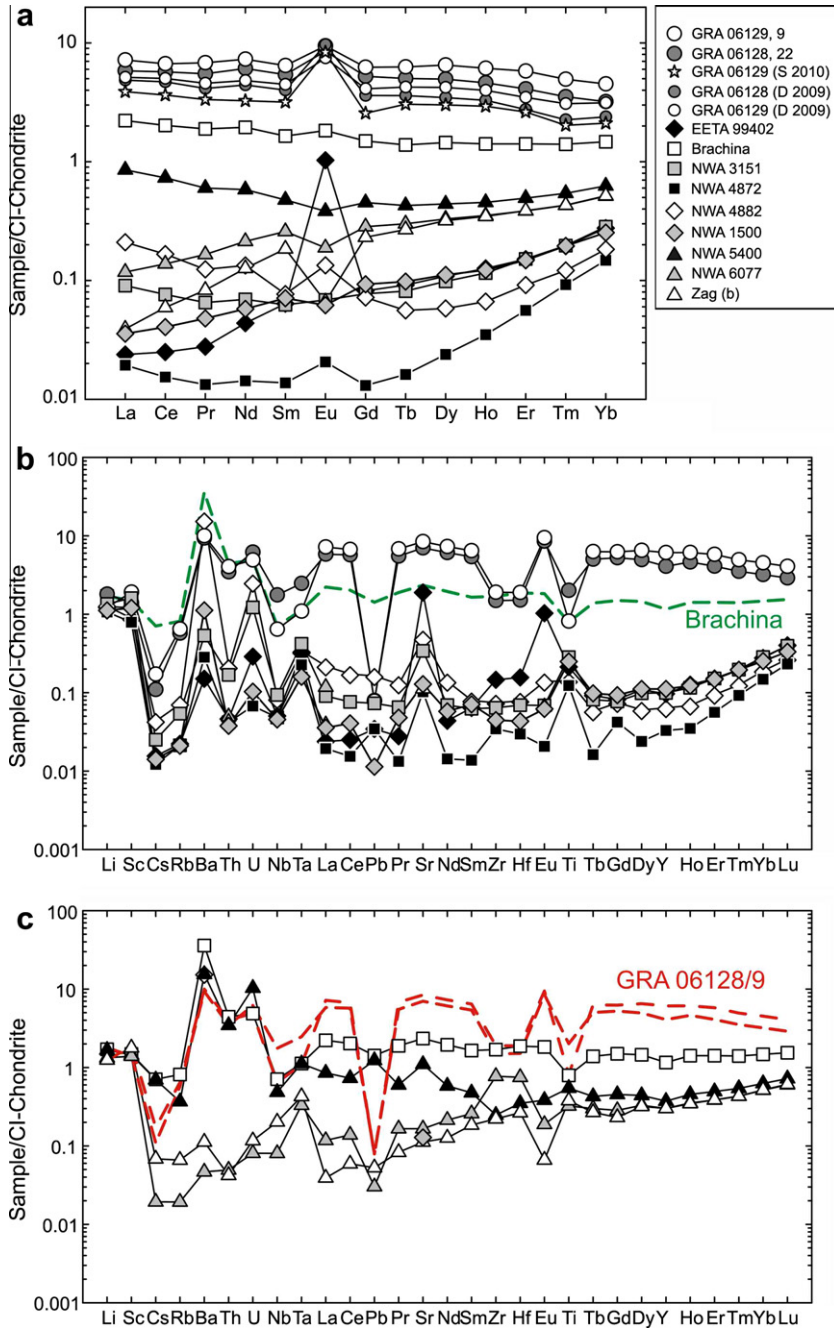


Fig. 7. (a) CI-chondrite normalised rare earth element patterns of GRA 06128/9, brachinites and brachinite-like achondrites. Published data measured by solution ICP-MS for GRA 06129 from Shearer et al. (2010) [S 2010], and by LA-ICP-MS analysis of fused beads for GRA 06128 and GRA 06129 from Day et al. (2009a) [D 2010]. (b) CI-normalised multi-element variation diagram for GRA 06128/9 and brachinites and (c) for brachinite-like achondrites and Brachina. Total errors are equal to or smaller than symbols. Normalisation data from McDonough and Sun (1995).

NWA 4882 and NWA 5400 all have anomalously high Ba (37–87 ppm) and Pb (0.4–3.6 ppm) contents, as well as elevated U, possibly reflecting low-temperature alteration products derived from hot desert alteration (Fig. 7b). Conversely, aliquots of EET 99402/7, NWA 1500, NWA 3151, NWA 4872, NWA 6077, and Zag (b) all have low Ba (<3 ppm) and Pb (<0.2 ppm). Brachinites and brachinite-like achondrites have Li and Sc contents similar to GRA 06128/9, and have generally low Nb/Ta. Moderately siderophile elements (MSE; e.g., Se, Sn, Pb, Ge, Ga, Cu, Co, Ni, Mo and W) range from 0.01 to 10 × CI-chondrite, with relatively consistent concentrations for Se (0.141–0.352 ppm), but more variable measured abundances for Sn (0.155–2.9 ppm), Pb (0.028–3 ppm), Ga, Ni and W (0.071–1.467 ppm; [Online annex](#)). GRA 06128/9 have pronounced enrichments in Ga and 0.25–0.33 ppm W; NWA 5400 has the highest W concentration (1.47 ppm) of all brachinites and brachinite-like achondrites.

### 3.3.2. $^{187}\text{Re}$ – $^{187}\text{Os}$ systematics and HSE abundances

Abundances of Os, Ir, Ru, Pt, Pd and Re and values of  $^{187}\text{Os}/^{188}\text{Os}$  are reported in Table 6, and Re–Os isotopic data for GRA 06128/9, brachinites and brachinite-like achondrites are shown in Fig. 8. All of the studied meteorites have present-day  $^{187}\text{Os}/^{188}\text{Os}$  within the range of chondrites (0.120–0.132; [Walker et al., 2002](#); [Fischer-Gödde et al., 2010](#)). GRA 06128/9 have  $^{187}\text{Os}/^{188}\text{Os}$  between 0.1261 and 0.1312, with five of the seven separate measurements lying close to a 4.56 Ga iron meteorite reference isochron. The two samples that lie furthest from the reference isochron have higher measured Re concentrations than calculated, suggesting open-system behaviour of Re (gain) or Os (loss). Brachinites have measured  $^{187}\text{Os}/^{188}\text{Os}$  of between 0.1204 and 0.1301. Only splits from NWA 1500, NWA 4872, NWA 4882, and Brachina plot close to the reference isochron, with all other samples having measured Re that is either higher or lower than calculated  $\text{Re}^*$  (concentration of Re calculated assuming chondritic  $^{187}\text{Os}/^{188}\text{Os}$  at the estimated time of sample crystallisation using the measured Os concentration and calculated Re/Os; Fig. 8).

None of the brachinite-like achondrites have Re–Os isotope systematics that lie on the reference isochron. Splits of NWA 6077 have measured  $^{187}\text{Os}/^{188}\text{Os}$  of between 0.1280 and 0.1282 and higher measured Re than predicted from the isotopic composition. Splits of Zag (b) have variable measured  $^{187}\text{Os}/^{188}\text{Os}$  (0.1255–0.1280) and higher measured Re than predicted from the isotopic composition. Replicates of homogenised powder of NWA 5400 have measured  $^{187}\text{Os}/^{188}\text{Os}$  of between 0.1265 and 0.1272 and low Re/Os.

New HSE abundance analyses of splits of GRA 06128/9 are in agreement with previous measurements ([Day et al., 2009a](#)), with CI-normalised HSE patterns that are significantly fractionated relative to chondrites, and characterised by increasing levels of depletion correlating with decreasing order of 50% condensation temperatures, but with positive Ru ‘anomalies’ (i.e., lower Ir, Pt and Pd relative to Ru). Rhenium, Ru and Os are at concentrations that are factors of ~2–4 times lower than CI-chondrites (Fig. 9a). Brachinites (Brachina; EET 99402; NWA 1500; NWA 4872; NWA 4882; NWA 3151) possess similar to lower concentrations of the HSE relative to GRA 06128/9, as well as similar HSE fractionations (i.e., low Ir, Pt and Pd relative to Ru, Fig. 9b). EET 99402 has the lowest HSE abundances of the brachinite suite. Brachinite-like achondrites Zag (b) and NWA 6077 show pronounced Pd depletions, yet otherwise exhibit relatively ‘flat’ HSE patterns, and have absolute abundances of the HSE abundances broadly similar to brachinites (Fig. 9c). Brachinite-like achondrite NWA 5400 has pronounced depletions in Pd and Re relative to Os, Ir, Ru and Pt, and Os concentrations that are 3–7 × CI-chondrites (Fig. 9c). CI-chondrite normalised Ir/Os (GRA 06128/9 =  $0.57 \pm 0.13$ ; Brachinites =  $0.50 \pm 0.13$ ; where errors represent ranges, rather than analytical uncertainties) and Pt/Os (GRA 06128/9 =  $0.38 \pm 0.07$ ; brachinites =  $0.20 \pm 0.08$ ) are low for GRA 06128/9 and brachinites, whereas these ratios are closer to chondritic values in brachinite-like achondrites (Ir/Os<sub>CI</sub> =  $0.98 \pm 0.10$ ; Pt/Os<sub>CI</sub> =  $0.93 \pm 0.29$ ). Like GRA 06128/9 and brachinites (GRA 06128/9 =  $0.27 \pm 0.09$ ; brachinites =  $0.18 \pm 0.08$ ), Pd/Os<sub>CI</sub> in brachinite-like achondrites are low ( $0.27 \pm 0.28$ ).

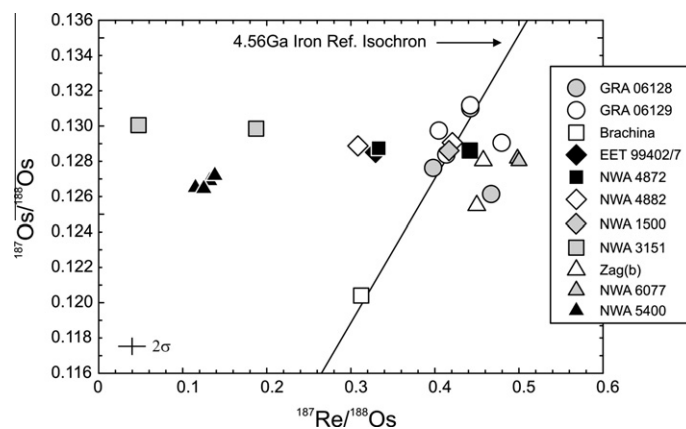


Fig. 8.  $^{187}\text{Re}/^{188}\text{Os}$ – $^{187}\text{Os}/^{188}\text{Os}$  diagram for GRA 06128/9, brachinites, and brachinite-like achondrites. Also shown is the iron isochron from [Smoliar et al. \(1996\)](#). The primordial reference isochron was obtained from Re–Os isotope systematics for iron meteorites and calculated for an age of 4.567 Ga using an initial  $^{187}\text{Os}/^{188}\text{Os}$  isotopic composition of 0.09517 (from [Walker et al., 2002](#) and adjusted to 4.567 Ga) and  $\lambda = 1.666 \times 10^{-11} \text{ a}^{-1}$  ([Smoliar et al., 1996](#)).

and similar to Pd/Os<sub>CI</sub> in ureilites ( $0.19 \pm 0.23$ ; Rankenburg et al., 2008). Ratios of Re/Os<sub>CI</sub> for GRA 06128/9, brachinites, and brachinite-like achondrites are  $1.05 \pm 0.08$ ,  $0.72 \pm 0.31$ , and  $0.68 \pm 0.45$ , respectively.

### 3.3.3. Oxygen isotopes

New laser fluorination oxygen isotope data for separate splits of EET 99402, 44 yield an average of  $\Delta^{17}\text{O} = -0.08 \pm 0.03\text{‰}$ . The range of  $\Delta^{17}\text{O}$  for brachinites now measured from a single laboratory (Geophysical Laboratory), and thoroughly treated to remove the effects of terrestrial alteration, is from  $-0.08\text{‰}$  to  $-0.31\text{‰}$  (Table 7;

Fig. 10). If brachinite-like achondrites are included in the comparison, the range is from the terrestrial fractionation line (i.e.,  $\Delta^{17}\text{O} = \text{zero}$ ; NWA 5400) to  $-0.31\text{‰}$  (Brachina). Multiple splits of the GRA 06128/9 meteorites yield an average  $\Delta^{17}\text{O}$  value of  $-0.208 \pm 0.005\text{‰}$  (Day et al., 2009a), which is within the range of values for brachinites and brachinite-like achondrites. If the brachinites and brachinite-like achondrites derive from the same parent body, the range in  $\Delta^{17}\text{O}$  would reflect oxygen isotope heterogeneity in the parent body resulting from partial differentiation and inefficient melting of a body with a complex heritage (e.g., Greenwood et al., 2005; Day et al., 2009a). To the extent that their values are overlapping, oxygen isotopes in GRA 06128, brachinites and brachinite-like achondrites allow for genetic links between the meteorites. The range in  $\delta^{18}\text{O}$  values for samples probably reflects mineralogical heterogeneity, as well as possible inherited O isotope characteristics from their source. Indeed, mineralogical heterogeneity can explain the  $\sim 1\text{‰}$  difference in  $\delta^{18}\text{O}$  values between splits of GRA 06129 from this study versus Shearer et al. (2010). There may also be a small calibration shift between the two laboratories, but this will not affect  $\Delta^{17}\text{O}$  values.

## 4. DISCUSSION

### 4.1. Genetic- and process-related links and possible parent bodies

There is geochemical and petrological evidence for possible process- and genetic-links between GRA 06128/9, brachinites and brachinite-like achondrites, including: (1) overlap in oxygen mass-independent isotopic compositions ( $\Delta^{17}\text{O}$ ; Fig. 10); (2) petrology (e.g., Warren and Kallemeyn, 1989; Mittlefehldt et al., 2003; Zeigler et al., 2008; Day et al., 2009a; Shearer et al., 2010); (3) similar oxidation conditions, and; (4) geochemistry, including the relative and absolute HSE abundances and volatile abundances. Lithological differences (i.e., olivine- versus plagioclase-dominated assemblages) do not preclude links between the meteorites, as

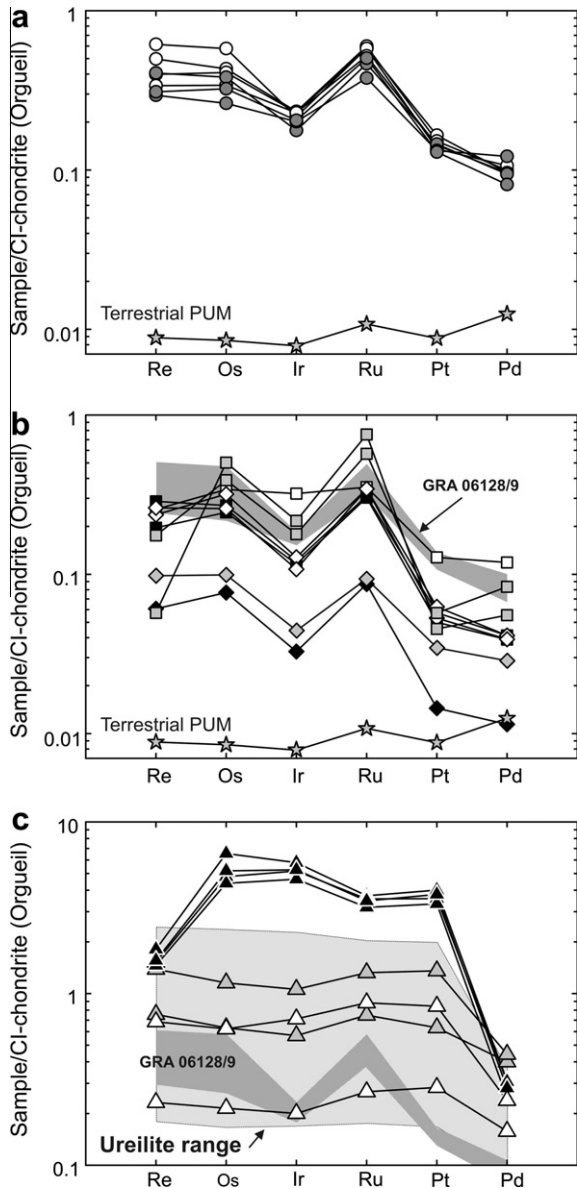


Fig. 9. CI-chondrite normalised whole-rock HSE patterns for (a) GRA 06128/9, (b) brachinites, and (c) brachinite-like achondrites. Symbols as for Fig. 7. CI-chondrite normalisation from Horan et al. (2003), ureilite range from Rankenburg et al. (2008) and PUM estimate from Becker et al. (2006). Total errors are equal to or smaller than symbols.

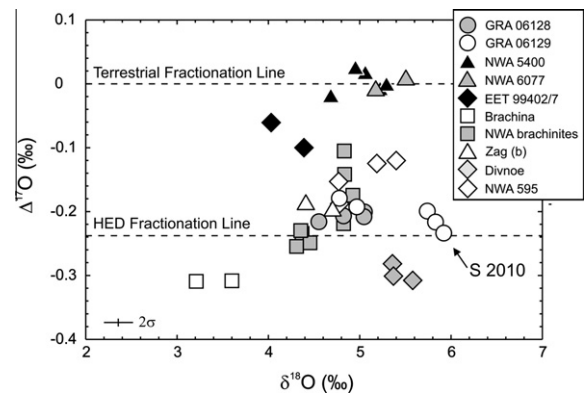


Fig. 10.  $\delta^{18}\text{O}$ - $\Delta^{17}\text{O}$  plot for GRA 06128/9 brachinites and some brachinite-like achondrites (NWA 5400; NWA 6077; Zag (b), Divnoe, NWA 595). These meteorites span a range of  $\Delta^{17}\text{O}$  values from the terrestrial fractionation line to below the range estimated for howardite, eucrite, diogenite meteorites (HED fractionation line; Greenwood et al., 2005). Data sources are given in Table 7.

diverse magmatic rock-types are a natural consequence of igneous differentiation processes, even on fully differentiated bodies (e.g., lunar crustal anorthosites, high-Mg suite rocks and mare basalts, or terrestrial layered mafic intrusions; c.f., Taylor, 1975; Day et al., 2008, 2010). For example, olivine-dominated brachinites, and brachinite-like achondrites could conceivably represent complementary ultramafic residues to GRA 06128/9 felsic melts (Day et al., 2009a). A similar scenario has been suggested for ureilite meteorites, which have olivine compositions that span a large range of Fe/Mg and are missing a plagioclase-rich melt component to complement their depleted peridotitic compositions (e.g., Cohen et al., 2004; Warren et al., 2006; Goodrich et al., 2007). Rare feldspathic clasts in polymict ureilites may represent remnants of this missing basaltic component (Cohen et al., 2004). Similarly, acapulcoite-lodranites, which represent anatectic melts of chondrites (acapulcoites) and partial melt residues that are also missing a ‘melt component’ (lodranites), span a range of mafic mineral compositions ( $F_{O_{86.7-96.9}}$ ), mineral trace-element compositions and  $\Delta^{17}O$ , yet lie on a  $\delta^{17}O$ – $\delta^{18}O$  line of slope  $\sim 0.5$ , and probably derive from the same parent body (e.g., Mittlefehldt et al., 1996; McCoy et al., 1997; Floss, 2000).

The new petrology and geochemical data for GRA 06128/9, EETA 99402/7, NWA 1500, NWA 3151, NWA 4872 and NWA 4882 provide strong evidence for a genetic link between these meteorites. Although these meteorites span a range in  $\Delta^{17}O$  values ( $-0.05\text{‰}$  to  $-0.25\text{‰}$ ; Fig. 10) they all exhibit remarkable consistency in the relative abundances of the HSE (Fig. 9) and have petrological characteristics and major- and trace-element abundances consistent with GRA 06128/9 representing differentiation complements to partially melted brachinites. These similarities attest to the strong possibility for a single parent body for these meteorites. Brachina has the lowest  $\Delta^{17}O$  value ( $-0.3\text{‰}$ ) of the studied brachinites, with only Divnoe showing similarly low  $\Delta^{17}O$  (Fig. 10). Brachina also has elevated incompatible element abundances (Fig. 7), and distinct Cr-spinel compositions compared with other brachinites (e.g., Table 3), as well as distinct measured  $^{187}Os/^{188}Os$  and relative HSE abundances to GRA 06128/9 and other brachinites (Figs. 8 and 9). In the case of  $^{187}Re$ – $^{187}Os$  and HSE abundance measurements of Brachina, we note that there may be a phase distribution and nugget effect for the sample that we measured (see Section 4.3), attributable to the limited available mass (0.063 g). Thus, there may be more than one brachinite parent body, but further work is required to address this possibility.

Although brachinite-like achondrites (NWA 5400, NWA 6077, Zag (b)) share similarities with brachinites, in detail these rocks appear distinct and probably originated from a different parent body compared to the brachinites and GRA 06128/9. Differences include more mafic silicate compositions that place brachinite-like achondrites as intermediate between brachinites and ureilites (Fig. 3), and the contrasting relative HSE abundances of brachinite-like achondrites, when compared with brachinites (Fig. 9). Furthermore, based on petrology, mineralogy and  $\Delta^{17}O$  values, there is strong evidence to suggest that NWA 5400 and NWA 6077 are paired.

The similarities and differences between brachinites and brachinite-like achondrites suggest process-related links, whereby similar differentiation and post-crystallisation processes occurred on a number of discrete oxidised and volatile-rich parent bodies. Analogies include basaltic achondrites with strong similarities to eucrites, but which possess different oxygen isotope systematics (Yamaguchi et al., 2002; Floss et al., 2005), or angrite meteorites which have been proposed to originate from at least two separate parent bodies (Mittlefehldt et al., 2002), yet require similar precursor compositions, oxidation and volatile states, and differentiation histories. Process-related links are common to ‘primitive’ achondrites such as acapulcoite-lodranites, ureilites, and GRA 06128/9, brachinites and brachinite-like achondrites, as described above. The similar melting histories of these meteorite groups point to a continuum of differentiation processes, from early anatexis and generation of FeS melts, to whole-sale melting, silicate–metal equilibrium and fully differentiated planets and planetesimals (e.g., McCoy et al., 2006).

#### 4.2. Alteration and open-system behaviour

GRA 06128/9, brachinites and brachinite-like achondrites represent early-formed Solar System achondrite finds from both the hot and cold deserts. Assuming derivation from a reservoir with uniform initial  $^{187}Os/^{188}Os$ , it would be anticipated that such achondrites would plot close to a primordial  $^{187}Re$ – $^{187}Os$  isochron; this curve is defined by iron meteorites, which crystallised between 0 and 40 Ma after Solar System formation (e.g., Smoliar et al., 1996). However, only a third of the measured splits from GRA 06128/9, brachinites and brachinite-like achondrites plot within typical uncertainties ( $\pm 0.2\%$ ) of the iron meteorite isochron (Fig. 8). The level of scatter about the isochron is greater than for chondrites (e.g., Walker et al., 2002) and similar to the scatter observed for  $^{187}Re$ – $^{187}Os$  systematics of ureilites (Rankenburg et al., 2007). Such scatter probably does not reflect analytical issues, given the level of analytical precision obtained for  $^{187}Os/^{188}Os$  and  $^{187}Re/^{188}Os$  measurements. Instead, the Re–Os isotopic systematics of GRA 06128/9, brachinites and brachinite-like achondrites most likely reflect late-stage open-system behaviour of Re due to terrestrial alteration. Rhenium mobilisation, rather than Os, is indicated by the limited range in Ir/Os and large range in Re/Os for these meteorites (e.g., Fig. 8). The variability in Re/Os among different splits of the same meteorite (e.g., Zag (b)) is most consistent with localised mobilisation (cm- to mm-scale), rather than loss or gain of Re from the bulk meteorites. Splits of GRA 06128/9 that deviate from the reference isochron are consistent with mobilisation of  $\leq 20\%$  Re. Some brachinites and brachinite-like achondrites show a greater percentage of Re mobilisation, and splits of the NWA 5400 powder show as much as 67% apparent loss of Re (note that replicate measurements of other samples were performed on individually ground fragments, rather than on a homogenised sample powder). The likely timing of such mobilisation is during residence of the meteorites on Earth, because all of the meteorites have  $^{187}Os/^{188}Os$  within the narrow range of chondrites.

Rhenium mobilisation probably occurred due to alteration of sulphide and metal. The susceptibility of sulphides and metals to terrestrial aqueous alteration, the primary hosts of HSE in the studied samples, is well known in chondrites (e.g., Horan et al., 2010). In the studied samples for example, sulphides and metals show variable degrees of break-down in NWA 5400 (c.f., Fig. 2d). LA-ICP-MS analyses of altered sulphide in NWA 5400 show that they typically have ~50–60% lower HSE concentrations compared to their unaltered counterparts, while relative abundances of Os, Ir, Pt, Pd and Ru are broadly similar between fresh and altered sulphides (Online annex). Fresh metal grains in NWA 5400 have higher similar HSE patterns to that of the bulk rock (Fig. 6), but higher Re/Os, possibly indicating the mobilisation of Re. If paired, the higher Re/Os measured in NWA 6077 would also support the interpretation that weathering effects acted on the split of NWA 5400 that we measured. Sulphides ( $\pm$  minor metal) in EETA 99402/7 and GRA 06128/9 control the HSE in the meteorites, with limited disturbance to these phases (Fig. 6). Mobilisation of the HSE in response to sulphide/metal break-down is supported by observations of Fe-S-rich veins cross-cutting fusion crust in GRA 06128 (Shearer et al., 2010). Although some of the isotopic deviations are large for isochron applications and preclude use of the Re–Os isotope system for a precise age determination of the meteorites, the degree of open-system behaviour appears to be minor to negligible for the other HSE (Os, Ir, Ru, Pt, Pd). This is indicated by the large variations in Re/Os measured for different splits of the meteorites, accompanied by limited variations in  $^{187}\text{Os}/^{188}\text{Os}$ , and the limited variations in the inter-element ratios of the other HSE (e.g., [Ir, Pt, Pd, Ru/Os]).

Alteration has also affected abundances of incompatible trace elements in some bulk meteorites. Modal recombination

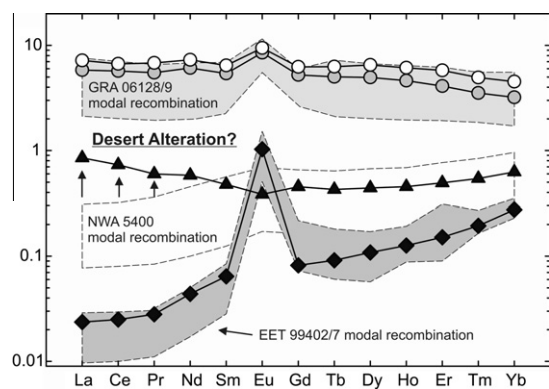


Fig. 11. Fields for modal recombination calculations of REE in GRA 06128/9, EET 99402 and NWA 5400 using mineral modes and LA-ICP-MS mineral REE abundance data versus whole-rock compositions measured by solution ICP-MS. Calculated REE concentrations for GRA 06128/9 and EET 99402 are identical, within uncertainty, of the measured whole-rock values. Calculated REE concentrations for NWA 5400 yield La, Ce, Pd and Nd concentrations below the measured whole-rock values, suggesting addition of these elements to the meteorite during terrestrial desert alteration.

using mineral modes and LA-ICP-MS trace element abundances of minerals in GRA 06128/9, EET 99402 and NWA 5400 show that it is possible to reproduce the REE patterns of bulk samples of the cold desert meteorites (GRA 06128/9, EET 99402/7), but that the measured La, Ce, Pr and Nd abundances in the NWA 5400 whole-rock are higher than predicted from modal recombination (Fig. 11). The probable cause of this enrichment is desert alteration and mobilisation/addition of some elements. Desert alteration would explain the dispersion in LREE, but also the similar absolute and relative abundances of the HREE for brachinite-like achondrites, and possibly for brachinites NWA 3151 and NWA 4882 (Fig. 7). Meteorites with LREE enrichments all show variable to high abundances of Ba, Sr, U and Pb, suggesting that these elements have also been compromised by hot desert alteration. For the purposes of modelling discussed below, we focus on elements that have been minimally affected by hot desert alteration. These elements include the REE from Eu to Yb, Os, Ir, Ru, Pt and Pd.

#### 4.3. Phase distribution and the mode-effect

Some brachinite and brachinite-like achondrites exhibit large differences in HSE concentrations between sub-sample fragments (e.g., NWA 6077; 40–50% RSD). These differences are considerably outside of analytical uncertainty for HSE abundance measurements ( $<\pm 1\%$ ), and do not reflect alteration effects. The majority of HSE measurements were performed on different powder aliquants from the same sample chip, with heterogeneous distribution of sulphide and metal. Similar heterogeneities in sample splits have been observed from HSE studies of chondritic meteorites (e.g., Walker et al., 2002; Horan et al., 2003; Fischer-Gödde et al., 2010) and ureilites (Rankenburg et al., 2008). As pointed out by these studies, inter-element ratios normally cancel out the effects of heterogeneous phase distribution. In contrast, a well-mixed powder was used for all HSE measurements of NWA 5400, and replicate measurements of this powder show relatively good agreement (HSE = 7–15.5% RSD;  $^{187}\text{Os}/^{188}\text{Os}$  reproducibility = 0.24%;  $n = 5$ ,  $2\sigma$ ), with the range of measured HSE abundances in the powder reflecting uneven distribution of HSE-rich trace phases (the ‘nugget effect’). We note that the variable HSE abundances measured in splits of NWA 6077, combined with the use of an altered sample powder for HSE determinations in NWA 5400, are consistent with pairing of these samples. The reason for significant HSE abundance dispersion in meteorite sub-samples is the mode-effect. The mode-effect (variations in modal mineral abundances) occurs where non-representative volumes of rock are analysed (see discussion in Spicuzza et al., 2007), resulting in variability in chemical measurements due to large grain-sizes ( $>1$  mm for some GRA 06128/9, brachinite and brachinite-like achondrite lithologies) and uneven phase distribution within the meteorites. This effect is reflected in whole-rock major- and trace-element variations for the GRA 06128/9 meteorites, and is probably also an issue for relatively coarse grained brachinites and brachinite-like achondrites.

#### 4.4. Chronology, conditions of volatility, reduction and precursor composition

The known chronologies of GRA 06128/9, brachinite and brachinite-like achondrites are summarised in the [Online annex](#). The chronology of GRA 06128/9 suggests crystallisation ages of >4.52–4.566 Ga (Nyquist et al., 2009; Day et al., 2009a; Shearer et al., 2010; Wimpenny et al., 2011), which are within uncertainty of the minimum crystallisation age of 4.54 Ga determined from Mn–Cr isotope systematics on NWA 5400 (Shukolyukov et al., 2010), and 4.565 Ga for Brachina (Wadhwa et al., 1998). GRA 06128/9, brachinites and brachinite-like achondrites have suffered complex and chronic post-formation thermal disturbance events from ~4.3 Ga until as late as 2.3 Ga, implying origins from parent bodies with similar post-crystallisation histories (e.g., Bogard et al., 1983; Swindle et al., 1998; Nyquist et al., 2009). Thus, despite a paucity of precise ages, it can be concluded that the parent body(ies) of GRA 06128/9, brachinites and brachinite-like achondrites probably melted and differentiated early in Solar System history.

A striking aspect of the petrology of achondrites deriving from limited degrees of partial melting is the systematic variation in Fe/Mg within mafic silicates (e.g., olivine and pyroxene) as a function of conditions of volatility and reduction at the time of differentiation within their respective parent bodies. For example, aubrite meteorites, which have witnessed large-scale melting processes, are virtually devoid of Fe in their mafic silicates, reflecting extreme reduction, as well as segregation of Fe-rich liquids (~IW –5,  $F_{O_{99.8-99.9}}$ ; e.g., Keil, 2010). Ureilites preserve a large range in Fe/Mg in their silicates (e.g., ~ $F_{O_{74-95}}$ ), at nearly constant Mn/Mg, suggesting near-constant degrees of partial melt extraction over a large range of redox conditions (Mittlefehldt, 1986; Goodrich et al., 1987, 2004) ([Online annex](#), Fig. S7). GRA 06128/9, brachinites, and brachinite-like achondrites represent some of the most oxidised of the recognised partially melted achondrites. GRA 06128/9 preserve evidence of  $fO_2$  of ~IW to IW + 1 during the last phase of thermal equilibration (Day et al., 2009a; Shearer et al., 2010), as reflected in the high Fe/Mg of the silicates (e.g.,  $F_{O_{38-40}}$  olivine). Brachinites are dominantly composed of olivine (>80%) with the highest Fe/Mg ( $F_{O_{64-72}}$ ) of all partially differentiated olivine-rich achondrites, including ureilites ( $F_{O_{76-92}}$ ; Goodrich et al., 2007), lodranites (~IW –2,  $F_{O_{86.7-96.9}}$ ; McCoy et al., 1997) and winonaites (~IW –2,  $F_{O_{94.7-99.7}}$ ; Benedix et al., 1998). Brachinites have been considered as oxidised materials from CI-chondrite like material by the oxidation reaction:  $MgSiO_3 + Fe + 0.5O_2 \rightleftharpoons (Mg, Fe)_2SiO_4$  (Nehru et al., 1992, 1996). Brachinite-like achondrites span a wider range of Fe/Mg for their mafic silicates ( $F_{O_{69-80}}$ ; Table 3), at the lower end of the ureilite range, and upper end of the brachinite range. However, it is notable that brachinites and brachinite-like achondrites together show a trend (like that of ureilites, but with more scatter) of near-constant Mn/Mg, reflecting similar degrees of partial melting over a range of redox conditions (Mittlefehldt et al., 2003; Goodrich et al., 2011) ([Online annex](#), Fig. S7). These features point to a range of  $fO_2$  conditions on the parent body(ies)

of GRA 06128/9, brachinites and brachinite-like achondrites, and even within the individual meteorite groups.

The oxidised nature of the meteorites is accompanied by elevated volatile contents, relative to most achondrites from fully- or partially-differentiated bodies. Radiogenic measured  $^{87}Sr/^{86}Sr$  (0.7043–0.7062; Nyquist et al., 2009) and comparatively high  $^{87}Rb/^{86}Sr$  (0.069–0.07) for GRA 06128/9 and Brachina ( $^{87}Rb/^{86}Sr = 0.187–0.300$ ;  $^{87}Sr/^{86}Sr = 0.70947–0.71408$ ; Bogard et al., 1983), as well as for brachinites and brachinite-like achondrites ( $^{87}Rb/^{86}Sr = 0.011–0.185$ ; excluding samples that show evidence from Ba and Pb abundances for desert alteration; Table 5) indicate a volatile-rich source. High K, Na, S, Rb, Cl and Pb contents also support generation of GRA 06128/9 from a volatile-rich source in their parent body (Day et al., 2009a,b). The volatile-rich nature of GRA 06128/9, brachinites and brachinite-like achondrites implies volatile-rich precursors similar to carbonaceous chondrites ([Online annex](#)), providing an important constraint on the origin and evolution of their parent bodies.

#### 4.5. Experimental evidence for generation of felsic asteroidal partial melts

Experiments on chondrites indicate that progressive partial melting produces a continuum of melt products ranging from Fe–Ni–S melts at relatively low temperatures (~988 °C), to basaltic melts at higher temperatures (>1050 °C; e.g., Jurewicz et al., 1991, 1995; Feldstein et al., 2001; Usui et al., 2010a,b). These melt products are consistent with observations of the compositions of various types of primitive achondrite meteorites (Mittlefehldt et al., 1996; McCoy et al., 1997; Benedix et al., 1998). Observations of plagioclase-rich materials in some meteorites (e.g., Benedix et al., 1998; Floss, 2000; Takeda et al., 2000; Ikeda and Prinz, 2001; Cohen et al., 2004; Goodrich et al., 2007), and the GRA 06128/9 meteorites in particular (Day et al., 2009a), have been interpreted to indicate that felsic melt compositions were produced by partial melting at intermediate temperatures between Fe–Ni–S melting and the main phase of basaltic melting in some asteroids (>1200 °C). Experimental studies have shown that quartz-normative felsic or andesitic compositions with >50% plagioclase may be generated by partial melting of volatile- and olivine-rich chondritic precursors (Morse, 1980; Sessler et al., 1982). The Na-rich composition of precursor material to GRA 06128/9 may also lower liquidus temperatures by up to 100 °C, shifting melt compositions to feldspar abundances (Tuttle and Bowen, 1958; Kushiro, 1975) that approach oligoclase contents in GRA 06128/9.

For equilibrium melting experiments conducted at  $fO_2$  conditions similar to those estimated for GRA 06128/9 on CR-, H-, and LL chondrites, silica-undersaturated liquids are generated because of high FeO contents. Such melts cannot be parental to GRA 06128/9 (e.g., Jurewicz et al., 1995; Usui et al., 2010a,b). Usui et al. (2010b) suggested that compositions analogous to GRA 06128/9 might not be achieved by melting experiments if the oxidation conditions preserved in mafic silicates were higher than originally experienced in the source of the parental magma,

as a result of post-magmatic events. There is ample evidence for post-magmatic equilibration of silicate phases in GRA 06128/9, as well as brachinite and brachinite-like achondrites, with granoblastic to equi-granular textures, pyroxene equilibration temperatures, and Mg/Fe disequilibrium between olivine and pyroxenes in GRA 06128/9. We note that comparison problems between melt experiments and GRA 06128/9 (and brachinites) may also be compounded if the rock has a major cumulate component (e.g., Shearer et al., 2010).

In contrast to equilibrium melting experiments, disequilibrium partial melting experiments (which have, thus far, not been conducted on carbonaceous-chondrite compositions) on a relatively volatile-rich L6 chondrite ( $\text{Na}_2\text{O} \sim 0.95$  wt.%) generated sodic- (up to 4.4 wt.%  $\text{Na}_2\text{O}$ ) and silica-rich (51–56 wt.%  $\text{SiO}_2$ ), high-normative plagioclase melts at  $\sim 10$ – $15\%$  melting (Feldstein et al., 2001). Furthermore, the Sr, Y, Ba and REE (La, Ce, Nd, Sm, Eu, Dy, Yb) abundances of some of the run products of these experiments are similar to the abundances of these elements measured in GRA 06128/9 (Day et al., 2009a; Shearer et al., 2010). Therefore, despite some uncertainties relating to melting conditions, melting experiments support the notion that the precursor starting composition of GRA 06128/9 can be represented by a volatile-rich chondritic source (c.f., Arai et al., 2008; Day et al., 2009a,b; Shearer et al., 2010).

A notable feature of segregation of oxidised, sodic and volatile-rich melt from olivine-dominated source regions is the potential to generate trends similar to the observed Fe/Mg distributions within mafic silicates in GRA 06128/9, brachinites and brachinite-like achondrites. Partial melting of chondritic precursors produce Fe–Ni–S melts and early silicate melts that are enriched in plagioclase and pyroxene; these are also more ferroan than the residue (c.f., Morse, 1980). In fact, the similar Fe/Mn, but much higher Fe/Mg for GRA 06128/9 in relation to brachinites, are what would be predicted for a melt complementary to a brachinite-like residue (Online annex, Fig. S7). Partial melting leads to the creation of residues that are increasingly magnesium-rich with increased extents of partial melting (c.f., terrestrial crust-mantle extraction). For example, Sunshine et al. (2007) performed MELTS model calculations (at QFM) on R-chondrite compositions and demonstrated that an olivine-rich residue ( $>98\%$  olivine) with  $\sim \text{Fo}_{65}$  could be produced by  $\sim 25\%$  partial melting. These authors found that melting of a chondrite produces early silicate partial melts that would be markedly more ferroan than the residue. Trends to raise Fo contents in restite olivines after prolonged disequilibrium melt experiments on the Leedey L6 chondrite ( $\text{Fo}_{74.6-80.5}$ ; Feldstein et al., 2001) are also consistent with this conclusion. Therefore, we suggest that the range of Fe/Mg observed in the mafic silicates of brachinites and brachinite-like achondrites is consistent with variable degrees of sodic, and high Fe/Mg melt extraction (c.f., melts similar to those responsible for generating GRA 06128/9); this is followed by prolonged equilibration at relatively high temperatures ( $>650$  °C), in their respective parent body(ies). Thermal equilibration would effectively homogenise major-element compositions

of minerals in both the melt (GRA 06128/9) and melt residues (e.g., brachinites and brachinite-like achondrites). Further, the Fe/Mg variations provide evidence for the origin of most brachinites and brachinite-like achondrites as residues resulting from partial melting. The origin of some brachinites as cumulates remains permissible under these conditions (i.e., localised pooling of melts during inefficient melt segregation), and can potentially explain features such as preferred grain orientation in some rocks (e.g., ALH 84025; EET 99402/7; Warren and Kallemeyn, 1989; Swindle et al., 1998; Mittlefehldt et al., 2003), but does not generally support the derivation of brachinites from a fully differentiated parent body (e.g., Mittlefehldt et al., 2003). Thus, based on the presented evidence, there is strong rationale for exploring unified differentiation models for GRA 06128/9, brachinites and brachinite-like achondrite petrogenesis.

#### 4.6. GRA 06128/9, brachinite and brachinite-like achondrite petrogenesis

New data for the HSE and MSE in GRA 06128/9, brachinite and brachinite-like achondrites are within a factor of 10 of CI-chondrite abundances, with the exception of EET 99402/7 ( $0.01$ – $0.1 \times$  CI-chondrite; Online annex). The HSE patterns of GRA 06128/9 and brachinites are distinctly fractionated, relative to CI chondrites. These HSE patterns are in strong contrast to the flat chondrite-normalised patterns of mantle or crustal rocks from other fully differentiated bodies, such as lunar mantle-derived mare basalts, lunar anorthositic crust, or most terrestrial peridotites (Becker et al., 2006; Day et al., 2007, 2010). Furthermore, the high HSE contents of GRA 06128/9, brachinites and brachinite-like achondrites, in combination with their chondrite-normalised fractionated HSE patterns, are inconsistent with an origin from chondritic impactor contamination (c.f., Day et al., 2010). The patterns of GRA 06128/9 and brachinites are compared with ureilites in Fig. 9, which exhibit a range of HSE patterns, but span a similar range of absolute HSE abundances.

Two broad generalizations governing the HSE patterns in these meteorites can be made. First, the HSE data for GRA 06128/9, brachinites and brachinite-like achondrites are consistent with a lack of large-scale silicate-metal equilibration in their parent body(ies), as would be expected from core formation (Day et al., 2009a). Such a global process would have decreased HSE abundances to well below those measured. Second, sulphide-rich segregated metallic melts probably played important roles in fractionating HSE/MSE and distributing these elements between melts and melt sources (Warren and Kallemeyn, 1989; Mittlefehldt et al., 2003; Day et al., 2009a). Here, we explore the nature of partial melting in GRA 06128/9, brachinites and brachinite-like achondrites through models of whole-rock REE and HSE abundances.

##### 4.6.1. REE modelling: silicate melts and residues

Disequilibrium melt experiments of the Leedey L6 chondrite performed at  $\sim 1200$  °C and  $f\text{O}_2$  of IW-1 (Feldstein et al., 2001) generated melt pockets after  $10$ – $15\%$  partial

melting with similar absolute and relative REE abundances as compared to GRA 06128/9 (IW to IW + 1; Fig. 12a). Assuming a CI-chondrite trace-element initial composition and olivine, low-Ca pyroxene and high-Ca pyroxene modal proportions similar to the Leedeey L6 chondrite, a simple non-modal batch melting model indicates approximately 13–30% partial melting of such a source can reproduce some of the trace-element compositions of GRA 06128/9 (Fig. 12a). The results of our model are also in agreement with models from Shearer et al. (2010), that required >10% partial melting using both batch and fractional melting models of L, CI and CM chondrite compositions. Partial melting of a volatile-rich chondritic source can, therefore, explain the Na-rich nature of GRA 06128/9, indicating they approach melt compositions in terms of trace-element composition.

The degree of melting estimated to generate GRA 06128/9 (13–30%) is broadly consistent with the 25–30%

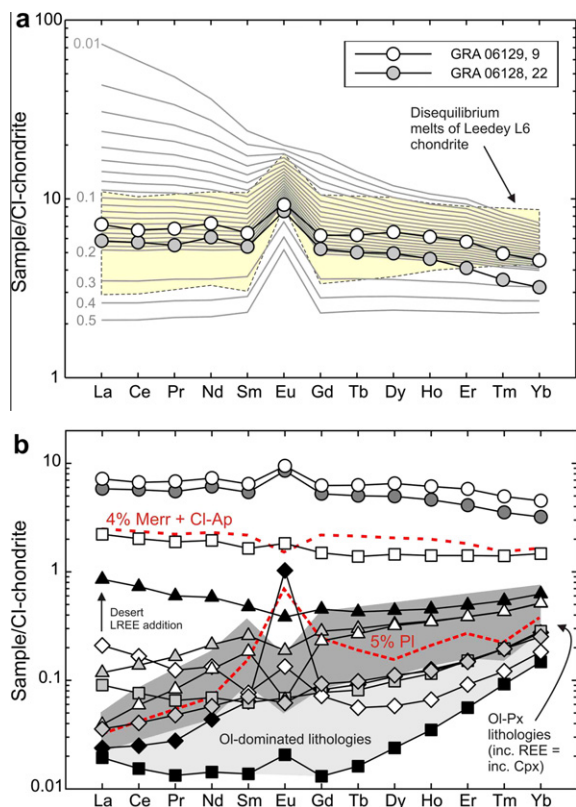


Fig. 12. Chondrite-normalised rare earth element patterns for (a) GRA 06128/9 versus 10–14% partial melt products of the Leedeey L6 chondrite (pale field with stippled border), and 1 (0.01) to 50 (0.5) percent batch melting of a CI-chondrite starting composition (grey lines, from McDonough and Sun, 1995) with Leedeey L6 chondrite modal olivine and pyroxene compositions (from Feldstein et al., 2001). (b) Brachinite and brachinite-like achondrites compared with GRA 06128/9 and calculated residues after melting with variable proportions of olivine (Ol), low-Ca pyroxene (Opx), and high-Ca pyroxene (Cpx). Also shown are melt residue compositions containing proportions of plagioclase and phosphate (as merrillite (Merr) and chlorapatite (Cl-Ap)). Mineral data are from this study.

partial melting and melt-removal required to generate the compositions of brachinites as residues (Mittlefehldt et al., 2003). Therefore, we have also modelled a range of olivine-orthopyroxene-clinopyroxene residue compositions expected to form as a consequence of felsic melt depletion, using brachinite mineral modes and measured trace element compositions of mineral phases. The residue compositions obtained have low La/Yb and negative Eu anomalies, and approach the compositions of brachinites and brachinite-like achondrites (Fig. 12b). As noted previously, many brachinites and brachinite-like achondrites have elevated LREE due to hot-desert alteration. For example, we attribute progressive change to this process in La/Yb from NWA 5400 ( $La/Yb_n = 1.4$ ) to NWA 6077 ( $La/Yb_n = 0.2$ ), to Zag (b) ( $La/Yb_n = 0.1$ ; Fig. 12b). However, MREE and HREE were not affected by this process. The relative and absolute abundances of MREE-HREE in aliquots of NWA 4872 and NWA 4882 are consistent with these rocks being dominated by olivine, whereas other brachinite and brachinite-like achondrites conform to olivine-pyroxene lithologies (increasing REE abundances in the proportions Ol:Opx:Cpx = 80:10–20:0–10 to 60–70:20–40:0–10; Fig. 12b).

Many of the brachinites contain phosphate and plagioclase as trace, minor, or even major phases (e.g., EET 99402/7 contains ~8% modal plagioclase). If these phases are included in residua calculations, it is possible to reproduce all brachinite and brachinite-like achondrite MREE-HREE compositions (Fig. 12b). For example, trace element abundances measured in EET 99402/7 are consistent with virtually no phosphate, and >5% modal plagioclase. Brachina, with the most elevated REE pattern of the brachinite suite, can be reproduced, after ~13–30% melt extraction, by addition of minor phosphate and plagioclase (not shown) to an olivine-ortho/clinopyroxene residue.

Model calculations emphasise the similar melt processing required on the parent body(ies) of GRA 06128/9, brachinites and brachinite-like achondrites. It is possible to conclude that, not only did moderate degrees of partial melting of asteroids generate felsic melt compositions, but that uneven distribution of trace phases (sulphides, phosphates, plagioclase) and inefficient melt extraction in the source regions led to a range of melt-depleted source rock compositions. These observations permit the origin of brachinites primarily as residues of partial melting (e.g., Nehru et al., 1983) and as minor cumulate materials within their parent body(ies) (e.g., Warren and Kallemeyn, 1989; Mittlefehldt et al., 2003).

#### 4.6.2. HSE modelling: Fe–Ni–S melts and residual sulphide and metal

The HSE are both strongly siderophile and strongly chalcophile, and are sensitive tracers of the earliest stages of chondritic melting, when the first melts to be generated are Fe–Ni–S-rich (e.g., Mittlefehldt et al., 1996). Consistent with this, the Fe–Ni–S veins present in some acapulcoite achondrites have been interpreted to represent frozen melts (Mittlefehldt et al., 1996; McCoy et al., 1997). Sulphide and metal grains are the primary hosts of the HSE in GRA 06128/9, brachinites and brachinite-like achondrites (Fig. 13). Calculated whole-rock abundances (from modal

abundance and HSE concentrations of sulphide + metal) closely match measured whole-rock HSE concentrations. For example, to explain the whole-rock HSE abundances measured in EET 99402/7 requires  $\sim 0.04 \pm 0.03\%$  troilite. GRA 06128/9 require between  $\sim 0.2\%$  and  $>2\%$  troilite and pentlandite, respectively, consistent with observed modal abundances of these phases in the meteorites (Day et al., 2009a). Brachinite-like achondrites require no more than  $\sim 0.05\%$  metal and  $0.3\%$  sulphide based on the composition of fresh metal and sulphide measured in NWA 5400.

As noted in Section 3.3.2, there are fundamental differences between the Pt/Os and Ir/Os values of brachinite-like achondrites, which have nearly chondritic-relative abundances of these elements, versus brachinites, and GRA 06128/9, which have lower ratios. Assuming precursor material with relative and absolute abundances of the HSE that were broadly chondritic, then HSE-rich materials

with abundances that are complementary to the sulphides and metals must be present elsewhere on the parent body(ies) of GRA 06128/9 and brachinites. These materials should be characterised by chondrite-normalised Pd/Os =  $1.45 \pm 0.26$ ; Pt/Os =  $1.41 \pm 0.24$ ; Ru/Os =  $0.83 \pm 0.14$ ; Ir/Os =  $1.28 \pm 0.20$ ; Re/Os =  $1.08 \pm 0.24$ , to complement relative abundances in the bulk brachinites and GRA 06128/9.

A possible mechanism for generating HSE fractionation in GRA 06128/9, brachinites and brachinite-like achondrites is by magmatic fractionation during melting of metal-bearing chondritic precursor materials. The distribution of HSE between a liquid metal phase and solid metal restite during partial melting in the Fe–Ni–S system is strongly dependent on the S-content of extracted melts, and on C and P that enter the metallic phase (Chabot and Jones, 2003; for the sake of simplicity and because of the

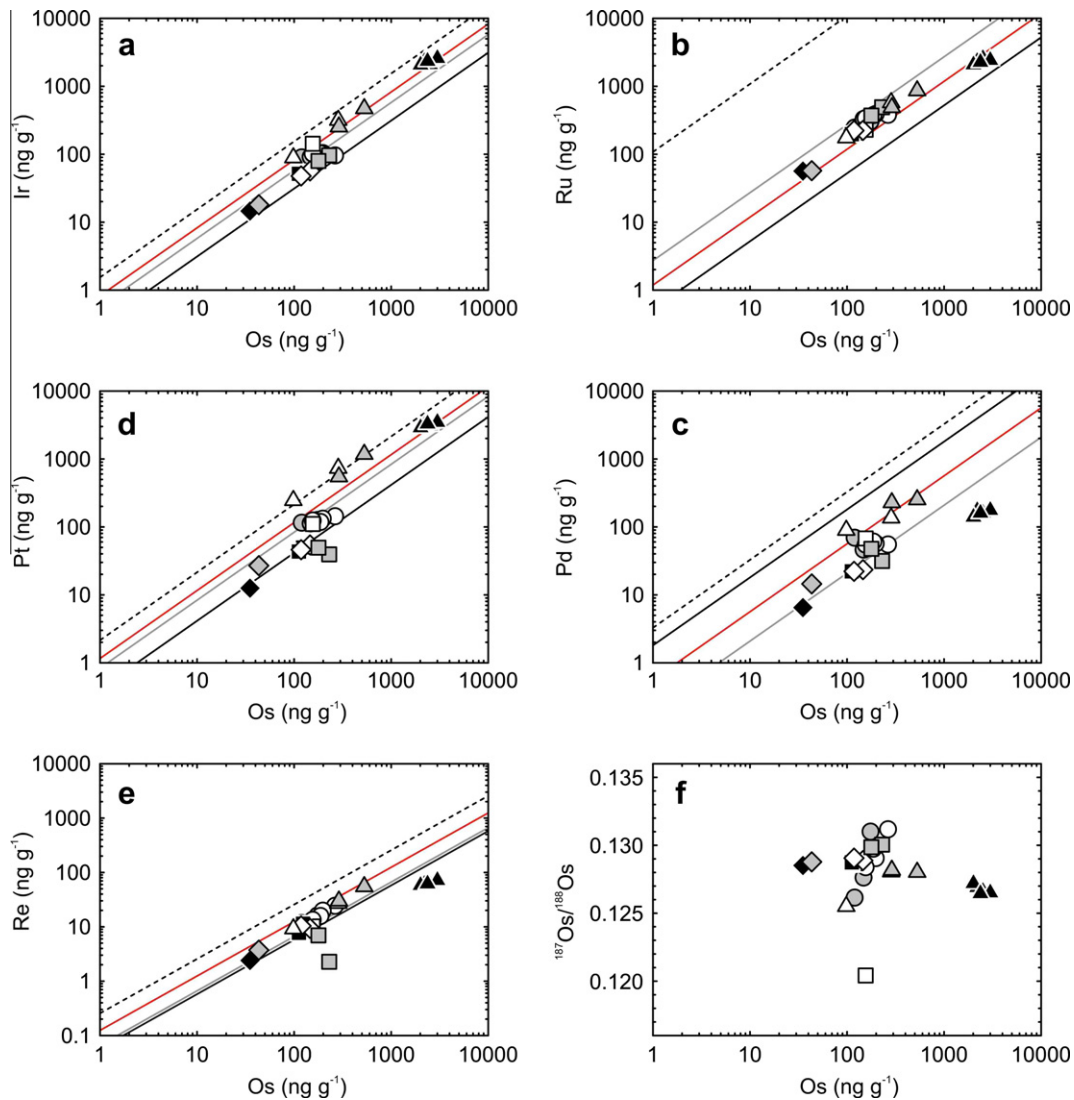


Fig. 13. Plots of Os abundance versus (a) Ir, (b) Ru, (c) Pd, (d) Pd, (e) Re abundances, and (f) present-day  $^{187}\text{Os}/^{188}\text{Os}$  in GRA 06128/9, brachinites and brachinite-like achondrites. Shown are compositional tie-lines of FeS (thick line) and pentlandite (red line) from GRA 06128/9, and metal (black line) and FeS (grey line) from NWA 5400. (For interpretation of the references to colour in this figure legend, the reader is referred to the web version of this article.)

lack of current evidence for elevated C or P in the parent body(ies) of GRA 06128/9, brachinites and brachinite-like achondrites, only S-content is considered in the following discussion). Therefore, HSE fractionations in GRA 06128/9, brachinites and brachinite-like achondrites could reflect partial extraction of metal liquids of variable S content from a chondritic starting composition. To explore this possibility we modelled batch-melting of metal with FeS removal and resultant residues using solid metal-liquid metal  $D$ -values from the parameterisation of Chabot and Jones (2003). The approach we used is similar to previous studies that modelled variable S contents during metal melt removal in ureilites (Rankenburg et al., 2008), chondritic components (Horan et al., 2010) and IVB iron meteorites (Walker et al., 2008). For the starting composition, we used CI-chondrite, Orgueil, due to its relatively elevated Pd/Os ( $\sim 1.3$ ), and assumed that all HSE were initially sited in metal. This was accompanied by HSE partitioning only between solid metal and liquid metal, consistent with high  $D$ -values for HSE ( $>10^4$ ) for metal-silicate at the low pressures of asteroidal interiors (e.g., Righter, 2003). It should

be noted that the choice of starting composition is important, because, although relative HSE fractionation between chondrites groups is minor compared to the observed HSE fractionation in GRA 06128/9, and brachinites in particular, the range of initial inter-element fractionation observed in chondrites is still significant (Pd/Os = 0.88–1.69). Because HSE preferentially partition into metal, the HSE concentration present in the metal will depend on the percentage of metal in the parent body, which is also a reflection of its oxidation state. To estimate initial metal abundance, we used the approach of Rankenburg et al. (2008), comparing total Fe and olivine composition in brachinites with the total Fe content of carbonaceous chondrites (e.g., Orgueil), which have relatively constant total Fe of  $\sim 24.5 \pm 1.5$  wt.% (Jarosewich, 1990). Given that total Fe in brachinites range from chondritic values to  $\sim 19$  wt.%, with relatively high Fe/Mg olivine ( $Fo_{64-72}$ ) yields no more than  $\sim 5\%$  Fe-metal loss.

It has previously been noted that the best measures of HSE fractionation during metallic liquid extraction for ureilites are plots of Pd/Os and Pt/Os (Rankenburg et al.,

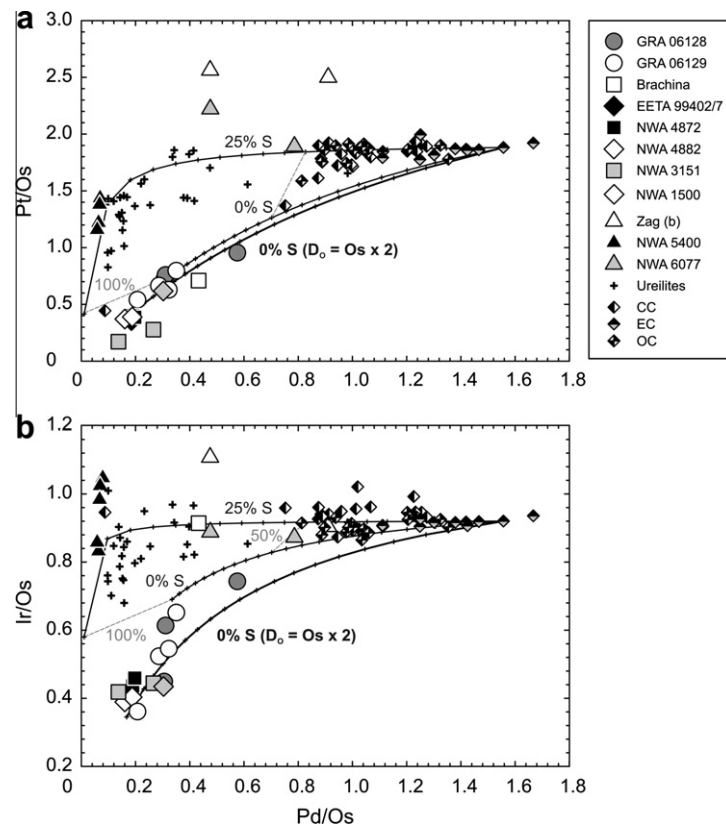


Fig. 14. Plots of Pd/Os versus (a) Pt/Os and (b) Ir/Os ratios for GRA 06128/9, brachinites, and brachinite-like achondrites, with calculated compositions of metal residues. Also shown are chondrite (Horan et al., 2003; Fischer-Gödde et al., 2010) and ureilite HSE compositions (Rankenburg et al., 2008). The melt calculations model the composition of residues that result from single episodes of batch melting. The starting HSE composition is the bulk composition of Orgueil with concentrations adjusted assuming that all of the HSE were originally in metal and that metal comprises 5% of the bulk. Curves show compositions of residues resulting from no sulphur, and 25% sulphur. Fractions of residue are labelled and are in increments of 5%. Solid metal-liquid metal  $D$  values were calculated using the parameterisation of Chabot and Jones (2003). The thick curve denotes  $D_o$  for Os that is two times greater than parameterised values (and greater than observed for IVB iron meteorites; Walker et al., 2008) required to explain brachinite and GRA 06128/9 Pd/Os and Ir/Os. Details of the models ( $D$ -values used from the parameterisation and equations are provided in the Online annex.

2008). While this plot is also effective for monitoring metallic liquid extraction in brachinite-like achondrites, the brachinites and GRA 06128/9 also show significant fractionation between traditionally 'compatible' HSE, Os and Ir. Given evidence for brachinites representing residues after 25–30% partial melting (c.f., lack of plagioclase in most samples, low abundances of silicate-compatible trace elements, and REE fractionation), this implies that Os, Ru and Re behaved compatibly, whereas Ir, Pt and Pd were relatively incompatible. This relative compatibility strongly contrasts with HSE behaviour in ureilites (Rankenburg et al., 2008), or in IVB iron meteorites (Walker et al., 2008). We have, therefore, performed model calculations for both Pt/Os–Pd/Os and for Ir/Os–Pd/Os (Fig. 14). Constructed curves for 0% and 25% S, using the parameterisation of Chabot and Jones (2003) are shown for Pd/Os versus Pt/Os and Ir/Os in Fig. 14.

If brachinite-like achondrites are treated separately from brachinites and GRA 06128/9, because of their different Pt/Os and Ir/Os, it is found that brachinite-like achondrites are similar to ureilites; this is in the sense that they fall along model residual compositions consistent with residual metal compositions after extraction of melts with high S contents (e.g., 25% S curve). In some respects, brachinite-like achondrites (and ureilites), have complementary characteristics to IVA, IIAB and IIIAB iron meteorites (c.f., Cook et al., 2004; Walker et al., 2005), possibly indicating a simple one-stage model for the removal of high-S metal melt from the brachinite-like achondrite source regions. By contrast, brachinites (and GRA 06128/9) fall close to the curve for 0% S, implying extraction of S-poor metal. In fact, the brachinites fall at Pt/Os and Pd/Os values that require total exhaustion of initial metal contents. The degree of metal exhaustion is dependent on temperature, initial metal/sulphide ratio in the starting material, and on the Pd/Os and Pt/Os values of the initial starting composition, regardless of the initial chondritic composition employed (Fig. 14). In this sense, the direct application of the parameterisation method fails for brachinites because the differences in D values for Pt and Ir versus Os are too small.

As described in Walker et al. (2008) there is an alternative method to that of the parameterisation method of Chabot and Jones (2003) for estimating changing D values for the HSE, which involves observation of linear trends on logarithmic plots of the HSE (e.g., Cook et al., 2004). The disadvantage of applying this technique to brachinites is that (1) the initial D(Ir) is normally chosen as an 'anchor' because its solid metal-liquid metal partitioning is the best experimentally constrained for the HSE, yet Ir appears unusually fractionated relative to the other HSE in brachinites and GRA 06128/9, and (2) the limited dataset for these meteorites does not define particularly well-correlated linear trends (e.g., Fig. 13). Instead, we estimated what the parameterisations would need to be in order to explain the HSE abundances in GRA 06128/9 and brachinites. Assuming 0% S in the metal, the simplest method for fitting the observed brachinite data is to increase  $D_o$  for Os from 2 to 4 and to retain parameterisations for  $D_o$  of Ir (1.5), Pt (0.81) and Pd (0.43; Chabot and Jones, 2003; Fig. 14). However, since Re/Os is minimally fractionated during

metallic partial melt extraction (because of similar solid metal-liquid metal D-values at 0–30% S; Rankenburg et al., 2008) and  $^{187}\text{Os}/^{188}\text{Os}$  for GRA 06128/9, and brachinites are within the range of chondritic meteorites, it appears that  $D_o$  for Pt, Pd and Ir are lower than predicted from parameterisations. Since  $D_o$  is defined as the D in the end member non-metal-free Fe–Ni system these arguments illustrate the problem of the relatively low S required during liquid metal-solid metal partitioning in GRA 06128/9 and brachinites, which does not allow the required fractionations by simple one-step batch melting of chondritic precursors. We suggest four possibilities to explain this discrepancy:

- 1) Multiple phases in the residue. In this scenario both metal and sulphide were retained in the brachinite residue during metal melt-solid melt partitioning. These conditions may satisfy the low calculated S-content of the calculated metal melt, because S is retained in the residue. Evidence for inefficient melt extraction and retention of sulphide ( $\pm$  metal) is evident in some brachinites (e.g., EET 99402/7 and ALH 84025; Warren and Kallemeyn, 1989). However, this scenario also requires high proportions of metal and appears inconsistent with the moderate degrees of partial melting (13–30%) involved in the genesis of GRA 06128/9 and brachinites, and the tendency for Fe–Ni–S melts to be the first to form during partial melting of chondritic pre-cursors.
- 2) Two-stage melt fractionation. In this case, after generation of an initial melt, secondary melting occurred. A simple example for this behaviour is to take the composition of a brachinite-like achondrite with high Pd/Os, such as NWA 6077 and to model fractional crystallisation behaviour. However, we find that any reasonable metal melt S-content (0–25%) and using parameterisation from Chabot and Jones (2003), or determination of D-values from iron meteorites (Walker et al., 2008) will not generate strong enough fractionation to account for (Pd, Pt, Ir)/Os observed in brachinites and GRA 06128/9.
- 3) Fractional fusion. Fractional fusion is where crystal compositional paths remain constant, but liquid paths have compositional breaks in response to temperature intervals, where addition of heat generates no melting (e.g., Presnall, 1969). Fractional fusion differs from equilibrium fusion in that liquids become immediately isolated from the residue as soon as they are formed, preventing further reaction. Such behaviour might result in the fractionation of HSE as a consequence of variable melt compositions during asteroidal partial melting. For example, generation of Fe–Ni–S melts at relatively low temperatures ( $\sim 988^\circ\text{C}$ ), to basaltic melts at higher temperatures ( $>1050^\circ\text{C}$ ) can potentially lead to such effects. If fractional fusion is responsible for the low Pt/Os, Pd/Os and Ir/Os observed in brachinites, and GRA 06128/9 there must be high Pt/Os, Pd/Os and Ir/Os melts, that are presumably S-rich, missing from our existing meteorite collections.

- 4) A non-chondritic starting composition. The parent body of brachinites and GRA 06128/9 did not have chondritic relative initial abundances of the HSE. At first glance this method for generating the low Ir/Os and Pd/Os values does not appear to be consistent with our understanding of nebular fractionation effects. For example, while the consistently low (Pd/Os)<sub>CI</sub> of GRA 06128/9 ( $0.27 \pm 0.09$ ) and brachinites ( $0.18 \pm 0.08$ ) are too low to be directly inherited from any known chondrite group (0.88–1.69; c.f., Horan et al., 2003; Fischer-Gödde et al., 2010), these ratios are similar to those of brachinite-like achondrites and ureilites, which do not show similar Ir/Os or Pt/Os to GRA 06128/9 and brachinites. This point appears to be reinforced by the fact that, if Ir/Os in GRA 06128/9 and brachinites reflect nebular fractionation effects, the large differences in Pd versus Ir and Os 50% condensation temperatures should have led to Pd/Os spanning several orders of magnitude difference between the different meteorite groups studied here, which is not the case. Indeed, the source composition of brachinites in this scenario would require extremely low Pt/Os and Ir/Os values, relative to CI-chondrites, which doesn't appear currently possible based on materials observed in the terrestrial collection of meteorites, or from our current understanding of nebular processes.

In summary, the absolute and relative abundances of the HSE in GRA 06128/9, brachinites and brachinite-like achondrites are consistent with removal of metal of variable S content, and in the case of GRA 06128/9 and brachinites, under unusual partitioning, or two-stage fractional crystallization of the HSE. However the unusual Pt/Os and Ir/Os of brachinites were generated, they are clearly distinct from brachinite-like achondrites, precluding a direct genetic-link between these meteorites, and consistent with their petrology (Section 4.1).

#### 4.7. Origins of GRA 06128/9, brachinites and brachinite-like achondrites

Given the presented evidence, GRA 06128/9, brachinites and brachinite-like achondrites may be process-related, with permissive evidence for genetic links between GRA 06128/9 and brachinites. A number of future observations would be expected based on these relationships. First, high-precision chronological work would be expected to yield crystallisation ages and thermal/shock disturbances that remain consistent for GRA 06128/9 and brachinites. Second, the meteorites should also share complementary behaviour in terms of both radiogenic (e.g., Sr, Nd, Hf, W) and stable (e.g., Li, Zn, Fe, Mg, Si) isotope systems (providing terrestrial alteration can be overcome for some of these systems). Third, if GRA 06128/9 and brachinites are genetically related, then it would be anticipated that single or closely-related asteroidal bodies will be located with both felsic and olivine-dominated mineral assemblages (Sunshine et al., 2009). Such bodies could have a carapace of felsic crust, or may show a crustal dichotomy of felsic

and olivine-dominated lithologies. Remote sensing of asteroids shows that, where detected, the preponderance of crust is basaltic. Nevertheless, feldspar-rich crust may not be uncommon in the asteroid belt. Feldspar does not typically have strong adsorptions in the near-infrared, but its relatively high albedo may be a diagnostic feature. However, bright asteroids identified to date (E-type asteroids) include adsorptions indicative of low-Fe pyroxenes (Clark et al., 2004), inconsistent with the known mineralogy of the GRA 06128/9 meteorites (Day et al., 2009a). Based on their possible genetic link, the GRA 06128/9 parent body may be found near possible brachinite parent bodies, identified among the olivine-rich asteroids based on reflectance spectra consistent with FeO-rich olivine found in brachinites (Sunshine et al., 2007).

GRA 06128/9 represent partial melts from a previously undifferentiated body, indicating that their volumetric extent can be broadly estimated. One scenario is that GRA 06128/9 represent 'pods' or 'dykes' of evolved material. An example is heterogeneous distribution of lithologies in the Caddo County IAB iron meteorite, where silicate inclusions (Takeda et al., 2000) have similar major-element compositions to GRA 06128/9. On the other hand, it is well-demonstrated that the contemporary flux of meteorites is biased and unrepresentative of Solar System materials because of the complex sequence of events required to bring a meteorite from its parent body to Earth (Warren, 1994). These biases include, but are not limited to, longevity of the parent body, location of asteroids near dynamically favourable delivery zones/resonances, impact-excavation and preservation of the meteorite from its parent body, and low-velocity collision with Earth. While these arguments do not constrain the size of parent bodies, they do imply that meteorites are probably representative portions of more extensive lithologies. The GRA 06128/9 meteorites, therefore, provide the first definitive evidence for generation of significant quantities of felsic melt on an asteroid parent body (Day et al., 2009a). Extensive masses of GRA 06128/9-like lithologies may be expected given the process and possible genetic links with brachinites, requiring 13–30% melting of their parent body. On a precursor chondritic parent body of 50 km diameter, and assuming no loss of volatiles or volcanic materials into space and 13–30% melting of the entire body, this would equate to  $6.5\text{--}19 \times 10^3$  km<sup>3</sup> of felsic material.

Identification of felsic melts such as GRA 06128/9 as early formed ( $\sim 4.56$  Ga; Day et al., 2009a; Shearer et al., 2010) partial melt products of a volatile-rich source has significant bearing on the thermal history of their parent body, and parent bodies to brachinites, brachinite-like achondrites, and possibly other primitive achondrites (e.g., ureilites, lodranite-acapulcoites). The short-lived ( $T^{1/2} = 7.17 \times 10^5$  a) radioactive isotope <sup>26</sup>Al is considered one of the most important heat sources during inception of asteroidal melting (e.g., Mittlefehldt, 2007). During heating of an asteroid immediately after formation it is possible to generate runaway melting as radioactive heat is produced and melting progresses. However, this is clearly not what occurred in partially differentiated primitive achondrite meteorites. In the case of GRA 06128/9, brachinites and brachinite-like

achondrites, we propose that early melting and segregation of Al-rich melts (c.f., GRA 06128/9) acted to halt melting on their parent body(ies). Similar suggestions have been made for the missing Al-rich melts to the ureilite (e.g., Cohen et al., 2004) and aubrite parent bodies (e.g., Keil, 2010), and the GRA 06128/9 meteorites and their relation to brachinites serves to reinforce this concept. Whether the process of Al-rich melt removal is restricted to volatile-rich parent bodies, or if there is an asteroidal ‘size’ threshold beyond which such a process can be effective is unclear. However, this mechanism offers a potential explanation for the apparent inefficiency of melting processes in primitive achondrite meteorite parent bodies, in addition to possible shock-melting processes on some asteroidal parent bodies (Rubin, 2007).

## 5. CONCLUSIONS

We report new petrological and geochemical data, including mineral and whole-rock trace-element data for GRA 06128/9, six brachinites (Brachina; EET 99402/7; NWA 1500; NWA 3151; NWA 4872; NWA 4882) and three brachinite-like ultramafic achondrites (NWA 5400; NWA 6077; Zag (b)). These new data support derivation of GRA 06128/9, brachinites and brachinite-like achondrites from volatile-rich and oxidised ‘chondritic’ precursor sources within asteroidal parent bodies. Chronological information suggests similar crystallisation ages for GRA 06128/9 and brachinites early in Solar System history and prolonged thermal and shock disturbance is also recorded for the samples. It is possible to generate residue compositions, such as brachinites and brachinite-like ultramafic achondrites by relatively inefficient removal of silica-saturated felsic melt compositions, like GRA 06128/9, through 13–30% partial melting of a chondritic source. The range in whole-rock trace element compositions for brachinites and brachinite-like achondrites can be explained by minor trapped phosphate and plagioclase in some samples, implying inefficient melt segregation. Moderate degrees of partial melting to form the GRA 06128/9 meteorites are also consistent with highly- (e.g., Os, Ir, Ru, Pt, Pd, Re) and moderately-siderophile (e.g., Mo, W) element abundances that are within a factor of ~2–10 times chondritic abundances, and so is also consistent with concomitant generation of Fe–Ni–S melts. However, the mechanism responsible for the HSE compositions of brachinite-like achondrites differs from GRA 06128/9 and brachinites.

A model is proposed whereby planetesimals, which formed from volatile-rich primitive ‘chondritic’ material, partially melted (13–30%) generating oxidised, high Fe/Mg and plagioclase-normative melts, with early evolution of Fe–Ni–S melts. These melts were then inefficiently extracted from their source generating a range of residue compositions from dominantly olivine-pyroxene residues to rocks with high proportions of sulphide, metal, plagioclase and phosphate. Melting was halted, possibly due to the exhaustion of short-lived radionuclides (e.g.,  $^{26}\text{Al}$ ) as a function of age and felsic melt removal; this was followed by a period of thermal equilibration punctuated by impact-related shock events as late as 2.3–2.7 Ga. These

observations are consistent with the compositions of brachinites and brachinite-like ultramafic achondrites, as well as the range of  $\Delta^{17}\text{O}$  values recorded in these rocks, which are potentially diagnostic of a parent body(ies) that did not witness large-scale differentiation. We argue that felsic material such as GRA 06128/9, and relatively high Fe/Mg olivine-rich rocks such as brachinites may be genetically related (i.e., same parent body), and that brachinite-like ultramafic achondrites probably formed by analogous processes, but on different parent bodies. The size, scale and preservation of GRA 06128/9 and brachinites, possibly as crudely formed evolved asteroidal crust (Day et al., 2009a) and variably depleted mantle material, respectively, are currently unclear, but may be revealed by remotely sensed data of asteroids in the inner main belt. The current classification of brachinites and brachinite-like achondrites as ‘primitive achondrites’ is somewhat misleading, given their association to felsic ‘non-primitive achondrites’ and their complex and extensive partial differentiation histories.

## ACKNOWLEDGEMENTS

We are grateful to G.M. Hupé, T. McCoy, I. Nickin, the Meteorite Working Group and the NASA JSC curatorial facility staff for provision and preparation of samples used in this study. We thank B. Hyde and L. Hallis for informal comments, S. Russell for editorial handling, and H. Downes, C. Shearer and an anonymous for constructive journal reviews. This work was supported by the NASA Cosmochemistry program: NNX10AG94G (R.J.W.), NNX07AI48G (D.R.), NNX08AH76G (W.F.M.), and NNX08AG54G (L.A.T.), and by SIO start-up funds to J.M.D.D.

## APPENDIX A. SUPPLEMENTARY DATA

Supplementary data associated with this article can be found, in the online version, at [doi:10.1016/j.gca.2011.12.017](https://doi.org/10.1016/j.gca.2011.12.017).

## REFERENCES

- Arai T., Tomiyama T., Saiki K. and Takeda H. (2008) Unique achondrites GRA 06128/06129: Andesitic partial melt from a volatile-rich parent body. *Lunar and Planetary Science Conference*, 39th, 2465 (abstr.).
- Barrat J. A., Yamaguchi A., Greenwood R. C., Benoit M., Cotton J., Bohn M. and Franchi I. A. (2008) Geochemistry of diogenites: still more diversity in their parental melts. *Meteor. Planet. Sci.* **43**, 1759–1775.
- Benedix G. K., McCoy T. J., Keil K., Bogard D. D. and Garrison D. H. (1998) A petrologic and isotopic study of winonaites: evidence for early partial melting, brecciation, and metamorphism. *Geochim. Cosmochim. Acta* **62**, 2535–2553.
- Becker H., Horan M. F., Walker R. J., Gao S., Lorand J.-P. and Rudnick R. L. (2006) Highly siderophile element composition of the Earth’s primitive upper mantle: constraints from new data on peridotite massifs and xenoliths. *Geochim. Cosmochim. Acta* **70**, 4528–4550.
- Birck J.-L., Roy-Barman M. and Capmas F. (1997) Re–Os isotopic measurements at the femtomole level in natural samples. *Geostand. Newslett.* **21**, 21–28.
- Bogard D. D., Nyquist L. E., Johnson P., Wooden J. and Bansal B. (1983) Chronology of Brachina. *Meteoritics* **18**, 269–270 (Abs.).

- Chabot N. L. and Jones J. H. (2003) The parameterization of solid metal–liquid metal partitioning of siderophile elements. *Meteorit. Planet. Sci.* **38**, 1425–1436.
- Choi B.-G., Ouyang X. and Wasson J. T. (1995) Classification and origin of IAB and III CD iron meteorites. *Geochim. Cosmochim. Acta* **59**, 593–612.
- Clark B.-E., Bus S. J., Rivkin A. S., McConnochie T., Sanders J., Shah S., Hiroi T. and Shepard M. (2004) E-type asteroid spectroscopy and compositional modelling. *J. Geophys. Res.* **109**. doi:10.1029/2003JE002200.
- Cohen B. A., Goodrich C. A. and Keil K. (2004) Feldspathic clast populations in polymict ureilites: stalking the missing basalts from the ureilite parent body. *Geochim. Cosmochim. Acta* **68**, 4249–4266.
- Cook D. L., Walker R. J., Horan M. F., Wasson J. T. and Morgan J. W. (2004) Pt–Re–Os systematics of group IIAB and IIIAB iron meteorites. *Geochim. Cosmochim. Acta* **68**, 1413–1431.
- Connolly, Jr., H. C., Smith C., Benedix G., Folco L., Richter K., Zipfel J., Yamaguchi A. and Chennaoui Aoudjehane H. (2008) The Meteoritical Bulletin, No. 93. *Meteorit. Planet. Sci.* **43**, 571–632.
- Craig J. R. and Kullerud G. (1968) The Cu–Fe–Ni–S System. *Carnegie Inst. Washington, Yearbook*, vol. 66, pp. 413–417.
- Day J. M. D., Floss C., Taylor L. A., Anand M. and Patchen A. D. (2006a) Evolved mare basalt magmatism, high Mg/Fe feldspathic crust, chondritic impactors, and the petrogenesis of Antarctic lunar breccia meteorites Meteorite Hills 01210 and Pecora Escarpment 02007. *Geochim. Cosmochim. Acta* **70**, 5957–5989.
- Day J. M. D., Taylor L. A., Floss C., Patchen A. D., Schnare D. W. and Pearson D. G. (2006b) Comparative petrology, geochemistry, and petrogenesis of evolved, low-Ti mare basalt meteorites from the LaPaz Icefield, Antarctica. *Geochim. Cosmochim. Acta* **70**, 1581–1600.
- Day J. M. D., Pearson D. G. and Taylor L. A. (2007) Highly siderophile element constraints on accretion and differentiation of the Earth–Moon system. *Science* **315**, 217–219.
- Day J. M. D., Pearson D. G. and Hulbert L. J. (2008) Rhenium–osmium isotope and platinum–group element constraints on the origin and evolution of the 1.27 Ga Muskox layered intrusion. *J. Petrol.* **49**, 1255–1295.
- Day J. M. D., Ash R. D., Liu Y., Bellucci J. J., Rumble D. I. I., McDonough W. F., Walker R. J. and Taylor L. A. (2009a) Early formation of evolved asteroidal crust. *Nature* **457**, 179–182.
- Day J. M. D., Walker R. J., Sunshine J. M., Ash R. D., Rumble D., Liu Y., McDonough W. F. and Taylor L. A. (2009b) The role of volatiles during asteroidal differentiation. *Geochim. Cosmochim. Acta* **73**, A269 (Abs.).
- Day J. M. D., Ash R. D., Liu Y., Bellucci J. J., Rumble D. I. I., McDonough W. F., Walker R. J. and Taylor L. A. (2009c) Asteroids and andesites – reply. *Nature* **459**. doi:10.1038/nature08078.
- Day J. M. D., Walker R. J., James O. B. and Puchtel I. S. (2010) Osmium isotope and highly siderophile element systematics of the lunar crust. *Earth Planet. Sci. Lett.* **289**, 595–605.
- Delaney J. S., Zanda B., Clayton R. N. and Mayeda T. (2000) Zag (b): a ferroan achondrite intermediate between brachinites and lodranites. *Lunar and Planetary Science Conference. XXXI*. 1745 (abstr.).
- Feldstein S. N., Jones R. H. and Papke J. J. (2001) Disequilibrium partial melting experiments of the Leedey L6 chondrite: textural controls on melting processes. *Meteorit. Planet. Sci.* **36**, 1421–1441.
- Fischer-Gödde M., Becker H. and Wombacher F. (2010) Rhodium, gold and other highly siderophile element abundances in chondritic meteorites. *Geochim. Cosmochim. Acta* **74**, 356–379.
- Floss C. (2000) Complexities on the acapulcoite-lodranite parent body: evidence from trace element distributions in silicate minerals. *Meteorit. Planet. Sci.* **35**, 1073–1085.
- Floss C., Taylor L. A., Promprated P. and Rumble, III, D. (2005) Northwest Africa 011: a ‘eucritic’ basalt from a non-eucrite parent body. *Meteorit. Planet. Sci.* **40**, 343–359.
- Goodrich C. A., Jones J. H. and Berkley J. L. (1987) Origin and evolution of the ureilite parent magmas: multi-stage igneous activity on a large parent body. *Geochim. Cosmochim. Acta* **51**, 2255–2273.
- Goodrich C. A., Scott E. R. D. and Fioretti A. M. (2004) Ureilitic breccias: clues to the petrologic structure and impact disruption of the ureilite parent body. *Chem. de Erde* **64**, 283–327.
- Goodrich C. A., Wlotzka F., Ross D. K. and Bartoschewitz R. (2006) Northwest Africa 1500: plagioclase-bearing monomict ureilite or ungrouped achondrite? *Meteorit. Planet. Sci.* **41**, 925–952.
- Goodrich C. A., Van Orman J. A. and Wilson L. (2007) Fractional melting and smelting of the ureilite parent body. *Geochim. Cosmochim. Acta* **71**, 2876–2895.
- Goodrich C. A., Kita N. T., Spicuzza M. J., Valley J. W., Zipfel J., Mikouchi T. and Miyamoto M. (2011) The Northwest Africa 1500 meteorite: not a ureilite, maybe a brachinite. *Meteorit. Planet. Sci.* **45**, 1906–1928.
- Greenwood R. C., Franchi I. A., Jambon A. and Buchanan P. C. (2005) Widespread magma oceans on asteroidal bodies in the early Solar System. *Nature* **435**, 916–918.
- Grossman J. N. (1998) The Meteoritical Society Bulletin, No. 82. *Meteorit. Planet. Sci.* **33**, A221–A239.
- Horan M. F., Walker R. J., Morgan J. W., Grossman J. N. and Rubin A. E. (2003) Highly siderophile elements in chondrites. *Chem. Geol.* **196**, 5–20.
- Horan M. F., Alexander C. M. O’ D. and Walker R. J. (2010) Highly siderophile element evidence for early solar system processes in components from ordinary chondrites. *Geochim. Cosmochim. Acta* **73**, 6984–6997.
- Ikeda Y. and Prinz M. (2001) Magmatic inclusions and felsic clasts in the Dar al Gani 319 polymict ureilite. *Meteorit. Planet. Sci.* **36**, 481–499.
- Irving A. J. and Rumble D. (2006) Oxygen isotopes in Brachina, SAH 99555, and Northwest Africa 1054. *Meteorit. Planet. Sci.* **41**, A84 (Abs.).
- Irving A. J., Kuehner S. M. and Rumble D. (2005) Brachinite NWA 3151 and (?) brachinite NWA 595. *Meteorit. Planet. Sci.* **40**, 5213 (Abs.).
- Irving A. J., Rumble D., Kuehner S. M., Gellissen M. and Hupé G. M. (2009) Ultramafic achondrite Northwest Africa 5400: a unique brachinite-like meteorite with terrestrial oxygen isotopic composition. *Lunar and Planetary Science Conference, 40th*. 2332 (abstr.).
- Jarosewich E. (1990) Chemical analyses of meteorites: a compilation of stony and iron meteorite analyses. *Meteoritics* **25**, 323–337.
- Jolliff B. L., Hughes J. M., Freeman J. J. and Zeigler R. A. (2006) Crystal chemistry of lunar merrillite and comparison to other meteoritic and planetary suites of whitlockite and merrillite. *Am. Mineral.* **91**, 1583–1595.
- Jurewicz A. J. G., Mittlefehldt D. W. and Jones J. H. (1991) Partial melting of the Allende (CV) meteorite: implications for the origin of basaltic meteorites. *Science* **252**, 695–698.
- Jurewicz A. J. G., Mittlefehldt D. W. and Jones J. H. (1995) Experimental partial melting of the St. Severin (LL) and Lost City (H) chondrites. *Geochim. Cosmochim. Acta* **59**, 391–408.
- Keil K. (2010) Enstatite achondrite meteorites (aubrites) and the histories of their asteroidal parent bodies. *Chem. Der Erde* **70**, 295–317.

- Kushiro I. (1975) On the nature of silicate melt and its significance in magma genesis: regularities in the shift of the liquidus boundaries involving olivine, pyroxene, and silica minerals. *Am. J. Sci.* **275**, 411–431.
- Liu Y., Taylor L. A., Ash R. D. and Day J. M. D. (2008) Mineralogy and petrology of a strange achondrite GRA 06129. *Lunar and Planetary Science Conference*, **39th**. 1830 (abstr.).
- McBride K. and McCoy T. (2000) EET 99402/EET 99407. *Antarct. Meteorit. Newslett.* **23**, 2. <http://curator.jsc.nasa.gov/antmet/index.cfm>.
- McCoy T., Scott E. R. D. and Haack H. (1993) Genesis of the IIICD iron meteorites: evidence from silicate-bearing inclusions. *Meteoritics* **28**, 552–560.
- McCoy T., Keil K., Clayton R. N., Mayeda T. K., Bogard D. D., Garrison D. H. and Wieler R. (1997) A petrologic and isotopic study of lodranites: evidence for early formation as partial melt residues from heterogeneous precursors. *Geochim. Cosmochim. Acta* **61**, 623–637.
- McCoy T., Mittlefehldt D. W. and Wilson L. (2006) Asteroid differentiation. In *Meteorites and the Early Solar System II* (eds. D. S. Lauretta and H. Y. McSween). University of Arizona Press, Tucson, pp. 733–745.
- McDonough W. F. and Sun S.-S. (1995) The composition of the Earth. *Chem. Geol.* **120**, 223–254.
- Mikouchi T. and Miyamoto M. (2008) Mineralogy and pyroxene cooling rate of unique achondrite meteorite GRA 06129. *Lunar and Planetary Science Conference*, 39th. 2297 (abstr.).
- Miller M. F. (2002) Isotopic fractionation and the quantification of  $^{17}\text{O}$  anomalies in the oxygen three-isotope system: an appraisal and geochemical significance. *Geochim. Cosmochim. Acta* **66**, 1881–1889.
- Mittlefehldt, D. W., 2007. Achondrites. In: *Meteorites, Comets and Planets* (ed. A. M. Davis). Treatise on Geochemistry Update 1. Elsevier, pp. 1–40. doi: [10.1016/B0-08-043751-6/01064-1](https://doi.org/10.1016/B0-08-043751-6/01064-1), (Chapter 1.11).
- Mittlefehldt D. W. (1986) Fe–Mn–Mg relations and of ureilite olivines and pyroxenes and the genesis of ureilites. *Geochim. Cosmochim. Acta* **50**, 107–110.
- Mittlefehldt D. W., Lindstrom M. M., Bogard D. D., Garrison D. H. and Field S. W. (1996) Acapulco- and Lodran-like achondrites: petrology, geochemistry, chronology and origin. *Geochim. Cosmochim. Acta* **60**, 867–882.
- Mittlefehldt D. W., Killgore M. and Lee M. T. (2002) Petrology and geochemistry of D'Orbigny, geochemistry of Sahara 99555, and the origin of angrites. *Meteorit. Planet. Sci.* **32**, 345–369.
- Mittlefehldt D. W., Bogard D. D., Berkley J. L. and Garrison D. H. (2003) Brachinites: igneous rocks from a differentiated asteroid. *Meteorit. Planet. Sci.* **38**, 1601–1625.
- Morse S. A. (1980) *Basalts and Phase Diagrams: An Introduction to the Quantitative Use of Phase Diagrams in Igneous Petrology*. Springer-Verlag, New York Berlin Heidelberg, 493pp.
- Nehru C. E., Prinz M., Delaney J. S., Dreibus G., Palme H., Spettel B. and Wänke H. (1983) Brachina: a new type of meteorite, not a chassignite. *Proceedings of the Lunar and Planetary Science Conference*, 10th. 817–832.
- Nehru C. E., Prinz M., Weisberg M. K., Edihara M. E., Clayton R. N. and Mayeda T. K. (1992) Brachinites: a new primitive achondrite group. *Meteoritics* **27**, 267 (Abs.).
- Nehru C. E., Prinz M., Weisberg M. K., Ebihara M. E., Clayton R. N. and Mayeda T. K. (1996) A new brachinite and petrogenesis of the group. *Lunar and Planetary Science Conference*, 27th, 943–944 (abstr.).
- Nyquist L. E., Shih C. -Y. and Reese Y. D. (2009) Early petrogenesis and late impact (?) metamorphism on the GRA 06128/9 parent body. *Lunar and Planetary Science Conference*, 40th, 1290 (abstr.).
- Petaev M. I., Barsukova L. D., Lipschutz M. E., Wang M.-S., Ariskin A. A., Clayton R. N. and Mayeda T. K. (1994) The Divnoe meteorite: petrology, chemistry, and oxygen isotopes and origin. *Meteoritics* **29**, 182–199.
- Presnall D. C. (1969) The geometric analysis of partial fusion. *Am. J. Sci.* **267**, 1178–1194.
- Prinz M., Wagoner D. G. and Hamilton P. J. (1980) Winonaites: a primitive achondritic group related to silicate inclusions in IAB irons. *Lunar and Planetary Science*, **XI**, 902–904 (abstr.).
- Prinz M., Nehru C. E., Delaney J. S. and Weisberg M. (1983) Silicates in IAB and IIICD irons, winonaites, lodranites, and Brachina: a primitive and a primitive-modified group. *Lunar and Planetary Science*, **XIV**. 616–617 (abstr.).
- Rankenburg K., Brandon A. D. and Humayun M. (2007) Osmium isotope systematics of ureilites. *Geochim. Cosmochim. Acta* **71**, 2402–2413.
- Rankenburg K., Humayun M., Brandon A. D. and Herrin J. S. (2008) Highly siderophile elements in ureilites. *Geochim. Cosmochim. Acta* **72**, 4642–4659.
- Righter K. (2003) Metal-silicate partitioning of siderophile elements and core formation in the early Earth. *Annu. Rev. Earth Planet. Sci.* **31**, 135–174.
- Rubin A. E. (2007) Petrogenesis of acapulcoites and lodranites: a shock-melting model. *Geochim. Cosmochim. Acta* **71**, 2383–2401.
- Rumble D., Farquhar J., Young E. D. and Christensen C. P. (1997) In situ oxygen isotope analysis with an excimer laser using  $\text{F}_2$  and  $\text{BrF}_5$  reagents and  $\text{O}_2$  gas as analyte. *Geochim. Cosmochim. Acta* **61**, 4229–4234.
- Rumble D., Miller M. F., Franchi I. A. and Greenwood R. C. (2007) Oxygen three-isotope fractionation lines in terrestrial silicate minerals: an inter-laboratory comparison of hydrothermal quartz and eclogitic garnet. *Geochim. Cosmochim. Acta* **71**, 3592–3600.
- Rumble D., Irving A. J., Bunch T. E., Wittke J. H. and Kuehner S. M. (2008) Oxygen isotopic and petrological diversity among brachinites NWA 4872, NWA 4874, NWA 4882 and NWA 4969: How many ancient parent bodies? *Lunar and Planetary Science Conference*, 39th. 1974 (abstr.).
- Satterwhite C. and McBride K. (2007) GRA 06128/GRA 06129. *Antarct. Meteorit. Newslett.* **30**, 2. <http://curator.jsc.nasa.gov/antmet/index.cfm>.
- Sessler R., Hess P. C. and Rutherford M. J. (1982) Liquidus relations in the forsterite–silica–anorthosite–albite system at 1 atmosphere. *Lunar and Planetary Science*, **XIII**, 710–711, Lunar and Planetary Institute, Houston. (abstr.).
- Shearer C. K., Burger P. V., Neal C., Sharp Z., Spivak-Birndorf L., Borg L., Fernandes V., Papike J. J., Karner J., Wadhwa M., Gaffney A. M., Shafer J., Geissman J., Atudorei N.-V., Herd C., Weiss B. P., King P. L., Crowther S. A. and Gilmour J. D. (2010) Non-basaltic asteroidal magmatism during the earliest stages of Solar System evolution. A view from Antarctic achondrites Graves Nunataks 8 and 06129. *Geochim. Cosmochim. Acta* **74**, 1172–1199.
- Shukolyukov A., Lugmair G., Day J. M. D., Walker R. J., Rumble D. III, Nakashima D., Nagao K. and Irving A. J. (2010) Constraints on the formation age, highly siderophile element budget and noble gas isotope compositions of Northwest Africa 5400: an ultramafic achondrite with terrestrial isotope characteristics. *Lunar and Planetary Science Conference*, 41st. 1492 (abstr.).
- Smoliar M. I., Walker R. J. and Morgan J. W. (1996) Re–Os ages of group IIA, IIIA, IVA and IVB iron meteorites. *Science* **271**, 1099–1102.
- Spicuzza M. J., Day J. M. D., Taylor L. A. and Valley J. W. (2007) Oxygen isotope constraints on the origin and differentiation of the Moon. *Earth Planet. Sci. Lett.* **253**, 254–265.

- Sunshine J. M., Bus S. J., Corrigan C. M., McCoy T. J. and Burbine T. H. (2007) Olivine-dominated asteroids and meteorites: distinguishing nebular and igneous histories. *Meteorit. Planet. Sci.* **42**, 155–170.
- Sunshine J. M., Day J. M. D., Ash R. D., McCoy T. J., Bus S. J., Klima R. J. and Hiroi T. (2009) Searching for the evolved crust of oxidized asteroids. *Lunar and Planetary Science Conference*, 40th, 1965.
- Swindle T. D., Kring D. A., Burkland M. K., Hill D. H. and Boynton W. V. (1998) Noble gases, bulk chemistry, and petrography of olivine-rich achondrites Eagles Nest and Lewis Cliff 88763: comparison to brachinites. *Meteorit. Planet. Sci.* **33**, 31–48.
- Takeda H., Bogard D. D., Mittlefehldt D. W. and Garrison D. H. (2000) Mineralogy, petrology, chemistry, and  $^{39}\text{Ar}$ – $^{40}\text{Ar}$  and exposure ages of the Caddo County IAB iron: evidence for early partial melt segregation of a gabbro area rich in plagioclase-diopside. *Geochim. Cosmochim. Acta* **64**, 1311–1327.
- Taylor S. R. (1975) *Lunar Science: A Post-Apollo View*. Pergamon Press, New York, 390pp.
- Taylor L. A. and Liu Y. (2009) Sulfide inclusions in diamonds: not monosulfide solid solution. *Russ. Geol. Geophys.* **50**, 1201–1211.
- Taylor L. A., Patchen A., Taylor D. H. S., Chambers J. G. and McKay D. S. (1996) X-ray digital imaging petrography of lunar mare soils: modal analyses of minerals and glasses. *Icarus* **124**, 500–512.
- Tuttle O. F. and Bowen N. L. (1958) Origin of granite in the light of experimental studies in the system  $\text{NaAlSi}_3\text{O}_8$ – $\text{KAlSi}_3\text{O}_8$ – $\text{SiO}_2$ – $\text{H}_2\text{O}$ . *Geol. Soc. Am. Mem.* **74**, p. 153.
- Treiman A. H., Morris R. V., Kring D. A., Mittlefehldt D. W. and Jones J. H. (2008) Petrography and origin of the unique achondrite GRA 06128 & 06129: preliminary results. *Lunar and Planetary Science Conference*, 39th. 2215 (abstr.).
- Usui T., Jones J. H. and Mittlefehldt D. W. (2010a) Low-degree partial melting experiments of CR and H chondrite compositions: implications for asteroidal magmatism recorded in GRA 06128 and GRA 06129. *Lunar and Planetary Science Conference*, 41st. 1186 (abstr.).
- Usui T., Jones J. H. and Mittlefehldt D. W. (2010b) Experimental study of the felsic asteroidal crust formation recorded in GRA 06128 and GRA 06129. *Meteorit. Planet. Sci.* **45**, A205 (Abs.).
- Valley J. W., Kitchen N. E., Kohn M. J., Niendorf C. R. and Spicuzza M. J. (1995) UWG-2, a garnet standard for oxygen isotope ratios: strategies for high precision and accuracy with laser heating. *Geochim. Cosmochim. Acta* **59**, 5223–5231.
- von Seckendorf V. and O'Neill H. St. C. (1993) An experimental study of Fe–Mg partitioning between olivine and orthopyroxene at 1173, 1273, and 1423 K and 1.6 Gpa. *Contrib. Mineral. Petrol.* **113**, 196–207.
- Wadhwa M., Shukolyukov A. and Lugmair G. W. (1998)  $^{53}\text{Mn}$ – $^{53}\text{Cr}$  systematics in Brachina: a record of one of the earliest phases of igneous activity on an asteroid. *Lunar and Planetary Science Conference*, 29th. 1480 (abstr.).
- Walker R. J., Horan M. F., Morgan J. W., Becker H., Grossman J. N. and Rubin A. E. (2002) Comparative  $^{187}\text{Re}$ – $^{187}\text{Os}$  systematics of chondrites: implications regarding early solar system processes. *Geochim. Cosmochim. Acta* **23**, 4187–4201.
- Walker R. J., McCoy T. J., Schulte R. F., McDonough W. F. and Ash R. D. (2005)  $^{187}\text{Re}$ – $^{188}\text{Os}$ ,  $^{190}\text{Pt}$ – $^{186}\text{Os}$  isotopic and highly siderophile element systematics of group IVA irons. *Lunar and Planetary Science Conference*, 36th. 1313 (abstr.).
- Walker R. J., McDonough W. F., Honesto J., Chabot N. L., McCoy T. J., Ash R. D. and Bellucci J. J. (2008) Modeling fractional crystallization of group IVB iron meteorites. *Geochim. Cosmochim. Acta* **72**, 2198–2216.
- Warren P. H. (1994) Lunar and martian meteorite delivery services. *Icarus* **111**, 338–353.
- Warren P. H. and Kallemeyn G. W. (1989) Allan Hills 84025: the second brachinite, far more differentiated than Brachina, and an ultramafic achondrite clast from L chondrite Yamato 75097. *Proceedings of the Lunar and Planetary Science Conference*, 19th. 475–486.
- Warren P. H., Ulf-Møller F., Huber H. and Kallemeyn G. W. (2006) Siderophile geochemistry of ureilites: a record of early stages of planetesimal core formation. *Geochim. Cosmochim. Acta* **70**, 2104–2126.
- Weisberg M. K., Smith C., Benedix G., Folco L., Righter K., Zipfel J., Yamaguchi A. and Chennai Aoudjehane H. (2009) The Meteoritical Bulletin, No. 95. *Meteorit. Planet. Sci.* **44**, 1–33.
- Wimpenny J., Yin Q. -Z. and Tollstrup D. (2011) Constraining the age of partial melting on the brachinite parent body by investigating Al–Mg systematics in Brachina and paired achondrites GRA 06128/9. *Lunar and Planetary Science Conference*, 42nd. 2473 (abstr.).
- Yamaguchi A., Clayton R. N., Mayeda T. K., Ebihara M., Oura Y., Miura Y., Haramura H., Misawa K., Kojima H. and Nagao K. (2002) A new source of basaltic meteorites inferred from Northwest Africa 011. *Science* **296**, 334–336.
- Zeigler R. A., Jolliff B., Korotev R., Rumble D., Carpenter P.K. and Wang A. (2008) Petrology, geochemistry and likely provenance of unique achondrite Graves Nunatak 06128. *Lunar and Planetary Science Conference*, 39th. 2456 (abstr.).

Associate editor: Sara S. Russell